Modeling and Computation in Vibration Problems, Volume 1

Numerical and semi-analytical methods

Online at: https://doi.org/10.1088/978-0-7503-3483-9

Modeling and Computation in Vibration Problems, Volume 1

Numerical and semi-analytical methods

Edited by
S Chakraverty
Department of Mathematics, National Institute of Technology Rourkela, Odisha, India

F Tornabene
Department of Innovation Engineering, University of Salento, Lecce, Italy

J N Reddy
J. Mike Walker'66 Department of Mechanical Engineering, Texas A&M University, College Station, USA

IOP Publishing, Bristol, UK

ISBN 978-0-7503-3483-9 (ebook)
ISBN 978-0-7503-3481-5 (print)
ISBN 978-0-7503-3484-6 (myPrint)
ISBN 978-0-7503-3482-2 (mobi)

DOI 10.1088/978-0-7503-3483-9

Version: 20211201

IOP ebooks

British Library Cataloguing-in-Publication Data: A catalogue record for this book is available from the British Library.

Published by IOP Publishing, wholly owned by The Institute of Physics, London

IOP Publishing, Temple Circus, Temple Way, Bristol, BS1 6HG, UK

US Office: IOP Publishing, Inc., 190 North Independence Mall West, Suite 601, Philadelphia, PA 19106, USA

Contents

Preface

The primary objective of this two-volume book is to bring together leading researchers of vibrations who are involved in the development of new computational and analytical/semi-analytical techniques. Vibration problems are commonly encountered in various systems of applied mathematics, physics, aeronautical, civil, architectural, marine, mechanical, nuclear, biological and other areas of science and technology. These systems need to be analyzed by easy, fast and efficient computational approaches. Different mathematical theories of vibration, numerical simulation, machine intelligence techniques, physical experiments with computational investigations and their various engineering and science applications are included in these two volumes. Accordingly, these volumes will provide an outstanding opportunity to learn from the contributions of well-known researchers of their ideas, experiences, and advances.

Volume 1 of this book contains numerical and semi-analytical methods including analytical methods in solving various vibration problems. A total of 14 chapters are included in this volume. Chapters 1–3 contain theoretical and modelling investigations of different vibration problems. Studies on nano-structural members are incorporated into chapters 4–9. Finally, chapters 10–14 address various applications of structural vibrations. More details of each chapter are outlined next.

Chapter 1 is contributed by Tornabene, Viscoti, and Dimitri. They have investigated an interesting problem of 'Higher-order theory for the modal analysis of doubly-curved shells with lattice layers and honeycomb cores.' They proposed an innovative method based on Higher Order Shear Deformation Theories (HSDTs) to study the free vibration response of composite lattice structures, with a single or double curvature. A general method for the homogenization of lattice layers made of honeycomb cells and grid patterns is presented, which predicts accurately the anisotropic equivalent elastic constants for a wide range of cell configurations with different heights, wall thicknesses, and geometric layups. The reliability of the strategy is successfully verified against solutions from finite element analyses, both in terms of frequencies and mode shapes, with a very good agreement.

The second chapter is contributed by Ahmad, Gupta, Sujata, and Poomani, titled, 'Particle impact damping technology: modelling and applications.' In this chapter a modelling technique is introduced to capture the interactions between the dynamics of the damping particles and the dynamics of the host structure with a particular focus on the discrete element method (DEM). Hertz's dissipative contact model for normal contact forces and Coulomb's friction model for tangential force are used to derive the governing equation. The vibration attenuation trend has been studied for the location of particle dampers, size of particles, fill fraction, and excitation energy.

Transverse vibration of thick functionally graded (FG) skew plates with various skew angles has been investigated by Pradhan and Chakraverty in chapter 3. Material properties of FG constituents may vary spatially along thickness direction in power-law form. A shear deformation plate theory is considered here to define the

constitutive relation, and the generalized eigenvalue problem is obtained by means of the Ritz method. The obtained results for natural frequencies are validated with those from the existing literature.

Chapter 4 is authored by Tornabene, Dimitri, and Brischetto, where mechanical modelling of functionally graded carbon nanotubes-reinforced composite materials and structures is studied. Variation of the material properties, such as thermal resistance, thermal conductivity and coefficient of thermal expansion, is included. Several higher-order shear deformation theories are used to investigate the problems of the vibration response, the dynamic stability, and the critical speed evaluation of thin and moderately thick structures with high values for the in-plane and transverse anisotropy; the governing equations are solved numerically by means of the Generalized Differential Quadrature (GDQ) method.

In chapter 5, contributed by Saxena and Sarkar, vibration of micro/nano structural members is investigated by discrete energy-based formulation. The authors focused on deriving a molecular-dynamics like discrete framework for different local and non-local continuum models such as beams and plates so that the models can simulate discontinuities. A major aspect of the formulation is that it unifies different local and non-local theories.

Chapter 6 includes the problem of 'Effect of thermal environment on nonlinear flutter of laminated composite plates reinforced with graphene nanoplates,' authored by Guo, Yang, Żur, Reddy, and Ferreira. The authors employed the element-free IMLS-Ritz method to obtain the flutter behavior of matrix cracked functionally graded multilayer graphene nanoplatelets (GPLs) reinforced composites (GPLRCs).

Malikan and Eremeyev have studied forced vibrations of piezo-flexomagnetic nano-actuator beams in chapter 7. The effect of excitation frequency on the piezomagnetic Euler–Bernoulli nanobeam taking the flexomagnetic material phenomenon is addressed here. The attained linear differential equation is transferred into an algebraic equation by using the Galerkin method. Then, the resulting linear algebraic equation is solved to determine the numerical values of dynamic deflections.

Nano-electromechanical systems have made significant advances in various sciences such as mechanics, medicine, and chemistry, due to their unique features and properties, especially in the fields of sensors and actuators. As such, vibration of size-dependent carbon nanotube-based biosensors in liquid is investigated by Sheikhmamoo, Mohammad-Sedighi, and Shishesaz in chapter 8. The equations and boundary conditions are derived using the Hamiltonian principle. The electrostatic and Casimir forces are the source of the nonlinearity in this problem. In this work, an analytical modified Adomian decomposition method is used to investigate the static response of the system. In the static section, the instability of the system and the pull-in voltage under the influence of surface tension effect and size effect are investigated.

Chapter 9, authored by Brischetto, Tornabene, and Dimitri, incorporates continuum 3D and 2D shell models for free vibration analysis of single-walled and double-walled carbon nanotubes. 3D shell solutions based on the exponential matrix methodology for the study of the free vibration response of simply supported

Single- and Double-Walled Carbon NanoTubes (SWCNTs and DWCNTs) are presented. A continuum approach based on the three-dimensional theory of elasticity is employed to represent discrete elements such as SWCNTs and DWCNTs. Proposed analytical 3D shell models are compared with some classical and refined 2D models based on the Generalized Differential Quadrature Method (GDQM) in the case of free vibration study of SWCNTs and DWCNTs with different lengths, diameters and equivalent elastic properties. Moreover, comparisons with well-known continuum beam models from the literature are proposed to analyze the differences between 3D, 2D and 1D approaches, depending on the carbon nanotube length and on the thickness of its walls.

Crack and interface interaction under quasi-static and dynamic loading is addressed by Pranavi, Reddy, Rajagopal, and Reddy in chapter 10. A thermodynamically consistent phase-field formulation for modelling the interactions between interfacial damage and bulk fracture in heterogeneous materials having matrix and inclusion phases with a matrix-inclusion interface is presented. A regularization scheme is considered for both the interface and the crack phase field. A coupled exponential cohesive zone law is adopted to model the interface which has the contributions of both normal and tangential displacement jump components. A novel nonlocal approach is devised to evaluate the smoothed values of jump at the regularized interface using element specific geometric information. The effects of stiff and soft interface on the mechanical response and the crack propagation is studied.

Industrial robotic systems have two essential functional sub-systems namely, gripper and wrist, that are prone to vibration-induced characteristics. This vibration is randomized in real-time and can be *in situ* and/or external impulse-based. Compliant Robotic Gripper (CRG) belongs to a selected niche of the first subsystem and these grippers are modular, semi-flexible and often small-enveloped with multi-task enabled ability. Accordingly, chapter 11 authored by Roy addresses vibration of compliant robotic grippers and wrists. The chapter includes modelling of vibration of CRG & CRW *ab initio*, for both *in situ* as well as external excitation. The author also discusses the local effects of vibration in this section, which are in the form of vibration accumulation at CRW and the consequences of external forcing on the robotic manipulator. Case-studies supported by test results are reported for a table-top small-sized semi-flexible robotic system, augmented with a tailor-made CRG.

Reinforced concrete (RC) beams are one of the critical structural elements in buildings. These elements suffer from distress and primarily cracks due to many reasons resulting into degradation of stiffness and strength. The mode shape-based approaches are very efficient techniques in damage identification in structural elements. As such, in chapter 12, authored by Panigrahi, Chourasia, and Bisht, a study of mode shape based approaches for health monitoring of reinforced concrete beams under transverse loading is presented. An analytical approach has been developed for identification of damage on a beam model considering damage in the beam. The mode shapes and modal curvatures have been computed both for an undamaged and damaged beam structure for damage identification. For validation

of the approach, simply-supported RC beams were subjected to an incrementally increasing static two-point loading in steps till ultimate failure. After each load step, vibration measurements were performed using sensors mounted at critical locations. The mode shapes and modal curvature graphs have been drawn to find out the location of developed crack pattern on the beam.

Chapter 13, authored by Gupta, Ahmad, Aditya, and Poomani, addresses the analysis and testing of honeycomb sandwich structures for spacecraft. Sandwich panels generally consist of three significant components, two thin face sheets and a thick core. The adhesive films are placed between face sheets and core to bond them. The honeycomb sandwich structure is widely used as a primary cylinder, payload mounting panels, shear webs and other support structures in a spacecraft. The experimental setup used in this work is described and then responses obtained through experiments and finite element computations are compared.

Finally, in chapter 14, numerical analysis of Qutb Minar (New Delhi, India) using non-linear plastic-damage macro model for constituent masonry is investigated by Chourasia and Panigrahi. A plastic–damage macro model, originally proposed to model plasticity in concrete, has been adapted to simulate the behavior of masonry present in Qutb Minar. The natural frequencies obtained from an idealized finite element model show better correlation with experimental values from previous studies. The material model implemented is characterized by a bi-dissipative and isotropic degradation of material during cyclic loading. A seismic simulation has been carried out for comparison between response in two cases—elastic and non-elastic material models for constituent masonry. The need to take account of the dynamic parameters and material non-linearity for a realistic seismic response prevision has also been established.

The Editors are certain that the contents of this book will be useful for academic researchers as well as engineers in industry. In academics, this book will be useful for graduate students and researchers of vibration problems of different fields. The Editors believe the integrated and holistic analytical, new theories, computationally efficient approaches presented in various chapters will certainly benefit readers for their future studies and research. The editors thank all the chapter contributors for their effort and support in preparing and submitting on time. Finally, the editors also thank the IOP team for their help and support throughout this project.

May 2021
S Chakraverty
F Tornabene
J N Reddy
Editors

Editor biographies

S Chakraverty

Professor S Chakraverty has 30 years of experience as a researcher and teacher. Presently he is working in the Department of Mathematics (Applied Mathematics Group), National Institute of Technology Rourkela, Odisha as a Senior (Higher Administrative Grade) Professor. Prior to this, he was with CSIR-Central Building Research Institute, Roorkee, India. After completing Graduation from St. Columba's College (Ranchi University), his career started from the University of Roorkee (now, Indian Institute of Technology Roorkee) and did MSc (Mathematics) and MPhil (Computer Applications) from there securing the first positions in the university. Dr Chakraverty received his PhD from IIT Roorkee in 1993. Thereafter he did his post-doctoral research at the Institute of Sound and Vibration Research (ISVR), University of Southampton, UK and at the Faculty of Engineering and Computer Science, Concordia University, Canada. He was also a visiting professor at Concordia and McGill universities, Canada, during 1997–1999 and visiting professor of University of Johannesburg, South Africa during 2011–2014. He has authored/edited 24 books, published 392 research papers (till date) in journals and conferences and two books are ongoing. He is in the Editorial Boards of various International Journals, Book Series and Conferences. Professor Chakraverty is the Chief Editor of *International Journal of Fuzzy Computation and Modelling* (IJFCM), Inderscience Publisher, Switzerland (http://www.inderscience.com/ijfcm), Associate Editor of *Computational Methods in Structural Engineering, Frontiers in Built Environment* and happens to be the Editorial Board member of Springer Nature Applied Sciences, IGI Research Insights Books, Springer Book Series of Modeling and Optimization in Science and Technologies, *Coupled Systems Mechanics* (Techno Press), *Curved and Layered Structures* (De Gruyter), *Journal of Composites Science* (MDPI), *Engineering Research Express* (IOP) and *Applications and Applied Mathematics: An International Journal*. He is also the reviewer of around 50 national and international Journals of repute and he was the President of the Section of Mathematical Sciences (including Statistics) of Indian Science Congress (2015–2016) and was the Vice President Orissa Mathematical Society (2011–2013). Professor Chakraverty is a recipient of prestigious awards viz. Indian National Science Academy (INSA) nomination under International Collaboration/Bilateral Exchange Program (with the Czech Republic), Platinum Jubilee ISCA Lecture Award (2014), CSIR Young Scientist Award (1997), BOYSCAST Fellow. (DST), UCOST Young Scientist Award (2007, 2008), Golden Jubilee Director's (CBRI) Award (2001), INSA International Bilateral Exchange Award ([2010–11 (selected but could not undertake), 2015 (selected)], Roorkee University Gold Medals (1987, 1988) for first positions in MSc and MPhil (Comp. Appl.) etc.

He is in the list of 2% world scientists recently (2020) in Artificial Intelligence & Image Processing category based on an independent study done by Stanford University scientists. His world rank is 1862 out of 215114 researchers throughout the globe.

IOP Publishing Top Cited Paper Award for one of the most cited articles from India, published across the entire IOP Publishing journal portfolio within the past three years (2018 to 2020). It also features in the top 1% of most cited papers in the Materials subject category. This data is from the citations recorded in Web of Science.

He has already guided nineteen (19) PhD students and twelve are ongoing. Professor Chakraverty has undertaken around 16 research projects as Principle Investigator funded by international and national agencies totaling about Rs.1.5 crores. He has hoisted around 8 international students with different international/national fellowships to work in his group as PDF, PhD, visiting researchers for different periods. A good number of international and national Conferences, Workshops, and Training programs have also been organised by him. His present research areas include differential equations (ordinary, partial and fractional), numerical analysis and computational methods, structural dynamics (FGM, Nano) and fluid dynamics, mathematical and uncertainty modeling, soft computing and machine intelligence (artificial neural network, fuzzy, interval and affine computations).

Following are his Google, Scopus, other related and Vidwan (Institute) links:

Google Scholar : https://scholar.google.co.in/citations?user=4EeFYt4AAAAJ&hl=en

Scopus ID: http://www.scopus.com/authid/detail.url?origin=resultslist&authorId=7005011457&zone=

ORCID ID: https://orcid.org/0000-0003-4857-644X

Publons: https://publons.com/researcher/685949/snehashish-chakraverty/

Researchgate: https://www.researchgate.net/profile/S_Chakraverty

Vidwan (Institute) Link: http://nitrkl.irins.org/profile/62073

My VIDEO Lectures: https://www.youtube.com/channel/UCEsAtWBMIvDTnrPH7Yn82wA/videos?view_as=subscriber

F Tornabene

Francesco Tornabene is an Assistant Professor and Lecturer at the School of Engineering, Department of Innovation Engineering, University of Salento. He was born on 13 January 1978 in Bologna, where he received the high school degree at Liceo Classico *San Luigi*, in 1997. In 2001 he achieved a National Patent Bologna (Italy) for the Industrial Invention: *Friction Clutch for High Performance Vehicles* Question BO2001A00442. He received from the University of Bologna - Alma Mater Studiorum, an MSc degree in *Mechanical Engineering* (Curriculum in *Structural Mechanics*), on 23 July 2003, discussing a thesis entitled: *Dynamic Behavior of Cylindrical Shells: Formulation and Solution*. In December 2003, he was admitted to the PhD course in *Structural Mechanics*, at the University of Bologna, reaching the first position in the competitive admission. In 2004, he received from the University

of Bologna a Thesis prize in memory of *Carlo Felice Jodi*; in 2007 he received the PhD degree in *Structural Mechanics* at the University of Bologna, discussing the Thesis entitled *Modeling and Solution of Shell Structures Made of Anisotropic Materials*. From 2007 to 2009 he received a research fellowship by the University of Bologna, working on the *Unified Formulation of Shell Structures Made of Anisotropic Materials. Numerical Analysis Using the Generalized Differential Quadrature Method and the Finite Element Method*. From 2011 to 2012 he became a junior researcher within the research program entitled *Advanced Numerical Schemes for Anisotropic Materials*; from 2012 to 2018 he was an Assistant Professor and Lecturer at the Alma Mater Studiorum - University of Bologna; from 2018 up to date he has been an Assistant Professor in Structural Mechanics and Lecturer at the University of Salento, Department of Innovation Engineering (Lecce). For a long time his scientific interests have included structural mechanics, solid mechanics, innovative and smart materials, computational mechanics and numerical techniques, damage and fracture mechanics. He is author of more than 260 scientific publications, and collaborates with many national or international researchers and professors all over the world, as visible from his scientific production. He is author of 11 books, see e.g. *Meccanica delle Strutture a Guscio in Materiale Composito. Il metodo Generalizzato di Quadratura Differenziale* (2012); *Mechanics of Laminated Composite Doubly-Curved Shell Structures. The Generalized Differential Quadrature Method and the Strong Formulation Finite Element Method* (2014); *Laminated Composite Doubly-Curved Shell Structures I. Differential Geometry. Higher-Order Structural Theories* (2016); *Laminated Composite Doubly-Curved Shell Structures II. Differential and Integral Quadrature. Strong Formulation Finite Element Method* (2016), *Anisotropic Doubly-Curved Shells. Higher-Order Strong and Weak Formulations for Arbitrarily Shaped Shell Structures* (2018), among many. He is member of the Editorial Board for 42 international journals (see, e.g. *Journal of Engineering*, *International Journal of Engineering & Applied Sciences*, *Composite Structures*, *Technologies*, *Journal of Applied and Computational Mechanics*, *Journal of Composites Science*, *Advanced Materials and Technologies*, *Heliyon, International Scholarly Research Notices, Mathematical Problems in Engineering, ISRN Mechanical Engineering, Journal of Computational Engineering, Advances in Aircraft and Spacecraft Science*, among others). He is also Editor-in-Chief for two international journals: *Curved and Layered Structures and Journal of Composites Science*; from 2019 he has been Associate Editor for the international journal *Mechanics Based Design of Structures and Machines*. In recent years he received different important awards, see e.g. *Highly Cited Researcher by Clarivate Analytics* (years 2018, 2019, 2020), *Ambassador of Bologna Award* for the organization of 21st International Conference on Composite Structures ICCS21, 4–7 September 2018, Bologna, Italy (2019), Member of the European Academy of Sciences (since 2018). He collaborates as a reviewer with more than 240 prestigious international journals in the structural mechanics field. From 2012, his teaching activities have included: dynamics of structures; computational mechanics; plates and shells; theory of structures; structural mechanics or mechanics of solids and structures. He is habilitated as Associate Professor and Full Professor in the area 08/B2 (Mechanics of Solids and Structures) and as Associate

Professor in Area 09/A1 (Aeronautical and Aerospace Engineering and Naval Architecture).

Assistant Professor at the Department of Innovation Engineering - University of Salento, Via per Monteroni, 73100, Lecce, Italy
E-mail Address: francesco.tornabene@unisalento.it

J N Reddy

Dr Reddy, the *O'Donnell Foundation Chair IV Professor* in J. Mike Walker '66 Department of Mechanical Engineering at Texas A &M University, is a highly-cited researcher, author of a large number of journal papers and 24 books (several with second, third, and fourth editions) on energy principles, variational methods, plates and shells, composite materials, mechanics of solids, and the finite element method (linear and nonlinear) and its applications. Dr Reddy has delivered over 180 plenary, keynote, and invited lectures at international conferences; and taught 116 short courses; he advised 50 postdoctoral fellows and research visitors, and guided and co-guided 120 graduate students (74 PhD and 46 MS students).

In research, Dr Reddy is known worldwide for his significant contributions to the field of applied mechanics through the authorship of widely used textbooks on the linear and nonlinear finite element analysis, variational methods, and composite materials and structures. His pioneering works on the development of shear deformation theories (that bear his name in the literature as the *Reddy third-order plate theory and the Reddy layerwise theory*) have had a major impact and have led to new research developments and applications. Some of the ideas on shear deformation theories and penalty finite element models of fluid flows have been implemented into commercial finite element computer programs like ABAQUS, NISA, and HyperXtrude.

Dr Reddy is the recipient of numerous professional awards from various professional organizations and societies. Recent significant national and international awards include: member of the US National Academy of Engineering, and foreign member of the Indian National Academy of Engineering, Canadian Academy of Engineering, Brazilian National Academy of Engineering, the Royal Academy of Engineering of Spain, the Chinese Academy of Engineering, a member of the European Academy of Sciences and Arts, Honorary Member of the European Association of Sciences, and the Academia Scientiarum et Artium Europaea (the European Academy of Sciences and Arts). He also received the *John von Neumann Medal* from the US Association of Computational Mechanics, the *Theodore von Karman Medal* from the American Society of Civil Engineers, and the *Stephan P. Timoshenko Medal* from American Society of Mechanical Engineers.

List of contributors

Akash Aditya
Structures Group, U. R. Rao Satellite Centre, Bangalore, India

Nazeer Ahmad
Structures Group, U. R. Rao Satellite Centre, Bangalore, India

R S Bisht
CSIR-Central Building Research Institute, Roorkee, India

Salvatore Brischetto
Department of Mechanical and Aerospace Engineering, Politecnico di Torino, Turin, Italy

S Chakraverty
Department of Mathematics, National Institute of Technology Rourkela, Rourkela, Odisha, India

Ajay Chourasia

CSIR-Central Building Research Institute, Roorkee, India

Rossana Dimitri
Department of Innovation Engineering, School of Engineering, University of Salento, Lecce, Italy

Victor A Eremeyev
Department of Mechanics of Materials and Structures, Gdansk University of Technology, 80-233 Gdansk, Poland
and
DICAAR, Università degli Studi di Cagliari, Via Marengo, 2, 09123 Cagliari, Italy

A J M Ferreira
Departamento de Engenharia Mecanica, Universidade do Porto, Porto, Portugal

Ankur Kumar Gupta
Structures Group, U. R. Rao Satellite Centre Bangalore, India

Hulun Guo
Department of Mechanics, Tianjin University, Tianjin, China

Mohammad Malikan
Department of Mechanics of Materials and Structures, Gdansk University of Technology, 80-233 Gdansk, Poland
and
DICAAR, Università degli Studi di Cagliari, Via Marengo, 2, 09123 Cagliari, Italy

S K Panigrahi
CSIR-Central Building Research Institute, Roorkee, India

D Poomani
Structures Group, U. R. Rao Satellite Centre, Bangalore, India

K K Pradhan
Department of Basic Science, Parala Maharaja Engineering College, Berhampur, Sitalapalli Ganjam, Odisha, India

Dhaladhuli Pranavi
IIT Hyderabad, India

Amirtham Rajagopal
IIT Hyderabad, India

J N Reddy
J. Mike Walker'66 Department of Mechanical Engineering, Texas A&M University, College Station, USA

K S S Reddy
IIT Hyderabad, India

Debanik Roy
Division of Remote Handling & Robotics, Bhabha Atomic Research Centre & Homi Bhabha National Institute, Department of Atomic Energy, Mumbai, India

Mukul Saxena
Discipline of Civil Engineering, IIT Indore, India

Saikat Sarkar
Discipline of Civil Engineering, IIT Indore, India

Hamid Mohammad Sedighi
Mechanical Engineering Department, Faculty of Engineering, Shahid Chamran University of Ahvaz, Ahvaz, Iran

Fatemeh Sheikhmamoo
Mechanical Engineering Department, Faculty of Engineering, Shahid Chamran University of Ahvaz, Ahvaz, Iran

Mohammad Shishesaz
Mechanical Engineering Department, Faculty of Engineering, Shahid Chamran University of Ahvaz, Ahvaz, Iran

Sujata
Structures Group, U. R. Rao Satellite Centre Bangalore, India

Francesco Tornabene
Department of Innovation Engineering, University of Salento, Lecce, Italy

Matteo Viscoti
Department of Innovation Engineering, School of Engineering, University of Salento, Lecce, Italy

Tianzhi Yang
School of Mechanical Engineering and Automation, Northeastern University, Shenyang, China

Krzysztof Kamil Żur
Faculty of Mechanical Engineering, Bialystok University of Technology, Bialystok, Poland

IOP Publishing

Modeling and Computation in Vibration Problems, Volume 1
Numerical and semi-analytical methods
S Chakraverty, F Tornabene and J N Reddy

Chapter 1

Higher order theory for the modal analysis of doubly-curved shells with lattice layers and honeycomb cores

Francesco Tornabene, Matteo Viscoti and Rossana Dimitri

This chapter proposes an innovative method based on Higher Order Shear Deformation Theories (HSDTs) to study the free vibration response of composite lattice structures, with a single or double curvature. We develop a general method for the homogenization of lattice layers made of honeycomb cells and grid patterns, which predicts accurately the anisotropic equivalent elastic constants for a wide range of cell configurations with different heights, wall thicknesses and geometric layups. A general lamination scheme is modelled following an Equivalent Single Layer (ESL) methodology, whereas the Generalized Differential Quadrature (GDQ) method is proposed to solve accurately the eigenvalue problems with a reduced computational cost. A systematic investigation is performed to check for the sensitivity of the dynamic response for shells with a varying honeycomb and grid layups, along with different geometries and boundary conditions. The reliability of the present strategy is successfully verified against solutions from classical finite elements, both in terms of frequencies and mode shapes, with a very good agreement among results.

1.1 Introduction

In recent decades, new frontiers in many engineering applications have seen a lot of endeavour in searching for optimum parameters of structures with respect to their mechanical response [1–3]. In order to seek the best performance, the design can be oriented looking at structural shapes, as well as a proper selection of the material constituents, keeping in mind the manufacturing issues [4, 5]. As suggested by Vasiliev [6, 7], one of the most challenging structures among doubly-curved shells can be found in latticed composite structures. They are conceived so that a particular shape can be assessed starting from a correct location of some stiffeners along the

doi:10.1088/978-0-7503-3483-9ch1

parametric lines of a surface. These kinds of structures are characterized by large versatility. Looking up the applications of these structures, several grid architectures can be found, with open and closed cell lattices, hierarchical cells, disordered or randomized. Some regular patterns can be additionally found in some applications, with a different location of hoops and helical ribs, as well as a varying distance between stiffeners and inclination angle. In this way, each beam element of a three-dimensional structure is essentially subjected to a compressive load.

Another interesting way for infilling doubly curved structures is represented by honeycomb cells. According to this technology, a periodic infill is defined within a layer, characterized by some geometric parameters like the internal cell angle, and geometry of the cell panels [8]. Different mechanical properties can be obtained for the same structure, with a proper selection of its geometrical parameters [9]. Nevertheless, the honeycomb cell can be easily applied to layered structures so that a general orthotropic softcore can be obtained starting from an isotropic raw material. The application of optimization design algorithms usually requires simple but accurate formulations based on iterative processes that check for the best periodic unit cell in the whole structure, and its equivalent elastic properties [10]. Among continuum models, it is possible to apply a homogenization process on the so-called Representative Volume Element (RVE), to determine its equivalent elasticity constants, independently of the unit cell scale. In other words, the so-called separation of scales principle must be guaranteed [11–13], as guaranteed by a Multiscale Aggregating Discontinuities (MAD) method [14] or a Continuum Strong Discontinuity Approach (MSDA) [15–17]. One of the most adopted tools for the homogenization of the unit cell is the well-known Finite Element Method (FEM) [18]. A comprehensive literature overview about a finite element modeling of lattice structures can be found in [19–21]. Since the strategy at issue is based on a structural decomposition, the homogenized properties must be properly assessed independently from the selected mesh [22]. A finite element-based homogenization of lattice structures must account for local deformation effects in line with the predefined shape functions per each element [23].

For honeycomb unit patterns, we can employ a large variety of formulations, based on different initial hypotheses. Starting from the pioneer works by Gibson and Ashby (G&A) [24], various homogenization theories have been developed in literature [25–27] that account for the actual microstructural nature. Most of them, however, cannot provide a unique value of the equivalent elasticity constants, since they follow the energy procedure based on the minimum potential energy principle, as suggested by Kelsey *et al* [28]. In order to determine a unique value of homogenized stiffness constants, Grediac [29] proposed a general procedure based on a linear interpolation between the extreme values of stiffness based on the out-of-plane cell slenderness. Scarpa and Tomlin [30] measured the equivalent constants for re-entrant cell units starting from finite element simulations. Malek and Gibson (M&G) [31] embedded a rigid node assumption in the definition of the homogenized cell model. Each element in the unit cell was modelled by means of a Timoshenko Beam Theory (TBT) [32], or an Euler–Bernoulli Beam Theory [33]. An improvement of the G&A formulae was also proposed by Sorohan *et al* [34], who introduced some correction factors in order to

account for the shear effects in the cell walls during a deformation process, as observed from FEM simulations, as well as experimental predictions.

Further shear correction factors were introduced by Fu and Yin [35] to improve the original formulation by G&A. In the work by Torabi *et al* [36] the above-mentioned formulation was applied for the flutter analysis of a cantilever trapezoidal honeycomb plate, employing the Differential Quadrature Method. Regarding the out-of-plane elastic properties, their mean value was computed by the authors between the extreme ones. Sorohan *et al* [37, 38] also provided an improved version of the M&G homogenization theory, based on an accurate geometrical description of the unit cell, with special attention to the geometry of nodes. In the original M&G model a rigid node assumption was embedded in the formulation. In this case, instead, its contribution to the total strain energy was computed by introducing an equivalent nodal length, based on the actual value of the node area. Following the same approach, a revision of G&A homogenization has been provided. Based on the recent work by Tornabene *et al* [39], a reliable formulation was proposed by the authors to determine the out-of-plane elastic constants for a large variety of honeycomb-based cells.

On the other hand, when a smearing technique is applied to anisogrid structures, after the proper definition of a generally-curved geometry, an important aspect is related to the periodicity of a unit pattern within the entire shell, or of a lattice layer. Differently from honeycomb cells, the cell geometry within a latticed structure comes out from the superimposition of various families of ribs which are assumed to be independent from each other. The overall mechanical properties for similar cell units are computed by considering the axial behaviour of each beam, accounting for its orientation with respect to the geometric principal axes of the shell structure. According to [4], each single rib contribution is computed independently from the presence of other beams within the unit cell.

In this way, cells with different numbers of rib families are obtained without considering the nodal stiffness, greater than the free area of the single rib. Based on this smearing technique it is also possible to assess a homogenized model by employing two different cell configurations with a different number of internal intersections. If only one node is embedded in the unit cell, a flake (F) unit pattern is identified, otherwise a star (S) cell layup is obtained. Actually, the rib family geometric parameters embedded in the model refer to the angle orientation and interspace between two adjacent beams [40].

The homogenized model of a shell structure can be described geometrically by means of the differential geometry basics, and a proper definition of the orthogonal reference system, together with the well-known Lamè Parameters and principal curvatures. The pioneering works by Calladine [41], Kraus [42] and Gould [43] applied this strategy to thin shells. The governing equations for the dynamic problem of curved shell structures are built on a bi-dimensional model that accounts for the through-the-thickness structural behaviour. In this perspective, two different strategies are proposed in this chapter: the Equivalent Single Layer (ESL) theory and the Layer-Wise (LW) approach [44]. In the former, we define the equivalent mechanical properties, in terms of elasticity constants, stress and strain field, for the entire shell thickness. A key aspect of this method is related to an accurate computation of such quantities, especially in the presence of very

complex lamination schemes and possible coupling effects. On the other hand, the LW approach can be considered as a generalization of the ESL theory, since the fundamental equations of the problem are written separately at each layer of the lamination scheme by introducing some general thickness functions [45], in respect of the compatibility conditions and of a consistent distribution of the stress/strain field. A recovery procedure based on the equilibrium equations provides the three-dimensional stress distribution within the shell structure [46]. Starting with the classical shell theories of Kirchhoff–Love [47, 48], Reissner and Mindlin [49–51], or Reddy [52–54], more advanced models in the recent literature embed possible warping and stretching functions. In such a context, a first attempt can be found in the works by Washizu [55] and Reddy [56], where the authors provide a general description of the displacement field in shell members with a single constant curvature, and introduce for the first time a unified notation for a compact computation of thickness functions. In the theory developed by Tornabene *et al* [57], a generalized ESL approach based on HSDTs has been recently employed for a static and dynamic analysis of doubly-curved structures with anisotropic materials. It is interesting to say that the introduction of anisotropy within a structure enhances its shear strain field, that can be well-captured only under a proper assumption of thickness functions. In the further works by Tornabene *et al* [58–60] the same set of fundamental equations has been also written for each layer of anisotropic structures with very complex geometries.

The dynamic behavior of lattice-based structures is a key aspect that must be accounted for optimum design purposes of shell members with high stiffness/weight ratios. In this perspective, some optimization algorithms can be found in [61–63], which compute numerically the modal frequencies of arbitrarily-shaped structures. Among many possible high-performance computational methods, in this chapter we propose the Generalized Differential Quadrature (GDQ) [64–69] as efficient tool to solve the dynamics of complicated shell geometries made of innovative materials [70–77], in a strong form. The proposed method stems from classical quadrature methods [78] and expresses the derivative of a smooth function as a weighted sum of the values assumed by the same function in a set of points. As stated in the pioneering work by Shu *et al* [79], the main performances of this method, in terms of accuracy, convergence, and stability, are related to the domain discrete point distribution and weighting coefficients selection. In a recent work [80], the GDQ method was successfully compared to a classical Ritz formulation for the modal analysis of isotropic and non-homogeneous thin-walled structures, while revealing a great accuracy even with a reduced number of degrees of freedom (DOFs). The high level of accuracy was also demonstrated in many convergence studies [81–84] involving the statics/dynamics and fracture mechanics nonlinear problems [85–94].

In the present chapter, we propose a homogenized model based on Higher Order Theories for the dynamic study of doubly-curved sandwich structures with a softcore layer made of latticed/honeycomb configurations. The governing equations of the problem together with the boundary conditions are here determined by applying the Hamiltonian Principle in a variational form, combined with different homogenization methods for both honeycomb layers and the latticed cores, to derive the equivalent anisotropic material properties. The GDQ method is, thus, applied to discretize the governing equations and boundary conditions of the problems, whose solutions are validated systematically with respect to refined 3D finite element-based solutions.

The rate of convergence analyses also demonstrate the stability and efficiency of the response, even for complex coupled mode shapes and a reduced computational effort, as implemented in the MATLAB code DiQuMASPAB, written by Tornabene *et al* [95].

1.2 Equivalent single layer shell theory

In this section we introduce all the theoretical basics of an ESL approach for lattice curved shells according to higher order theories. Particular attention is given to the structural geometry, the field variable assumptions, the RVE homogenization methods, and the derivation of the fundamental equations. According to an ESL strategy, all the geometric, kinematic and equilibrium features of the structure are referred to an equivalent middle surface, starting from a general three-dimensional formulation of the problem.

1.2.1 Geometrical description of the shell

We start considering the theoretical issues related to the geometry of a lattice structure with different curvatures. Generally speaking, pantographic structures and honeycomb shells present a three-dimensional extension, and their mathematical description usually turns out to be a challenging issue, especially for complicated shapes. In such cases, an orthogonal curvilinear reference system must be properly introduced to simplify the geometrical description of a generally-shaped structure, based on the definition of a principal coordinate system along the parametric directions α_1 and α_2, in the reference mid-surface, and the outward coordinate ζ in the thickness direction. Based on an indicial notation, it is $\zeta = \alpha_3$. As a consequence, the position vector $\mathbf{R}(\alpha_1, \alpha_2, \zeta)$ of a generic point of the structure can be written as follows [57]

$$\mathbf{R}(\alpha_1, \alpha_2, \zeta) = \mathbf{r}(\alpha_1, \alpha_2) + \frac{h(\alpha_1, \alpha_2)}{2} z\, \mathbf{n}(\alpha_1, \alpha_2) \tag{1.1}$$

where $\mathbf{r}(\alpha_1, \alpha_2)$ is the projection of the arbitrary point on the reference surface, $\mathbf{n}(\alpha_1, \alpha_2)$ the normal unit vector, and $h(\alpha_1, \alpha_2)$ the shell thickness (see figure 1.1). In equation (1.1), the position along the thickness coordinate ζ with respect to the middle surface is defined with a dimensionless coordinate $z = 2\zeta/h(\alpha_1, \alpha_2) \in [-1, 1]$. By computing the partial derivatives $\mathbf{r}_{,1}$ and $\mathbf{r}_{,2}$ of the reference surface position vector with respect to α_1 and α_2, respectively, it is possible to define at each point the Lamè Parameters of the middle layer $A_1(\alpha_1, \alpha_2)$ and $A_2(\alpha_1, \alpha_2)$

$$A_1(\alpha_1, \alpha_2) = \sqrt{\mathbf{r}_{,1} \cdot \mathbf{r}_{,1}}, \quad A_2(\alpha_1, \alpha_2) = \sqrt{\mathbf{r}_{,2} \cdot \mathbf{r}_{,2}} \tag{1.2}$$

The normal unit vector $\mathbf{n}(\alpha_1, \alpha_2)$ is thus defined as

$$\mathbf{n}(\alpha_1, \alpha_2) = \frac{\mathbf{r}_{,1} \times \mathbf{r}_{,2}}{A_1 A_2} \tag{1.3}$$

whereas, the principal radii of curvature $R_1(\alpha_1, \alpha_2)$ and $R_2(\alpha_1, \alpha_2)$ are computed as

$$R_1(\alpha_1, \alpha_2) = -\frac{\mathbf{r}_{,1} \cdot \mathbf{r}_{,1}}{\mathbf{r}_{,11} \cdot \mathbf{n}}, \quad R_2(\alpha_1, \alpha_2) = -\frac{\mathbf{r}_{,2} \cdot \mathbf{r}_{,2}}{\mathbf{r}_{,22} \cdot \mathbf{n}} \tag{1.4}$$

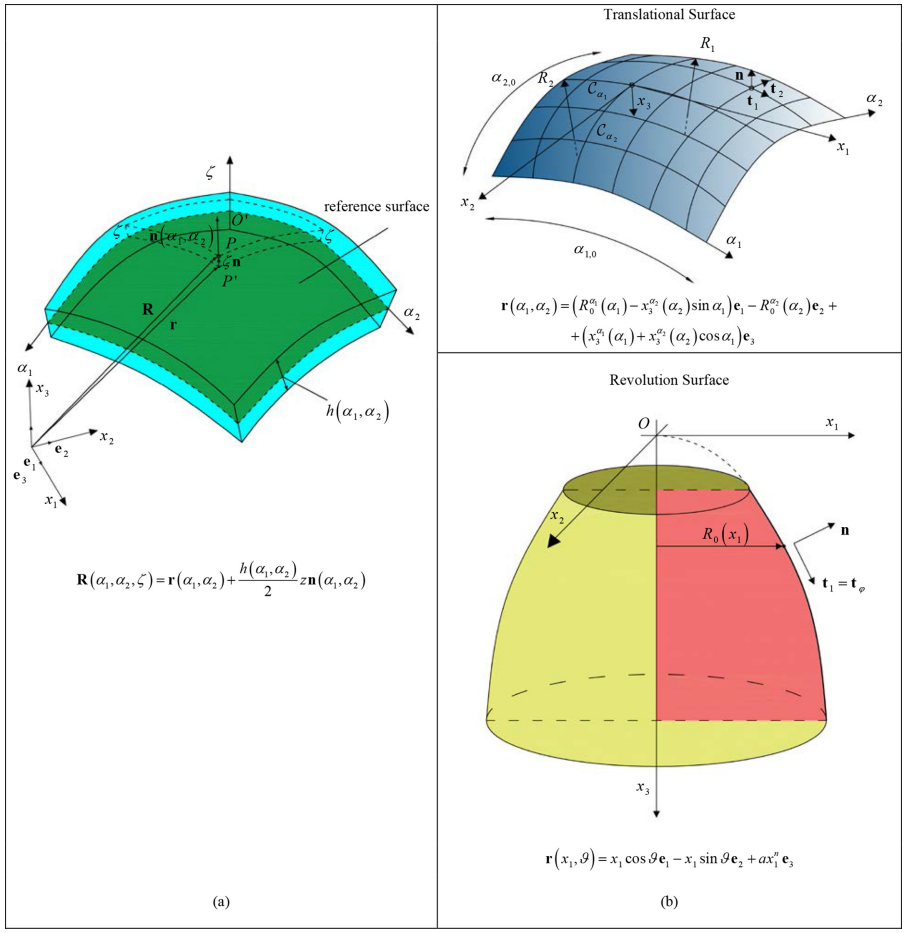

Figure 1.1. Geometric representation of a generic doubly-curved shell.

Note that the in-plane coordinates $\alpha_i \in [\alpha_i^0, \alpha_i^1]$, for $i = 1, 2$, whereas ζ is limited in the thickness direction as $\zeta(\alpha_1, \alpha_2) \in [-h(\alpha_1, \alpha_2)/2, h(\alpha_1, \alpha_2)/2]$. For a laminated structure, the overall thickness $h(\alpha_1, \alpha_2)$ is determined as [57]

$$h(\alpha_1, \alpha_2) = \sum_{k=1}^{l} h_k(\alpha_1, \alpha_2) \tag{1.5}$$

where $h_k(\alpha_1, \alpha_2) = \zeta_{k+1}(\alpha_1, \alpha_2) - \zeta_k(\alpha_1, \alpha_2)$ is the thickness for the kth layer of a l-laminate, with $k = 1, \ldots, l$.

1.2.2 Kinematic formulation

In what follows the displacement field represents the primary unknown. Therefore, we introduce a procedure for defining equivalent quantities in the mid-structure, and

we determine the 3D displacement field vector $\mathbf{U}(\alpha_1, \alpha_2, \zeta, t) = [U_1 \ U_2 \ U_3]^T$ in the curvilinear reference system O', α_1, α_2, ζ in the following form [57]

$$\begin{aligned} U_1(\alpha_1, \alpha_2, \zeta, t) &= \sum_{\tau=0}^{N+1} F_\tau^{\alpha_1}(\zeta) u_1^{(\tau)}(\alpha_1, \alpha_2, t) \\ U_2(\alpha_1, \alpha_2, \zeta, t) &= \sum_{\tau=0}^{N+1} F_\tau^{\alpha_2}(\zeta) u_2^{(\tau)}(\alpha_1, \alpha_2, t) \\ U_3(\alpha_1, \alpha_2, \zeta, t) &= \sum_{\tau=0}^{N+1} F_\tau^{\alpha_3}(\zeta) u_3^{(\tau)}(\alpha_1, \alpha_2, t) \end{aligned} \tag{1.6}$$

or in the compact notation

$$\mathbf{U}(\alpha_1, \alpha_2, \zeta, t) = \sum_{\tau=0}^{N+1} \mathbf{F}_\tau \mathbf{u}^{(\tau)} \tag{1.7}$$

where $\mathbf{F}_\tau = \mathbf{F}_\tau(\zeta)$ is a diagonal matrix collecting the thickness functions $F_\tau^{\alpha_i}(\zeta)$, with $i = 1, 2, 3$

$$\mathbf{F}_\tau(\zeta) = \begin{bmatrix} F_\tau^{\alpha_1} & 0 & 0 \\ 0 & F_\tau^{\alpha_2} & 0 \\ 0 & 0 & F_\tau^{\alpha_3} \end{bmatrix} \tag{1.8}$$

In equation (1.6) a generalized displacement field component vector $\mathbf{u}^{(\tau)}(\alpha_1, \alpha_2, t) = [u_1^{(\tau)} \ u_2^{(\tau)} \ u_3^{(\tau)}]^T$ with $\tau = 0, \ldots, N+1$ is defined for each τth order of the kinematic expansion, defined on the reference surface. In order to take into account the interaction between adjacent layers, for $\tau = N+1$ we introduce the well-known Murakami's function, together with a power series expansion for $\tau = 0, \ldots, N$

$$F_\tau = \begin{cases} \zeta^\tau & \text{for} \quad \tau = 0, 1, \ldots, N \\ (-1)^k z_k & \text{for} \quad \tau = N+1 \end{cases} \tag{1.9}$$

where $z_k = z_k(\zeta) \in [-1, \ 1]$ is defined for the kth layer as follows

$$z_k = \frac{2}{\zeta_{k+1} - \zeta_k}\zeta - \frac{\zeta_{k+1} + \zeta_k}{\zeta_{k+1} - \zeta_k} \tag{1.10}$$

In what follows we introduce a compact notation, as already proposed in [57] in order to identify easily higher order theories, namely

$$\text{ED} - \begin{matrix} [F_0^{\alpha_1}][F_1^{\alpha_1}]\ldots[F_N^{\alpha_1}][Z] \\ [F_0^{\alpha_2}][F_1^{\alpha_2}]\ldots[F_N^{\alpha_2}][Z] \\ [F_0^{\alpha_3}][F_1^{\alpha_3}]\ldots[F_N^{\alpha_3}][Z] \end{matrix} \tag{1.11}$$

where E stands for the ESL approach, D refers to the displacement field, Z is the Murakami's function (1.9) and N is the variable expansion order.

The kinematic relations for the ESL higher order theory are, thus, defined as

$$\boldsymbol{\varepsilon} = \mathbf{D}\, U = \mathbf{D}_\zeta \left(\sum_{i=1}^{3} \mathbf{D}_\Omega^{\alpha_i} \right) \mathbf{U} = \mathbf{D}_\zeta (\mathbf{D}_\Omega^{\alpha_1} + \mathbf{D}_\Omega^{\alpha_2} + \mathbf{D}_\Omega^{\alpha_3}) \mathbf{U} \tag{1.12}$$

where $\boldsymbol{\varepsilon}(\alpha_1, \alpha_2, \alpha_3, t) = [\varepsilon_1 \;\; \varepsilon_2 \;\; \gamma_{12} \;\; \gamma_{13} \;\; \gamma_{23} \;\; \varepsilon_3]^T$ is the three-dimensional strain vector [57] and $\mathbf{D}$ is the differential operator split in two different parts $\mathbf{D}_\zeta$ and $\mathbf{D}_\Omega^{\alpha_i}$ $i = 1, 2, 3$, such that

$$\mathbf{D}_\zeta = \begin{bmatrix} \frac{1}{H_1} & 0 & 0 & 0 & 0 & 0 & 0 & 0 & 0 \\ 0 & \frac{1}{H_2} & 0 & 0 & 0 & 0 & 0 & 0 & 0 \\ 0 & 0 & \frac{1}{H_1} & \frac{1}{H_2} & 0 & 0 & 0 & 0 & 0 \\ 0 & 0 & 0 & 0 & \frac{1}{H_1} & 0 & \frac{\partial}{\partial \zeta} & 0 & 0 \\ 0 & 0 & 0 & 0 & 0 & \frac{1}{H_2} & 0 & \frac{\partial}{\partial \zeta} & 0 \\ 0 & 0 & 0 & 0 & 0 & 0 & 0 & 0 & \frac{\partial}{\partial \zeta} \end{bmatrix} \tag{1.13}$$

$$\mathbf{D}_\Omega^{\alpha_1} = \begin{bmatrix} \frac{1}{A_1}\frac{\partial}{\partial \alpha_1} & 0 & 0 \\ \frac{1}{A_1 A_2}\frac{\partial A_2}{\partial \alpha_1} & 0 & 0 \\ -\frac{1}{A_1 A_2}\frac{\partial A_1}{\partial \alpha_2} & 0 & 0 \\ \frac{1}{A_2}\frac{\partial}{\partial \alpha_2} & 0 & 0 \\ -\frac{1}{R_1} & 0 & 0 \\ 0 & 0 & 0 \\ 1 & 0 & 0 \\ 0 & 0 & 0 \\ 0 & 0 & 0 \end{bmatrix} \quad \mathbf{D}_\Omega^{\alpha_2} = \begin{bmatrix} 0 & \frac{1}{A_1 A_2}\frac{\partial A_1}{\partial \alpha_2} & 0 \\ 0 & \frac{1}{A_2}\frac{\partial}{\partial \alpha_2} & 0 \\ 0 & \frac{1}{A_1}\frac{\partial}{\partial \alpha_1} & 0 \\ 0 & -\frac{1}{A_1 A_2}\frac{\partial A_2}{\partial \alpha_1} & 0 \\ 0 & 0 & 0 \\ 0 & -\frac{1}{R_2} & 0 \\ 0 & 0 & 0 \\ 0 & 1 & 0 \\ 0 & 0 & 0 \end{bmatrix} \quad \mathbf{D}_\Omega^{\alpha_3} = \begin{bmatrix} 0 & 0 & \frac{1}{R_1} \\ 0 & 0 & \frac{1}{R_2} \\ 0 & 0 & 0 \\ 0 & 0 & 0 \\ 0 & 0 & \frac{1}{A_1}\frac{\partial}{\partial \alpha_1} \\ 0 & 0 & \frac{1}{A_2}\frac{\partial}{\partial \alpha_2} \\ 0 & 0 & 0 \\ 0 & 0 & 0 \\ 0 & 0 & 1 \end{bmatrix} \tag{1.14}$$

By introducing the through-the-thickness assumptions (1.7) for the displacement field within three-dimensional congruence relations (1.12), the ESL formulation of kinematic equation comes out

$$\boldsymbol{\varepsilon} = \sum_{\tau=0}^{N+1} \sum_{i=1}^{3} \mathbf{D}_\zeta \mathbf{D}_\Omega^{\alpha_i} \mathbf{F}_\tau \mathbf{u}^{(\tau)} = \sum_{\tau=0}^{N+1} \sum_{i=1}^{3} \mathbf{Z}^{(\tau)\alpha_i} \mathbf{D}_\Omega^{\alpha_i} \mathbf{u}^{(\tau)} = \sum_{\tau=0}^{N+1} \sum_{i=1}^{3} \mathbf{Z}^{(\tau)\alpha_i} \boldsymbol{\varepsilon}^{(\tau)\alpha_i} \tag{1.15}$$

which is redefined for the τth order as

$$\boldsymbol{\varepsilon}^{(\tau)\alpha_i} = \mathbf{D}_\Omega^{\alpha_i} \mathbf{u}^{(\tau)} \quad \text{for} \quad \tau = 0, 1, 2, \ldots, N, N+1 \quad i = 1, 2, 3 \tag{1.16}$$

where

$$\mathbf{Z}^{(\tau)\alpha_i} = \begin{bmatrix} \frac{F_\tau^{\alpha_i}}{H_1} & 0 & 0 & 0 & 0 & 0 & 0 & 0 & 0 \\ 0 & \frac{F_\tau^{\alpha_i}}{H_2} & 0 & 0 & 0 & 0 & 0 & 0 & 0 \\ 0 & 0 & \frac{F_\tau^{\alpha_i}}{H_1} & \frac{F_\tau^{\alpha_i}}{H_2} & 0 & 0 & 0 & 0 & 0 \\ 0 & 0 & 0 & 0 & \frac{F_\tau^{\alpha_i}}{H_1} & 0 & \frac{\partial F_\tau^{\alpha_i}}{\partial \zeta} & 0 & 0 \\ 0 & 0 & 0 & 0 & 0 & \frac{F_\tau^{\alpha_i}}{H_2} & 0 & \frac{\partial F_\tau^{\alpha_i}}{\partial \zeta} & 0 \\ 0 & 0 & 0 & 0 & 0 & 0 & 0 & 0 & \frac{\partial F_\tau^{\alpha_i}}{\partial \zeta} \end{bmatrix} \tag{1.17}$$

1.2.3 Homogenization of the lattice core and equivalent elastic behaviour

Let us now introduce the constitutive elastic relations defining the equivalent behavior of the shells based on an ESL approach and a homogenization procedure. Thus, the elastic relationships both in a static and kinematic sense are consistently supported by relation (1.15), defined in the curvilinear geometric reference system $O'\alpha_1\alpha_2\zeta$. The assessment of the elasticity constants is essentially based on possible material symmetries, which define the so-called material reference system denoted with $O'\hat{\alpha}_1^{(k)}\hat{\alpha}_2^{(k)}\hat{\zeta}^{(k)}$, for the kth lamina. In composite laminates, the outward geometric unit vector $\hat{\zeta}^{(k)}$ for the kth lamina corresponds to the one for the whole structure ζ, in the global geometric reference system [57]. For this reason, a simplified notation can be adopted, such that $O'\hat{\alpha}_1^{(k)}\hat{\alpha}_2^{(k)}\hat{\zeta}^{(k)} = O'\hat{\alpha}_1^{(k)}\hat{\alpha}_2^{(k)}\zeta$. As mentioned before, for a completely anisotropic material in the kth lamina, the constitutive behavior in the material reference system can be expressed as follows

$$\begin{bmatrix} \hat{\sigma}_1^{(k)} \\ \hat{\sigma}_2^{(k)} \\ \hat{\tau}_{12}^{(k)} \\ \hat{\tau}_{13}^{(k)} \\ \hat{\tau}_{23}^{(k)} \\ \hat{\sigma}_3^{(k)} \end{bmatrix} = \begin{bmatrix} C_{11}^{(k)} & C_{12}^{(k)} & C_{16}^{(k)} & C_{14}^{(k)} & C_{15}^{(k)} & C_{13}^{(k)} \\ C_{12}^{(k)} & C_{22}^{(k)} & C_{26}^{(k)} & C_{24}^{(k)} & C_{25}^{(k)} & C_{23}^{(k)} \\ C_{16}^{(k)} & C_{26}^{(k)} & C_{66}^{(k)} & C_{64}^{(k)} & C_{65}^{(k)} & C_{63}^{(k)} \\ C_{14}^{(k)} & C_{24}^{(k)} & C_{64}^{(k)} & C_{44}^{(k)} & C_{45}^{(k)} & C_{43}^{(k)} \\ C_{15}^{(k)} & C_{25}^{(k)} & C_{65}^{(k)} & C_{45}^{(k)} & C_{55}^{(k)} & C_{53}^{(k)} \\ C_{13}^{(k)} & C_{23}^{(k)} & C_{63}^{(k)} & C_{43}^{(k)} & C_{53}^{(k)} & C_{33}^{(k)} \end{bmatrix} \begin{bmatrix} \hat{\varepsilon}_1^{(k)} \\ \hat{\varepsilon}_2^{(k)} \\ \hat{\gamma}_{12}^{(k)} \\ \hat{\gamma}_{13}^{(k)} \\ \hat{\gamma}_{23}^{(k)} \\ \hat{\varepsilon}_3^{(k)} \end{bmatrix} \tag{1.18}$$

where $\hat{\boldsymbol{\sigma}}^{(k)}(\hat{\alpha}_1^{(k)}, \hat{\alpha}_2^{(k)}, \zeta, t)$ and $\hat{\boldsymbol{\varepsilon}}^{(k)}(\hat{\alpha}_1^{(k)}, \hat{\alpha}_2^{(k)}, \zeta, t)$ refer to the 3D stress and strain state for the kth lamina, respectively. The constitutive relation (1.18) can be written in a compact matrix form as [57]

$$\hat{\boldsymbol{\sigma}}^{(k)} = \mathbf{C}^{(k)}\,\hat{\boldsymbol{\varepsilon}}^{(k)} \tag{1.19}$$

where $\mathbf{C}^{(k)}$ stands for the elastic stiffness matrix. When the constitutive equations are written in the geometric reference system, the possible discrepancy in (1.18) between the material symmetry axes and the principal reference system of the shell requires a proper transformation of the material properties with respect to the geometric reference system $O'\alpha_1\alpha_2\zeta$ by means of matrix $\mathbf{T}^{(k)}$. Defining with θ_k the angle between α_1 and $\hat{\alpha}_1^{(k)}$, $\mathbf{T}^{(k)}$ can be written as [57]

$$\mathbf{T}^{(k)} = \begin{bmatrix} \cos^2\theta_k & \sin^2\theta_k & -2\sin\theta_k\cos\theta_k & 0 & 0 & 0 \\ \sin\theta_k & \cos^2\theta_k & 2\sin\theta_k\cos\theta_k & 0 & 0 & 0 \\ \sin\theta_k\cos\theta_k & -\sin\theta_k\cos\theta_k & \cos^2\theta_k - \sin^2\theta_k & 0 & 0 & 0 \\ 0 & 0 & 0 & \cos\theta_k & -\sin\theta_k & 0 \\ 0 & 0 & 0 & \sin\theta_k & \cos\theta_k & 0 \\ 0 & 0 & 0 & 0 & 0 & 1 \end{bmatrix} \tag{1.20}$$

The transformed stiffness matrix $\bar{\mathbf{C}}^{(k)}$ in the reference system $O'\alpha_1\alpha_2\zeta$ is defined as

$$\bar{\mathbf{C}}^{(k)} = \mathbf{T}^{(k)}\mathbf{C}^{(k)}\mathbf{T}^{(k)T} \tag{1.21}$$

or in extended matrix form as [57]

$$\bar{\mathbf{C}}^{(k)} = \begin{bmatrix} \bar{C}_{11}^{(k)} & \bar{C}_{12}^{(k)} & \bar{C}_{16}^{(k)} & \bar{C}_{14}^{(k)} & \bar{C}_{15}^{(k)} & \bar{C}_{13}^{(k)} \\ \bar{C}_{12}^{(k)} & \bar{C}_{22}^{(k)} & \bar{C}_{26}^{(k)} & \bar{C}_{24}^{(k)} & \bar{C}_{25}^{(k)} & \bar{C}_{23}^{(k)} \\ \bar{C}_{16}^{(k)} & \bar{C}_{26}^{(k)} & \bar{C}_{66}^{(k)} & \bar{C}_{64}^{(k)} & \bar{C}_{65}^{(k)} & \bar{C}_{63}^{(k)} \\ \bar{C}_{14}^{(k)} & \bar{C}_{24}^{(k)} & \bar{C}_{64}^{(k)} & \bar{C}_{44}^{(k)} & \bar{C}_{45}^{(k)} & \bar{C}_{43}^{(k)} \\ \bar{C}_{15}^{(k)} & \bar{C}_{25}^{(k)} & \bar{C}_{65}^{(k)} & \bar{C}_{45}^{(k)} & \bar{C}_{55}^{(k)} & \bar{C}_{53}^{(k)} \\ \bar{C}_{13}^{(k)} & \bar{C}_{23}^{(k)} & \bar{C}_{63}^{(k)} & \bar{C}_{43}^{(k)} & \bar{C}_{53}^{(k)} & \bar{C}_{33}^{(k)} \end{bmatrix} \tag{1.22}$$

Thus, the constitutive relation between the 3D stress field $\boldsymbol{\sigma}^{(k)}(\alpha_1, \alpha_2, \zeta, t) = [\sigma_1^{(k)} \ \sigma_2^{(k)} \ \tau_{12}^{(k)} \ \tau_{13}^{(k)} \ \tau_{23}^{(k)} \ \sigma_3^{(k)}]^T$ and the strain field $\boldsymbol{\varepsilon}^{(k)}(\alpha_1, \alpha_2, \zeta, t) = [\varepsilon_1^{(k)} \ \varepsilon_2^{(k)} \ \gamma_{12}^{(k)} \ \gamma_{13}^{(k)} \ \gamma_{23}^{(k)} \ \varepsilon_3^{(k)}]^T$ in the global reference system $O'\alpha_1\alpha_2\zeta$ reads as

$$\boldsymbol{\sigma}^{(k)} = \bar{\mathbf{C}}^{(k)}\boldsymbol{\varepsilon}^{(k)} \quad \text{for} \quad k = 1, 2, \ldots, l \tag{1.23}$$

To define the equivalent elastic constants for a lattice material, we require some homogenization procedures capable of studying a wide range of cell and pantographic grid configurations in a general and efficient manner. The homogenization of a lattice layer made of various orders of ribs can be assessed taking into account the axial contribution of each single rib in the RVE. Namely, some simple load cases must be defined starting from the elastic constants definition (1.18) for the kth lamina, in the material reference system. In addition, each beam contribution to the overall stiffness can be computed for the whole pattern independently from the coupling effects of further stiffeners. As stated by Vasiliev *et al* [6, 7], each rib in a unit cell is very slender in all the configurations of

manufacturing interest, such that the influence of the rigid node zone is not charged with the role of physical constraint for the adjacent area. Therefore, the equivalent elastic properties of each unit cell can be written considering the superimposition of each single beam stiffness in the same reference system. As a consequence, it is convenient to define the single axial contribution assuming that each beam is made of an isotropic medium. This means that we have to define the Young's modulus E_i, density ρ_i and shear modulus G_i, for each ith element, while assuming a global orthotropic behaviour due to the slenderness of the single frame within the cell. If a local reference system $\hat{x}_1^{(i)}\hat{x}_2^{(i)}\hat{x}_3^{(i)}$ is defined for each stiffener along its principal axes, an overall constitutive elastic relationship can be written as

$$\begin{bmatrix} \sigma_1^{(i)} \\ \sigma_2^{(i)} \\ \tau_{12}^{(i)} \\ \tau_{13}^{(i)} \\ \tau_{23}^{(i)} \\ \sigma_3^{(i)} \end{bmatrix} = \begin{bmatrix} C_{11}^{(i)} & C_{12}^{(i)} & C_{16}^{(i)} & 0 & 0 & C_{13}^{(i)} \\ C_{12}^{(i)} & C_{22}^{(i)} & C_{26}^{(i)} & 0 & 0 & C_{23}^{(i)} \\ C_{16}^{(i)} & C_{26}^{(i)} & C_{66}^{(i)} & 0 & 0 & C_{36}^{(i)} \\ 0 & 0 & 0 & C_{44}^{(i)} & C_{45}^{(i)} & 0 \\ 0 & 0 & 0 & C_{45}^{(i)} & C_{55}^{(i)} & 0 \\ C_{13}^{(i)} & C_{23}^{(i)} & C_{36}^{(i)} & 0 & 0 & C_{33}^{(i)} \end{bmatrix} \begin{bmatrix} \varepsilon_1^{(i)} \\ \varepsilon_2^{(i)} \\ \gamma_{12}^{(i)} \\ \gamma_{13}^{(i)} \\ \gamma_{23}^{(i)} \\ \varepsilon_3^{(i)} \end{bmatrix} \tag{1.24}$$

where $\boldsymbol{\sigma}^{(i)}(\hat{x}_1^{(i)}, \hat{x}_2^{(i)}, \hat{x}_3^{(i)}, t) = [\sigma_1^{(i)} \ \sigma_2^{(i)} \ \tau_{12}^{(i)} \ \tau_{13}^{(i)} \ \tau_{23}^{(i)} \ \sigma_3^{(i)}]^T$ and $\boldsymbol{\varepsilon}^{(i)}(\hat{x}_1^{(i)}, \hat{x}_2^{(i)}, \hat{x}_3^{(i)}, t) = [\varepsilon_1^{(i)} \ \varepsilon_2^{(i)} \ \gamma_{12}^{(i)} \ \gamma_{13}^{(i)} \ \gamma_{23}^{(i)} \ \varepsilon_3^{(i)}]^T$ are the stress and strain vector in the local reference system. Nevertheless, the equivalent density ρ of the unit cell can be computed starting from the width of each rib, δ_i, together with the interspace a_i between two adjacent frames characterized by same inclination angle with respect to the α_1-direction. Eventually, one gets

$$\rho = \sum_{i=1}^{n} \rho_i \frac{\delta_i}{a_i} \tag{1.25}$$

with n the number of rib families within the unit pattern. Accounting for the stretching effect acting on each single rib, we define the non-reduced elastic constants of the constitutive relation (1.24) as

$$\begin{aligned} C_{11}^{(i)} &= C_{33}^{(i)} = E_i \\ C_{44}^{(i)} &= G_i = \frac{E_i}{2(1+\nu_i)} \\ C_{22}^{(i)} &= C_{12}^{(i)} = C_{13}^{(i)} = C_{23}^{(i)} = C_{55}^{(i)} = C_{66}^{(i)} = 0 \end{aligned} \tag{1.26}$$

Starting from the orthotropic relation (1.24), the actual contribution of the single frame to the equivalent stiffness of the unit cell can be derived from the application

of a rotation transformation by an angle ϕ_i, which corresponds to the rib inclination with respect to the geometric principal reference direction α_1. Thus, the equivalent elastic properties of a unit cell made of n rib families can be written as

$$
\begin{aligned}
C_{11}^{(k)} &= \sum_{i=1}^{n} E_i \frac{\delta_i}{a_i} \cos^4 \phi_i, & C_{22}^{(k)} &= \sum_{i=1}^{n} E_i \frac{\delta_i}{a_i} \sin^4 \phi_i, \\
C_{12}^{(k)} &= C_{66}^{(k)} = \sum_{i=1}^{n} E_i \frac{\delta_i}{a_i} \sin^2 \phi_i \cos^2 \phi_i, & C_{16}^{(k)} &= \sum_{i=1}^{n} E_i \frac{\delta_i}{a_i} \cos^3 \phi_i \sin \phi_i, \\
C_{26}^{(k)} &= \sum_{i=1}^{n} E_i \frac{\delta_i}{a_i} \cos \phi_i \sin^3 \phi_i, & C_{44}^{(k)} &= \sum_{i=1}^{n} G_i \frac{\delta_i}{a_i} \cos^2 \phi_i, \\
C_{45}^{(k)} &= \sum_{i=1}^{n} G_i \frac{\delta_i}{a_i} \cos \phi_i \sin \phi_i, & C_{55}^{(k)} &= \sum_{i=1}^{n} G_i \frac{\delta_i}{a_i} \sin^2 \phi_i, \\
C_{33}^{(k)} &= \sum_{i=1}^{n} E_i \frac{\delta_i}{a_i}, & C_{13}^{(k)} &= C_{23}^{(k)} = C_{36}^{(k)} = 0
\end{aligned}
\tag{1.27}
$$

Hereafter we introduce the following effective notation to identify the main properties of a unit cell

$$
\mathrm{S/F}\left[(\phi_i)_a^{\delta}\right] \quad i = 1, \ldots, n \tag{1.28}
$$

where (S) and (F) refer to the star and flake pattern configuration, respectively, depending on the number of rigid nodes in the RVE; n is the number of rib families, and angle ϕ_i refers to the ith frame family.

For a laminated structure with a latticed softcore, different elastic properties can be determined, depending on the cellular geometry of the unit pattern. This means that it is possible to obtain a large variety of elastic performances by simply tailoring the geometric parameters even for an isotropic medium implementation. More specifically, the overall properties of a lattice cell unit are mainly related to the wall slenderness determined by the following dimensionless parameters

$$
\alpha = \frac{s_2}{l}, \quad \beta = \frac{s}{l}, \quad \gamma = \frac{b}{l} \tag{1.29}
$$

A schematic representation of the geometric quantities that defines a honeycomb cell can be found in figure 1.2. Each unit cell is intended to be made of an isotropic medium with bulk density ρ_s, Young modulus E_s, Poisson's ratio ν_s, and shear stiffness $G_s = E_s/(2(1 + \nu_s))$.

To account for the geometric characteristics of a lattice honeycomb cell, the following nomenclature can be introduced

$$
\mathrm{H} \;\; c/C \;\; \vartheta \;\; (l, l_2, \; s) \tag{1.30}
$$

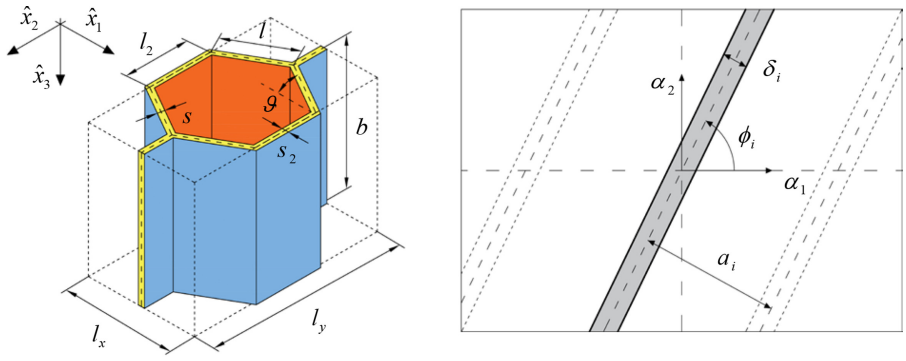

Figure 1.2. Lattice core grid patterns. (a) Honeycomb cell, (b) Frame infill.

where c/C stands for a classic ($s_2 = s$) or commercial ($s_2 = 2s$) geometric layup. These two cell configurations refer to lattices obtained by two different manufacturing processes. In detail, a commercial cell configuration features a double thickness vertical wall, since it comes out from the juxtaposition of two corrugated sheets. The geometric parameters of the honeycomb cell are reported in figure 1.2 for the sake of clarity. Generally speaking, according to [24], a general cellular material can be modelled as an equivalent orthotropic continuum, where a homogenization procedure should express the unit cell elasticity by means of the engineering constants. In such a context, a local material reference system is defined, as visible in figure 1.2, where the local axis $\hat{x}_1$ is taken perpendicularly to the vertical cell wall, $\hat{x}_2$ is parallel to the same ribbon, and $\hat{x}_3$ coincides with the opposite of the outward unit vector $\mathbf{n}(\alpha_1, \alpha_2)$ of the shell defined in (1.3), so that a right-handed system is obtained. Equivalent elastic properties of the honeycomb cell consider the in-plane moduli E_1 and E_2 in the $\hat{x}_1$ and $\hat{x}_2$ directions, respectively, the shear modulus G_{12}, the stretching stiffness E_3, the out-of-plane shear moduli G_{13} and G_{23}, together with the Poisson's ratios ν_{12}, ν_{21}, ν_{13}, ν_{31}, ν_{23} and ν_{32}. In what follows, the equivalent density of the cell is determined as proposed by Gibson and Ashby [24], namely

$$\rho = \frac{A_s}{A} = \rho_s \frac{\beta(\alpha + 2)}{2\cos\vartheta(\alpha + \sin\vartheta)} \tag{1.31}$$

where A_s is the effective area of the cell and A its bulk value. At the same time, the elastic moduli are determined as proposed by Sorohan *et al* [34]

$$E_1 = k_1 E_s \beta^3 \frac{\cos\vartheta}{(\alpha + \sin\vartheta)\sin^2\vartheta}, \quad E_2 = k_2 E_s \beta^3 \frac{\alpha + \sin\vartheta}{\cos^3\vartheta}, \quad E_3 = E_s \frac{\rho}{\rho_s} \tag{1.32}$$

and the equivalent shear stiffnesses are defined as

$$G_{12} = k_{12} E_s \beta^3 \frac{\alpha + \sin\vartheta}{\alpha^2(1 + 2\alpha)\cos\vartheta}, \quad G_{13} = G_s \beta \frac{\cos\vartheta}{\alpha + \sin\vartheta} \tag{1.33}$$

with

$$
\begin{aligned}
k_1 &= \frac{1}{1+\beta^2(2.4+1.5\nu_s+\cot^2\vartheta)} \\
k_2 &= \frac{1}{1+\beta^2\left(2.4+1.5\nu_s+\tan^2\vartheta+\dfrac{2\alpha}{\cos^2\vartheta}\right)} \\
k_{12} &= \frac{1+2\alpha}{1+2\alpha+\beta^2\left(\dfrac{2.4+1.5\nu_s}{\alpha}(2+\alpha+\sin\vartheta)\right.} \\
&\quad \left.+\frac{\alpha+\sin\vartheta}{\alpha^2}((\alpha+\sin\vartheta)\tan^2\vartheta+\sin\vartheta)\right)
\end{aligned}
\tag{1.34}
$$

Moreover, the in-plane Poisson's ratios are computed as

$$
v_{12} = c_{12}\frac{\cos^2\vartheta}{(\alpha+\sin\vartheta)\sin\vartheta}, \qquad v_{21} = c_{21}\frac{(\alpha+\sin\vartheta)\sin\vartheta}{\cos^2\vartheta} \tag{1.35}
$$

The out-of-plane transverse deformation coefficients are calculated taking into account the symmetry of the stiffness matrix (1.18) of the homogenized material

$$
\begin{aligned}
\nu_{13} &= \frac{E_1}{E_s}\nu_s, \qquad \nu_{31} = \nu_s \\
\nu_{23} &= \frac{E_2}{E_s}\nu_s, \qquad \nu_{32} = \nu_s
\end{aligned}
\tag{1.36}
$$

In addition, the shear modulus G_{23} follows the approach by Kelsey *et al* [28] based on the minimum potential energy's principle, for which an upper-bound value G_{23}^U and a lower-bound value G_{23}^L can be computed as

$$
G_{23}^U = G_s\beta\frac{\alpha+\sin^2\vartheta}{(\alpha+\sin\vartheta)\cos\vartheta} \tag{1.37}
$$

$$
G_{23}^L = G_s\beta\frac{\alpha+\sin\vartheta}{(1+\alpha)\cos\vartheta} \tag{1.38}
$$

where G_s is the shear modulus of the constituent material. On the other hand, the linear interpolation procedure proposed by Grediac [29] between extreme values G_{23}^U and G_{23}^L has been demonstrated to be inadequate for re-entrant cells, and it is reliable only for a limited type of cell configurations [30, 39]. Due to this limitation, as highlighted in the work by Fu and Yin [35], we apply the following interpolation formula

$$
G_{23} = G_{23}^L + \frac{A\gamma}{B\gamma^2+C}(G_{23}^U - G_{23}^L) \tag{1.39}
$$

where $A = 2/5$, $B = 3/4$ and $C = 1/4$ are some calibrated constants. It is worth noticing that the interpolation (1.39) fits Torabi's formula [36], when $\gamma \to 0.5$, whereas for $\gamma \to 10$ a lower bound value of shear modulus is steadily reached.

An ESL model is developed hereafter, such that the three-dimensional constitutive relation (1.23) is computed for each single layer of the lamination scheme. Based on the kinematic assumptions (1.7), we must consider the strain field coming from the adopted thickness functions matrix $\mathbf{F}_\tau = \mathbf{F}_\tau(\zeta)$ for each τth order of expansion. Nevertheless, a generalized stress component vector $\mathbf{S}^{(\tau)\alpha_i}(\alpha_1, \alpha_2, t) = [N_1^{(\tau)\alpha_i} \;\; N_2^{(\tau)\alpha_i} \;\; N_{12}^{(\tau)\alpha_i} \;\; N_{21}^{(\tau)\alpha_i} \;\; T_1^{(\tau)\alpha_i} \;\; T_2^{(\tau)\alpha_i} \;\; P_1^{(\tau)\alpha_i} \;\; P_2^{(\tau)\alpha_i} \;\; S_3^{(\tau)\alpha_i}]^T$ must be defined for each unknown variable order of the displacement field, by computing all the stress components along the thickness coordinate ζ, while keeping in mind the presence of possible coupling effects, due to the anisotropic behavior. In addition, the equivalent constitutive relation must account for the interlaminar phenomena. In this way, the ESL generalized strain component vector $\boldsymbol{\varepsilon}^{(\tau)\alpha_i}(\alpha_1, \alpha_2, t)$ is directly related to $\mathbf{S}^{(\tau)\alpha_i}(\alpha_1, \alpha_2, t)$ thanks to a generalized constitutive matrix. A formulation independent from the thickness coordinate is obtained, since ζ is computed in the definition of equivalent elastic and kinematic quantities. Based on the equivalence between the actual elastic strain energy and the homogenized one, the generalized anisotropic ESL Hooke's relation comes out [57]

$$\mathbf{S}^{(\tau)\alpha_i} = \sum_{\eta=0}^{N+1} \sum_{j=1}^{3} \mathbf{A}^{(\tau\eta)\alpha_i\alpha_j} \boldsymbol{\varepsilon}^{(\eta)\alpha_j} \quad \text{for} \quad \tau = 0, 1, 2, \ldots, N, N+1, \alpha_i = \alpha_1, \alpha_2, \alpha_3 \tag{1.40}$$

where the generalized elastic matrix $\mathbf{A}^{(\tau\eta)\alpha_i\alpha_j}$, for $\tau = 0, 1, 2, \ldots, N, N+1$ and $\alpha_i = \alpha_1, \alpha_2, \alpha_3$ reads as follows

$$\mathbf{A}^{(\tau\eta)\alpha_i\alpha_j} = \left[\begin{array}{ccccccc|ccc}
A_{11(20)}^{(\tau\eta)[00]\alpha_i\alpha_j} & A_{12(11)}^{(\tau\eta)[00]\alpha_i\alpha_j} & A_{16(20)}^{(\tau\eta)[00]\alpha_i\alpha_j} & A_{16(11)}^{(\tau\eta)[00]\alpha_i\alpha_j} & A_{14(20)}^{(\tau\eta)[00]\alpha_i\alpha_j} & A_{14(20)}^{(\tau\eta)[00]\alpha_i\alpha_j} & A_{15(11)}^{(\tau\eta)[00]\alpha_i\alpha_j} & A_{14(10)}^{(\tau\eta)[01]\alpha_i\alpha_j} & A_{15(10)}^{(\tau\eta)[01]\alpha_i\alpha_j} & A_{13(10)}^{(\tau\eta)[01]\alpha_i\alpha_j} \\
A_{12(11)}^{(\tau\eta)[00]\alpha_i\alpha_j} & A_{22(02)}^{(\tau\eta)[00]\alpha_i\alpha_j} & A_{26(11)}^{(\tau\eta)[00]\alpha_i\alpha_j} & A_{26(02)}^{(\tau\eta)[00]\alpha_i\alpha_j} & A_{24(11)}^{(\tau\eta)[00]\alpha_i\alpha_j} & A_{25(02)}^{(\tau\eta)[00]\alpha_i\alpha_j} & A_{24(01)}^{(\tau\eta)[01]\alpha_i\alpha_j} & A_{25(01)}^{(\tau\eta)[01]\alpha_i\alpha_j} & A_{23(01)}^{(\tau\eta)[01]\alpha_i\alpha_j} \\
A_{16(20)}^{(\tau\eta)[00]\alpha_i\alpha_j} & A_{26(11)}^{(\tau\eta)[00]\alpha_i\alpha_j} & A_{66(20)}^{(\tau\eta)[00]\alpha_i\alpha_j} & A_{66(11)}^{(\tau\eta)[00]\alpha_i\alpha_j} & A_{46(20)}^{(\tau\eta)[00]\alpha_i\alpha_j} & A_{56(11)}^{(\tau\eta)[00]\alpha_i\alpha_j} & A_{46(10)}^{(\tau\eta)[01]\alpha_i\alpha_j} & A_{56(10)}^{(\tau\eta)[01]\alpha_i\alpha_j} & A_{36(10)}^{(\tau\eta)[01]\alpha_i\alpha_j} \\
A_{16(11)}^{(\tau\eta)[00]\alpha_i\alpha_j} & A_{26(02)}^{(\tau\eta)[00]\alpha_i\alpha_j} & A_{66(11)}^{(\tau\eta)[00]\alpha_i\alpha_j} & A_{66(02)}^{(\tau\eta)[00]\alpha_i\alpha_j} & A_{46(11)}^{(\tau\eta)[00]\alpha_i\alpha_j} & A_{56(02)}^{(\tau\eta)[00]\alpha_i\alpha_j} & A_{46(01)}^{(\tau\eta)[01]\alpha_i\alpha_j} & A_{56(01)}^{(\tau\eta)[01]\alpha_i\alpha_j} & A_{36(01)}^{(\tau\eta)[01]\alpha_i\alpha_j} \\
A_{14(20)}^{(\tau\eta)[00]\alpha_i\alpha_j} & A_{24(11)}^{(\tau\eta)[00]\alpha_i\alpha_j} & A_{46(20)}^{(\tau\eta)[00]\alpha_i\alpha_j} & A_{46(11)}^{(\tau\eta)[00]\alpha_i\alpha_j} & A_{44(20)}^{(\tau\eta)[00]\alpha_i\alpha_j} & A_{45(11)}^{(\tau\eta)[00]\alpha_i\alpha_j} & A_{44(10)}^{(\tau\eta)[01]\alpha_i\alpha_j} & A_{45(10)}^{(\tau\eta)[01]\alpha_i\alpha_j} & A_{34(10)}^{(\tau\eta)[01]\alpha_i\alpha_j} \\
A_{15(11)}^{(\tau\eta)[00]\alpha_i\alpha_j} & A_{25(02)}^{(\tau\eta)[00]\alpha_i\alpha_j} & A_{56(11)}^{(\tau\eta)[00]\alpha_i\alpha_j} & A_{56(02)}^{(\tau\eta)[00]\alpha_i\alpha_j} & A_{45(11)}^{(\tau\eta)[00]\alpha_i\alpha_j} & A_{55(02)}^{(\tau\eta)[00]\alpha_i\alpha_j} & A_{45(01)}^{(\tau\eta)[01]\alpha_i\alpha_j} & A_{55(01)}^{(\tau\eta)[01]\alpha_i\alpha_j} & A_{35(01)}^{(\tau\eta)[01]\alpha_i\alpha_j} \\
\hline
A_{14(10)}^{(\tau\eta)[10]\alpha_i\alpha_j} & A_{24(01)}^{(\tau\eta)[10]\alpha_i\alpha_j} & A_{46(10)}^{(\tau\eta)[10]\alpha_i\alpha_j} & A_{46(01)}^{(\tau\eta)[10]\alpha_i\alpha_j} & A_{44(10)}^{(\tau\eta)[10]\alpha_i\alpha_j} & A_{45(01)}^{(\tau\eta)[10]\alpha_i\alpha_j} & A_{44(00)}^{(\tau\eta)[11]\alpha_i\alpha_j} & A_{45(00)}^{(\tau\eta)[11]\alpha_i\alpha_j} & A_{34(00)}^{(\tau\eta)[11]\alpha_i\alpha_j} \\
A_{15(10)}^{(\tau\eta)[10]\alpha_i\alpha_j} & A_{25(01)}^{(\tau\eta)[10]\alpha_i\alpha_j} & A_{56(10)}^{(\tau\eta)[10]\alpha_i\alpha_j} & A_{56(01)}^{(\tau\eta)[10]\alpha_i\alpha_j} & A_{45(10)}^{(\tau\eta)[10]\alpha_i\alpha_j} & A_{55(01)}^{(\tau\eta)[10]\alpha_i\alpha_j} & A_{45(00)}^{(\tau\eta)[11]\alpha_i\alpha_j} & A_{55(00)}^{(\tau\eta)[11]\alpha_i\alpha_j} & A_{35(00)}^{(\tau\eta)[11]\alpha_i\alpha_j} \\
A_{13(10)}^{(\tau\eta)[10]\alpha_i\alpha_j} & A_{23(01)}^{(\tau\eta)[10]\alpha_i\alpha_j} & A_{36(10)}^{(\tau\eta)[10]\alpha_i\alpha_j} & A_{36(01)}^{(\tau\eta)[10]\alpha_i\alpha_j} & A_{34(10)}^{(\tau\eta)[10]\alpha_i\alpha_j} & A_{35(01)}^{(\tau\eta)[10]\alpha_i\alpha_j} & A_{34(00)}^{(\tau\eta)[11]\alpha_i\alpha_j} & A_{35(00)}^{(\tau\eta)[11]\alpha_i\alpha_j} & A_{33(00)}^{(\tau\eta)[11]\alpha_i\alpha_j}
\end{array}\right] \tag{1.41}$$

As visible in (1.41), the stiffness matrix is conveniently split into blocks in order to collect the zeroth and first order derivatives of $\mathbf{F}_\tau$ components with respect to ζ. The definition of all the terms of $\mathbf{A}^{(\tau\eta)\alpha_i\alpha_j}$ is strictly related to the basic material assumptions. Generally speaking, we employ the three-dimensional constitutive coefficients $\bar{C}_{nm}^{(k)}$ with $n, m = 1, \ldots 6$, which are redefined as reduced elastic constants

$\bar{Q}_{nm}^{(k)}$, under in-plane stress assumptions. Moreover, by assuming a linear shape function throughout the thickness, for the in-plane displacement field, we introduce the well-known shear correction factor $\kappa(\zeta) = 5/6$ [49, 50], such that the equivalent elastic constants for the homogenized material $\bar{B}_{nm}^{(k)}$ take the following form [57]

$$\bar{B}_{nm}^{(k)} = \begin{cases} \bar{E}_{nm}^{(k)} & \text{for} \quad n, m = 1, 2, 3, 6 \\ \kappa(\zeta)\bar{E}_{nm}^{(k)} & \text{for} \quad n, m = 4, 5 \end{cases} \tag{1.42}$$

where $\bar{E}_{nm}^{(k)} = \bar{C}_{nm}^{(k)}$ or $\bar{E}_{nm}^{(k)} = \bar{Q}_{nm}^{(k)}$, in agreement with the stress state hypotheses.

Thus, an effective expression for each generalized elastic constant of (1.41) is summarized as follows [57]

$$\begin{aligned} & A_{nm(pq)}^{(\tau\eta)[fg]\alpha_i\alpha_j} = \sum_{k=1}^{l} \int_{\zeta_k}^{\zeta_{k+1}} \bar{B}_{nm}^{(k)} \frac{\partial^f F_\eta^{\alpha_j}}{\partial \zeta^f} \frac{\partial^g F_\tau^{\alpha_i}}{\partial \zeta^g} \frac{H_1 H_2}{H_1^p H_2^q} d\zeta && \text{for } \tau, \eta = 0, 1, 2, \ldots, N, N+1 \\ & && \text{for } n, m = 1, 2, 3, 4, 5, 6 \\ & && \text{for } p, q = 0, 1, 2 \\ & \frac{\partial^0 F_\tau^{\alpha_i}}{\partial \zeta^0} = F_\tau^{\alpha_i}, \quad \frac{\partial^0 F_\eta^{\alpha_j}}{\partial \zeta^0} = F_\eta^{\alpha_j} && \text{for } \alpha_i, \alpha_j = \alpha_1, \alpha_2, \alpha_3 \\ & && \text{for } f, g = 0, 1 \end{aligned} \tag{1.43}$$

1.2.4 Governing equations

We determine now the fundamental equations of motion for shells with a lattice core, in an ESL setting. These equations are written taking into account the elastic strain energy and inertial contribution of the structure, to solve a dynamic eigenvalue problem. The dynamic equilibrium can be computed from the Hamiltonian Principle in its variational form [57] within a time interval $[t_1, t_2]$

$$\delta \int_{t_1}^{t_2} (T - \Phi) dt = 0 \quad \rightarrow \quad \int_{t_1}^{t_2} (\delta T - \delta \Phi) dt = 0 \tag{1.44}$$

with T the kinetic energy and Φ the shell elastic strain energy. Based on the ESL approach, we account for the thickness functions set (1.7), while defining a differential operator $\mathbf{D}_\Omega^{*\alpha_i}$ for each direction in the reference system $\alpha_1, \alpha_2, \alpha_3$

$$\mathbf{D}_\Omega^{*\alpha_1} = \begin{bmatrix} \left(\mathbf{D}_\Omega^{*\alpha_1}\right)_{11} & \left(\mathbf{D}_\Omega^{*\alpha_1}\right)_{12} & \left(\mathbf{D}_\Omega^{*\alpha_1}\right)_{13} & \left(\mathbf{D}_\Omega^{*\alpha_1}\right)_{14} & \left(\mathbf{D}_\Omega^{*\alpha_1}\right)_{15} & \left(\mathbf{D}_\Omega^{*\alpha_1}\right)_{16} & \left(\mathbf{D}_\Omega^{*\alpha_1}\right)_{17} & \left(\mathbf{D}_\Omega^{*\alpha_1}\right)_{18} & \left(\mathbf{D}_\Omega^{*\alpha_1}\right)_{19} \\ 0 & 0 & 0 & 0 & 0 & 0 & 0 & 0 & 0 \\ 0 & 0 & 0 & 0 & 0 & 0 & 0 & 0 & 0 \end{bmatrix} \tag{1.45}$$

$$\mathbf{D}_\Omega^{*\alpha_2} = \begin{bmatrix} 0 & 0 & 0 & 0 & 0 & 0 & 0 & 0 & 0 \\ \left(\mathbf{D}_\Omega^{*\alpha_2}\right)_{21} & \left(\mathbf{D}_\Omega^{*\alpha_2}\right)_{22} & \left(\mathbf{D}_\Omega^{*\alpha_2}\right)_{23} & \left(\mathbf{D}_\Omega^{*\alpha_2}\right)_{24} & \left(\mathbf{D}_\Omega^{*\alpha_2}\right)_{25} & \left(\mathbf{D}_\Omega^{*\alpha_2}\right)_{26} & \left(\mathbf{D}_\Omega^{*\alpha_2}\right)_{27} & \left(\mathbf{D}_\Omega^{*\alpha_2}\right)_{28} & \left(\mathbf{D}_\Omega^{*\alpha_2}\right)_{29} \\ 0 & 0 & 0 & 0 & 0 & 0 & 0 & 0 & 0 \end{bmatrix} \tag{1.46}$$

$$\mathbf{D}_{\Omega}^{*\alpha\,3} = \begin{bmatrix} 0 & 0 & 0 & 0 & 0 & 0 & 0 & 0 & 0 \\ 0 & 0 & 0 & 0 & 0 & 0 & 0 & 0 & 0 \\ (\mathbf{D}_{\Omega}^{*\alpha\,3})_{31} & (\mathbf{D}_{\Omega}^{*\alpha\,3})_{32} & (\mathbf{D}_{\Omega}^{*\alpha\,3})_{33} & (\mathbf{D}_{\Omega}^{*\alpha\,3})_{34} & (\mathbf{D}_{\Omega}^{*\alpha\,3})_{35} & (\mathbf{D}_{\Omega}^{*\alpha\,3})_{36} & (\mathbf{D}_{\Omega}^{*\alpha\,3})_{37} & (\mathbf{D}_{\Omega}^{*\alpha\,3})_{38} & (\mathbf{D}_{\Omega}^{*\alpha\,3})_{39} \end{bmatrix} \tag{1.47}$$

The equilibrium equations can be written in terms of generalized stress resultants $\mathbf{S}^{(\tau)\alpha_i}(\alpha_1, \alpha_2, t)$ and generalized displacement field $\mathbf{u}^{(\tau)}(\alpha_1, \alpha_2, t)$ located on the reference surface, for each τth order of expansion, namely

$$\sum_{i=1}^{3} \mathbf{D}_{\Omega}^{*\alpha\,i} \mathbf{S}^{(\tau)\alpha\,i} = \sum_{\eta=0}^{N+1} \mathbf{M}^{(\tau\eta)} \ddot{\mathbf{u}}^{(\eta)} \quad \text{for} \quad \tau = 0, 1, 2, \ldots, N, N+1 \tag{1.48}$$

The inertial shell properties are collected in the τth order generalized mass matrix $\mathbf{M}^{(\tau\eta)}$

$$\mathbf{M}^{(\tau\eta)} = \begin{bmatrix} I^{(\tau\eta)\alpha\,1\alpha\,1} & 0 & 0 \\ 0 & I^{(\tau\eta)\alpha\,2\alpha\,2} & 0 \\ 0 & 0 & I^{(\tau\eta)\alpha\,3\alpha\,3} \end{bmatrix} \quad \text{for} \quad \tau, \eta = 0, 1, 2, \ldots, N, N+1 \tag{1.49}$$

where the mass matrix terms $I^{(\tau\eta)\alpha\,i\alpha\,j}$ in each principal direction are defined as [57]

$$I^{(\tau\eta)\alpha\,i\alpha\,j} = \sum_{k=1}^{l} \int_{\zeta_k}^{\zeta_{k+1}} \rho^{(k)} F_{\tau}^{\alpha\,i} F_{\eta}^{\alpha\,j} H_1 H_2 d\zeta \qquad \text{for} \quad \alpha_i, \alpha_j = \alpha_1, \alpha_2, \alpha_3 \tag{1.50}$$

accounting for the weight distribution along the shell thickness. On the other hand, the differential operators in (1.45)–(1.47) are defined as

$$\begin{aligned}
(\mathbf{D}_{\Omega}^{*\alpha\,1})_{11} = (\mathbf{D}_{\Omega}^{*\alpha\,2})_{23} = (\mathbf{D}_{\Omega}^{*\alpha\,3})_{35} &= \frac{1}{A_1}\frac{\partial}{\partial\alpha_1} + \frac{1}{A_1 A_2}\frac{\partial A_2}{\partial\alpha_1}, \\
(\mathbf{D}_{\Omega}^{*\alpha\,1})_{12} = -(\mathbf{D}_{\Omega}^{*\alpha\,2})_{24} &= -\frac{1}{A_1 A_2}\frac{\partial A_2}{\partial\alpha_1}, \\
(\mathbf{D}_{\Omega}^{*\alpha\,1})_{14} = (\mathbf{D}_{\Omega}^{*\alpha\,2})_{22} = (\mathbf{D}_{\Omega}^{*\alpha\,3})_{36} &= \frac{1}{A_2}\frac{\partial}{\partial\alpha_2} + \frac{1}{A_1 A_2}\frac{\partial A_1}{\partial\alpha_2}, \\
(\mathbf{D}_{\Omega}^{*\alpha\,1})_{13} = -(\mathbf{D}_{\Omega}^{*\alpha\,2})_{21} &= \frac{1}{A_1 A_2}\frac{\partial A_1}{\partial\alpha_2}, \\
(\mathbf{D}_{\Omega}^{*\alpha\,1})_{17} = (\mathbf{D}_{\Omega}^{*\alpha\,2})_{28} = (\mathbf{D}_{\Omega}^{*\alpha\,3})_{39} &= -1, \\
(\mathbf{D}_{\Omega}^{*\alpha\,1})_{15} = -(\mathbf{D}_{\Omega}^{*\alpha\,3})_{31} &= \frac{1}{R_1}, \\
(\mathbf{D}_{\Omega}^{*\alpha\,1})_{16} = (\mathbf{D}_{\Omega}^{*\alpha\,1})_{18} = (\mathbf{D}_{\Omega}^{*\alpha\,1})_{19} &= 0, \\
(\mathbf{D}_{\Omega}^{*\alpha\,2})_{26} = -(\mathbf{D}_{\Omega}^{*\alpha\,3})_{32} &= \frac{1}{R_2}, \\
(\mathbf{D}_{\Omega}^{*\alpha\,3})_{33} = (\mathbf{D}_{\Omega}^{*\alpha\,3})_{34} = (\mathbf{D}_{\Omega}^{*\alpha\,3})_{37} = (\mathbf{D}_{\Omega}^{*\alpha\,3})_{38} &= 0 \\
(\mathbf{D}_{\Omega}^{*\alpha\,2})_{25} = (\mathbf{D}_{\Omega}^{*\alpha\,2})_{27} = (\mathbf{D}_{\Omega}^{*\alpha\,2})_{29} &= 0,
\end{aligned} \tag{1.51}$$

If the generalized stress resultants $\mathbf{S}^{(\tau)\alpha_i}$ in (1.48) are expressed in terms of generalized strain resultants $\boldsymbol{\varepsilon}^{(\tau)\alpha_i}$ via the anisotropic Hooke's law (1.40) and ESL approach, it is possible to define the equilibrium problem directly by means of the kinematic primary unknowns $\mathbf{u}^{(\eta)}(\alpha_1, \alpha_2, t) = [u_1^{(\eta)}\ u_2^{(\eta)}\ u_3^{(\eta)}]^T$ with $\eta = 0, \ldots, N+1$. Taking into account the definition (1.16) of the strain component vector $\boldsymbol{\varepsilon}^{(\tau)\alpha_i}$ for each principal direction $\alpha_i = \alpha_1, \alpha_2, \alpha_3$ coming from relations (1.15), the fundamental equations are derived for a doubly-curved shell with a generally-oriented lattice core [57]

$$\sum_{\eta=0}^{N+1} \mathbf{L}^{(\tau\eta)}\mathbf{u}^{(\eta)} = \sum_{\eta=0}^{N+1} \mathbf{M}^{(\tau\eta)}\ddot{\mathbf{u}}^{(\eta)} \qquad \text{for} \quad \tau = 0, 1, 2, \ldots, N, N+1 \tag{1.52}$$

where

$$\mathbf{L}^{(\tau\eta)} = \sum_{i=1}^{3}\sum_{j=1}^{3} \mathbf{D}_{\Omega}^{*\alpha_i}\mathbf{A}^{(\tau\eta)\alpha_i\alpha_j}\mathbf{D}_{\Omega}^{\alpha_j} = \begin{bmatrix} L_{11}^{(\tau\eta)\alpha_1\alpha_1} & L_{12}^{(\tau\eta)\alpha_1\alpha_2} & L_{13}^{(\tau\eta)\alpha_1\alpha_3} \\ L_{21}^{(\tau\eta)\alpha_2\alpha_1} & L_{22}^{(\tau\eta)\alpha_2\alpha_2} & L_{23}^{(\tau\eta)\alpha_2\alpha_3} \\ L_{31}^{(\tau\eta)\alpha_3\alpha_1} & L_{32}^{(\tau\eta)\alpha_3\alpha_2} & L_{33}^{(\tau\eta)\alpha_3\alpha_3} \end{bmatrix} \tag{1.53}$$

and $\tau, \eta = 0, \ldots, N+1$.

The fundamental equation (1.52) can be written in extended form as

$$\begin{bmatrix} \mathbf{L}^{(00)} & \mathbf{L}^{(01)} & \cdots & \cdots & \mathbf{L}^{(0(N))} & \mathbf{L}^{(0(N+1))} \\ \mathbf{L}^{(10)} & \mathbf{L}^{(11)} & \cdots & \cdots & \mathbf{L}^{(1(N))} & \mathbf{L}^{(1(N+1))} \\ \vdots & \vdots & \ddots & & \vdots & \vdots \\ \vdots & \vdots & & \ddots & \vdots & \vdots \\ \mathbf{L}^{((N)0)} & \mathbf{L}^{((N)1)} & \cdots & \cdots & \mathbf{L}^{((N)(N))} & \mathbf{L}^{((N)(N+1))} \\ \mathbf{L}^{((N+1)0)} & \mathbf{L}^{((N+1)1)} & \cdots & \cdots & \mathbf{L}^{((N+1)(N))} & \mathbf{L}^{((N+1)(N+1))} \end{bmatrix} \begin{bmatrix} \mathbf{u}^{(0)} \\ \mathbf{u}^{(1)} \\ \vdots \\ \vdots \\ \mathbf{u}^{(N)} \\ \mathbf{u}^{(N+1)} \end{bmatrix} =$$
$$= \begin{bmatrix} \mathbf{M}^{(00)} & \mathbf{M}^{(01)} & \cdots & \cdots & \mathbf{M}^{(0(N))} & \mathbf{M}^{(0(N+1))} \\ \mathbf{M}^{(10)} & \mathbf{M}^{(11)} & \cdots & \cdots & \mathbf{M}^{(1(N))} & \mathbf{M}^{(1(N+1))} \\ \vdots & \vdots & \ddots & & \vdots & \vdots \\ \vdots & \vdots & & \ddots & \vdots & \vdots \\ \mathbf{M}^{((N)0)} & \mathbf{M}^{((N)1)} & \cdots & \cdots & \mathbf{M}^{((N)(N))} & \mathbf{M}^{((N)(N+1))} \\ \mathbf{M}^{((N+1)0)} & ((N+1)1) & \cdots & \cdots & \mathbf{M}^{((N+1)(N))} & \mathbf{M}^{((N+1)(N+1))} \end{bmatrix} \begin{bmatrix} \ddot{\mathbf{u}}^{(0)} \\ \ddot{\mathbf{u}}^{(1)} \\ \vdots \\ \vdots \\ \ddot{\mathbf{u}}^{(N)} \\ \ddot{\mathbf{u}}^{(N+1)} \end{bmatrix} \tag{1.54}$$

The complete expressions of the fundamental coefficients can be found in [57].

For a free vibration study of doubly-curved shell, we select an harmonic solution for the fundamental equation (1.52), such that the unknown vector $\mathbf{u}^{(\tau)} = [u_1^{(\tau)}\ u_2^{(\tau)}\ u_3^{(\tau)}]^T$ is described in terms of the mode shape $\mathbf{U}^{(\tau)} = [U_1^{(\tau)}(\alpha_1, \alpha_2)\ \ U_2^{(\tau)}(\alpha_1, \alpha_2)\ \ U_3^{(\tau)}(\alpha_1, \alpha_2)]^T$ and the corresponding circular frequency $\omega = 2\pi f$ as

$$\mathbf{u}^{(\tau)}(\alpha_1, \alpha_2, t) = \mathbf{U}^{(\tau)}(\alpha_1, \alpha_2)e^{i\omega t} \tag{1.55}$$

It is worth remembering that the $(N+1)$th expansion order is embedded in the model if we adopt the Murakami's strategy (1.9) for describing possible interlaminar

effects, otherwise the maximum order is equal to N. Thus, the free vibration equations can be set as [57]

$$\sum_{\eta=0}^{N+1} \mathbf{L}^{(\tau\eta)}\mathbf{U}^{(\eta)} + \omega^2 \sum_{\eta=0}^{N+1} \mathbf{M}^{(\tau\eta)}\mathbf{U}^{(\eta)} = \mathbf{0} \qquad \text{for} \quad \tau = 0,\, 1,\, 2,\, \ldots,\, N,\, N+1 \tag{1.56}$$

For the definition of the external boundary constraints, it is useful to express the generalized stress resultants set $\mathbf{S}^{(\tau)\alpha_i}$ in terms of the DOFs of (1.52), taking into account the constitutive elastic relation (1.40), as well as the compatibility equation (1.16), i.e.

$$\begin{bmatrix} N_1^{(\tau)\alpha_i} \\ N_2^{(\tau)\alpha_i} \\ N_{12}^{(\tau)\alpha_i} \\ N_{21}^{(\tau)\alpha_i} \\ T_1^{(\tau)\alpha_i} \\ T_2^{(\tau)\alpha_i} \\ P_1^{(\tau)\alpha_i} \\ P_2^{(\tau)\alpha_i} \\ S_3^{(\tau)\alpha_i} \end{bmatrix} = \sum_{\eta=0}^{N+1} \begin{bmatrix} O_{11}^{(\tau\eta)\alpha_i\alpha_1} & O_{21}^{(\tau\eta)\alpha_i\alpha_2} & O_{31}^{(\tau\eta)\alpha_i\alpha_3} \\ O_{12}^{(\tau\eta)\alpha_i\alpha_1} & O_{22}^{(\tau\eta)\alpha_i\alpha_2} & O_{32}^{(\tau\eta)\alpha_i\alpha_3} \\ O_{13}^{(\tau\eta)\alpha_i\alpha_1} & O_{23}^{(\tau\eta)\alpha_i\alpha_2} & O_{33}^{(\tau\eta)\alpha_i\alpha_3} \\ O_{14}^{(\tau\eta)\alpha_i\alpha_1} & O_{24}^{(\tau\eta)\alpha_i\alpha_2} & O_{34}^{(\tau\eta)\alpha_i\alpha_3} \\ O_{15}^{(\tau\eta)\alpha_i\alpha_1} & O_{25}^{(\tau\eta)\alpha_i\alpha_2} & O_{35}^{(\tau\eta)\alpha_i\alpha_3} \\ O_{16}^{(\tau\eta)\alpha_i\alpha_1} & O_{26}^{(\tau\eta)\alpha_i\alpha_2} & O_{36}^{(\tau\eta)\alpha_i\alpha_3} \\ O_{17}^{(\tau\eta)\alpha_i\alpha_1} & O_{27}^{(\tau\eta)\alpha_i\alpha_2} & O_{37}^{(\tau\eta)\alpha_i\alpha_3} \\ O_{18}^{(\tau\eta)\alpha_i\alpha_1} & O_{28}^{(\tau\eta)\alpha_i\alpha_2} & O_{38}^{(\tau\eta)\alpha_i\alpha_3} \\ O_{19}^{(\tau\eta)\alpha_i\alpha_1} & O_{29}^{(\tau\eta)\alpha_i\alpha_2} & O_{39}^{(\tau\eta)\alpha_i\alpha_3} \end{bmatrix} \begin{bmatrix} u_1^{(\eta)} \\ u_2^{(\eta)} \\ u_3^{(\eta)} \end{bmatrix} \tag{1.57}$$

with $\tau = 0, \ldots, N+1$. Based on the Hamiltonian Principle (1.44), and the application of the Gauss' Theorem for integration purposes, one obtains the equilibrium relations (1.48). Actually, since two different integrals are derived at this stage in any time interval $[t_1, t_2]$, it is possible to derive both the kinematic and static external constraints. Hereafter, we consider two different sets of BCs, namely a fully clamped (C) and a free (F) restraint, defined as [57]

Clamped (C)

$$\begin{aligned} &u_1^{(\tau)} = u_2^{(\tau)} = u_3^{(\tau)} = 0 \qquad \text{for} \quad \tau = 0,\, 1,\, 2,\, \ldots,\, N,\, N+1, \\ &\qquad \text{at} \quad \alpha_1 = \alpha_1^0 \quad or \quad \alpha_1 = \alpha_1^1, \qquad \alpha_2^0 \leqslant \alpha_2 \leqslant \alpha_2^1 \\ &u_1^{(\tau)} = u_2^{(\tau)} = u_3^{(\tau)} = 0 \qquad \text{for} \quad \tau = 0,\, 1,\, 2,\, \ldots,\, N,\, N+1, \\ &\qquad \text{at} \quad \alpha_2 = \alpha_2^0 \quad or \quad \alpha_2 = \alpha_2^1, \qquad \alpha_1^0 \leqslant \alpha_1 \leqslant \alpha_1^1 \end{aligned} \tag{1.58}$$

Free (C)

$$\begin{aligned} &N_1^{(\tau)} = 0, \quad N_{12}^{(\tau)} = 0, \quad T_1^{(\tau)} = 0 \qquad \text{for} \quad \tau = 0,\, 1,\, 2,\, \ldots,\, N,\, N+1, \\ &\qquad \text{at} \quad \alpha_1 = \alpha_1^0 \quad \text{or} \quad \alpha_1 = \alpha_1^1, \qquad \alpha_2^0 \leqslant \alpha_2 \leqslant \alpha_2^1 \\ &N_{21}^{(\tau)} = 0, \quad N_2^{(\tau)} = 0, \quad T_2^{(\tau)} = 0 \qquad \text{for} \quad \tau = 0,\, 1,\, 2,\, \ldots,\, N,\, N+1, \\ &\qquad \text{at} \quad \alpha_2 = \alpha_2^0 \quad \text{or} \quad \alpha_2 = \alpha_2^1, \qquad \alpha_1^0 \leqslant \alpha_1 \leqslant \alpha_1^1 \end{aligned} \tag{1.59}$$

For a smart definition of shell edges, we adopt the following nomenclature

$$\begin{aligned}
&\text{Westedge (W)} \rightarrow && {\alpha_1}^0 \leqslant \alpha_1 \leqslant {\alpha_1}^1, && \alpha_2 = {\alpha_2}^0 \\
&\text{Southedge (S)} \rightarrow && \alpha_1 = {\alpha_1}^1, && {\alpha_2}^0 \leqslant \alpha_2 \leqslant {\alpha_2}^1 \\
&\text{Eastedge (E)} \rightarrow && {\alpha_1}^0 \leqslant \alpha_1 \leqslant {\alpha_1}^1, && \alpha_2 = {\alpha_2}^1 \\
&\text{North edge(N)} \rightarrow && \alpha_1 = {\alpha_1}^0, && {\alpha_2}^0 \leqslant \alpha_2 \leqslant {\alpha_2}^1
\end{aligned} \tag{1.60}$$

1.2.5 Assembly procedure of the discrete governing equations

Once the analytical expression of the fundamental equation (1.56) has been derived for the eigenvalue problem, we provide a discrete version to solve the problem numerically. In the present formulation, we employ the GDQ method to solve the problem in a strong form. First of all, a set of $I_N \times I_M$ discrete points is identified within the computational domain. For each point, a coordinate location $(\alpha_{1i}, \alpha_{2j})$ with $i = 1, \ldots, I_N$ and $j = 1, \ldots, I_M$ must be provided with respect to the curvilinear reference system (1.1). In the present work, a non-uniform bidimensional Chebyshev–Gauss–Lobatto's (CGL) distribution has been selected [57], due to its capability to yield accurate and stable results, as verified in [57, 59, 60, 65, 70], namely

$$\alpha_{rp} = \left(1 - \cos\left(\frac{p-1}{I_P - 1}\pi\right)\right)\frac{({\alpha_r}^1 - {\alpha_r}^0)}{2} + {\alpha_r}^0 \qquad \begin{array}{l} \text{for} \quad I_P = I_N, I_M, \\ \text{for} \quad r = 1, 2, \\ \text{for} \quad p = 1, 2, \ldots, I_P, \\ \text{for} \quad \alpha_{rp} \in \left[{\alpha_{rp}}^0, {\alpha_{rp}}^1\right] \end{array} \tag{1.61}$$

The GDQ method allows one to express directly the nth order derivative of a function as a linear combination of its values assumed in a fixed point distribution. If $f(x)$ is a one-variable function with $x \in [x_0, x_1]$ and x_i is a discrete point belonging to a discrete distribution of I_N points within its domain, it gives

$$\left.\frac{d^n f(x)}{dx^n}\right|_{x=x_i} \cong \sum_{j=1}^{I_N} \varsigma_{ij}^{(n)} f(x_j) \qquad i = 1, 2, \ldots, I_N \tag{1.62}$$

The weighting coefficients are computed from the recursive relation provided by Shu [64]

$$\begin{aligned}
\varsigma_{ij}^{(1)} &= \frac{\mathcal{L}^{(1)}(x_i)}{(x_i - x_j)\mathcal{L}^{(1)}(x_j)}, \quad \varsigma_{ij}^{(n)} = n\left(\varsigma_{ij}^{(1)}\varsigma_{ii}^{(n-1)} - \frac{\varsigma_{ij}^{(n-1)}}{x_i - x_j}\right) && i \neq j \\
\varsigma_{ii}^{(n)} &= -\sum_{j=1 j\neq i}^{N} \varsigma_{ij}^{(n)} && i = j
\end{aligned} \tag{1.63}$$

depending on the properties of the interpolating polynomials $\mathcal{L}$. On the other hand, based on the integral fundamental theorems, from equation (1.62) we can similarly derive the well-known Generalized Integral Quadrature (GIQ) procedure [57], which approximates the integral of a function as follows

$$\int_{x_i}^{x_j} f(x)dx = \sum_{k=1}^{I_T} (w_{jk} - w_{ik}) f(x_k) \tag{1.64}$$

in the closed interval $[x_i, x_j]$. In equation (1.64) the weighting coefficients w_{ik} and w_{jk} can be derived from (1.63).

Accordingly, the partial derivation of a bi-dimensional function $f(\alpha_1, \alpha_2)$ with respect to α_1 and α_2 up to the nth and mth order within the bi-dimensional discretization (α_i, α_j) is defined numerically as

$$\begin{aligned} \frac{\partial^n f(\alpha_1, \alpha_2)}{\partial \alpha_1^n}\bigg|_{\alpha_1=\alpha_{1i},\, \alpha_2=\alpha_{2j}} &\cong \sum_{k=1}^{I_N} \varsigma_{\alpha_1(ik)}^{(n)} f(\alpha_{1k}, \alpha_{2j}) \\ & i = 1, 2, \ldots, I_N, \quad j = 1, 2, \ldots, I_M \\ \frac{\partial^m f(\alpha_1, \alpha_2)}{\partial \alpha_2^m}\bigg|_{\alpha_1=\alpha_{1i},\, \alpha_2=\alpha_{2j}} &\cong \sum_{l=1}^{I_M} \varsigma_{\alpha_2(jl)}^{(m)} f(\alpha_{1i}, \alpha_{2j}) \\ & i = 1, 2, \ldots, I_N, \quad j = 1, 2, \ldots, I_M \end{aligned} \tag{1.65}$$

with $i = 1, \ldots, I_N$ and $j = 1, \ldots, I_M$. At the same time, the mixed derivative of $(n + m)$th order of $f(\alpha_1, \alpha_2)$ is expressed as [57]

$$\begin{aligned} \frac{\partial^{n+m} f(\alpha_1, \alpha_2)}{\partial \alpha_1^n \partial \alpha_2^m}\bigg|_{\alpha_1=\alpha_{1i},\, \alpha_2=\alpha_{2j}} &\cong \sum_{k=1}^{I_N} \varsigma_{\alpha_1(ik)}^{(n)} \left(\sum_{l=1}^{I_M} \varsigma_{\alpha_2(jl)}^{(m)} f(\alpha_{1k}, \alpha_{2l}) \right) \\ & i = 1, 2, \ldots, I_N, \quad j = 1, 2, \ldots, I_M \end{aligned} \tag{1.66}$$

Now, the discrete form of the fundamental equation (1.56) for the eigenvalue problem is obtained in a strong formulation, taking into account each expansion order of the kinematic ESL assumption (1.7)

$$\mathbf{K}\boldsymbol{\delta} = \omega^2 \mathbf{M}\boldsymbol{\delta} \tag{1.67}$$

$\mathbf{K}$ and $\mathbf{M}$ being the stiffness and inertia matrix written for the whole domain. Nevertheless, $\boldsymbol{\delta}$ is the global DOFs array, which is conveniently separated as $\boldsymbol{\delta} = [\boldsymbol{\delta}_b \ \boldsymbol{\delta}_d]^T$ to account for the external points of the structure denoted with 'b', and those of the internal ones of the computational domain labelled with 'd'. As a consequence, also $\mathbf{K}$ and $\mathbf{M}$ are properly rearranged, such that equation (1.67) becomes [57]

$$\begin{bmatrix} \mathbf{K}_{bb} & \mathbf{K}_{bd} \\ \mathbf{K}_{db} & \mathbf{K}_{dd} \end{bmatrix} \begin{bmatrix} \boldsymbol{\delta}_b \\ \boldsymbol{\delta}_d \end{bmatrix} = \omega^2 \begin{bmatrix} \mathbf{0} & \mathbf{0} \\ \mathbf{0} & \mathbf{M}_{dd} \end{bmatrix} \begin{bmatrix} \boldsymbol{\delta}_b \\ \boldsymbol{\delta}_d \end{bmatrix} \tag{1.68}$$

Employing a kinematic condensation, it is possible to reduce the size of (1.68) that yields the following expression

$$(\mathbf{M}_{dd}^{-1}(\mathbf{K}_{dd} - \mathbf{K}_{db}\mathbf{K}_{bb}^{-1}\mathbf{K}_{bd}) - \omega^2\mathbf{I})\boldsymbol{\delta}_d = \mathbf{0} \tag{1.69}$$

Equation (1.68) points out also a problem related to the definition of BCs near the corners of the shell. According to the identification of edges in (1.60), the discrete corner point belongs to two different sides of the structure. Therefore, the definition of external constraints is not immediate, as the discrete form of BCs is univocally defined at each point. To this end, a possible solution is to consider in these points the sum of the external constraints defined in (1.59). In this way, the free corner condition can be easily set, since it comes from a combination of some basic constraint cases.

1.3 Numerical applications

In the present section we perform some numerical examples to validate the proposed approach against some reference 3D finite element-based predictions. The focus has been on various parameters occurring in the generalized problem at issue, namely the presence of variable curvatures within a structure, the introduction of latticed materials, and different stacking sequences along the shell thickness.

As far as the geometry is concerned, the structure is described with respect to the reference surface (1.1), in line with the ESL strategy. As summarized in figure 1.1, two categories of shells are distinguished among the proposed examples. First, a helicoidal panel is described as a translational surface if a principal coordinate system is set. It leads to the following position vector [57]

$$\begin{aligned}\mathbf{r}(\alpha_1, \alpha_2) = &-a\cos(\alpha_1 + \alpha_2)\sinh(\alpha_1 - \alpha_2)\mathbf{e}_1 - a\sin(\alpha_1 + \alpha_2)\sinh(\alpha_1 - \alpha_2)\,\mathbf{e}_2 \\ &+ a(\alpha_1 - \alpha_2)\,\mathbf{e}_3\end{aligned} \tag{1.70}$$

This kind of structure consists of a curve described with the principal coordinate α_1 sliding over another one described from the other principal line α_2. On the other hand, a revolution surface is obtained from a curve along α_1 direction getting around a reference rotation axis. The parallel direction denotes a principal parametric set of lines along α_2. In the following, the principal coordinate reference surface equation is reported for a revolution paraboloid of nth order [57]

$$\mathbf{r}(x_1, \vartheta) = x_1\cos\vartheta\,\mathbf{e}_1 - x_1\sin\vartheta\,\mathbf{e}_2 + ax_1^n\,\mathbf{e}_3 \tag{1.71}$$

In equations (1.70)–(1.71), the parameter a is used to fix the geometry scaling. This parameter assumes a different meaning depending on the selected shell structure. As a matter of fact, a rectangular plate can be described as a translational surface (1.70) in which both generatrix and directrix curves consist of a straight line.

As extensively discussed in the previous sections, the main advantage of employing a lattice medium in the structure is to come across a general orthotropic behaviour of the structure, even though an isotropic material with spherical elastic symmetry is assumed. In this way, it is possible to perform a topological

optimization of the cell unit to assess *a priori* the dynamic properties of the shell, by simply tuning the unit cell geometry rather than the entire structure or its BCs. Moreover, a lattice material turns into a very lightweight performing structure. In the present chapter two different approaches have been applied to define the central layer of shells. In figure 1.2 one can find all the geometric quantities employed in the model for both a honeycomb cell (a) and single grid family (a), based on thin-walled hypotheses.

The accuracy of the approach is affected by the complexity of the selected stacking sequence. Two main aspects must be considered, namely, the complexity of the single layer stiffness matrix (1.22) and the relative thickness of adjacent laminae. According to [24], a lattice honeycomb structure can be obtained in a lot of engineering applications, embedding both nanomaterials, aerospace, and civil applications. For this reason, the validation of the dynamic behaviour is compulsory for both thin and thick layers within a laminate.

As also stated by Vasiliev *et al* [6, 7], the manufacturing process of a lattice grid structure consists of a central thick core made by various stiffeners, together with two outer thinner isotropic sheets, which cannot be considered as structural contributions. However, since the dynamic behaviour must be assessed within the whole structure, in the present work we employ two isotropic thin skins for a lattice grid layer.

The first set of examples studies the accuracy of the proposed homogenization method to model the honeycomb core. A rectangular plate is considered with in-plane dimensions $L_x \simeq L_y \simeq 0.4$ m, which is assumed to be completely clamped (C) at each edge. The plate is made of an isotropic aluminum material, also for outer external skins, whereas a three-layer configuration is considered for each case.

As far as the honeycomb unit cell layup is concerned, examples with three different RVEs have been developed employing various internal cell angles ϑ, as depicted in figure 1.3, together with a conceptual three-dimensional representation of the sandwich panel. In particular, the hexagonal honeycomb cell is characterized by $\vartheta = 30°$, the rectangular one is denoted with $\vartheta = 0°$. Note that we revert to an auxetic behaviour in the case of re-entrant honeycomb, with $\vartheta = -30°$. In order to assess the smearing technique with a right set of cell configurations, different plates have been developed with various cell wall thicknesses, accounting for both the case of thin and thick layer. In all the analyses, the central honeycomb core lies within two external layers with $h_1 = h_3 = 0.001$ m. For each case, a refined 3D FEM model is employed for a large number of DOFs, and the first ten mode frequencies are calculated, together with their corresponding eigenvectors. The FEM-based outcomes are treated as reference solutions for the validation check of the proposed homogenized GDQ model.

The influence of the through-the-thickness axiomatic assumptions are, then, investigated by adopting different higher order theories. The results are summarized in tables 1.1–1.3, while a geometric representation of the FEM model can be found in figure 1.4, along with its homogenized scheme. The finite element model discretizes the outer layers with parabolic 20-nodes bricks, while the internal grid assumes higher order shell elements, to yield a conforming mesh, and an optimized interpolation of the problem.

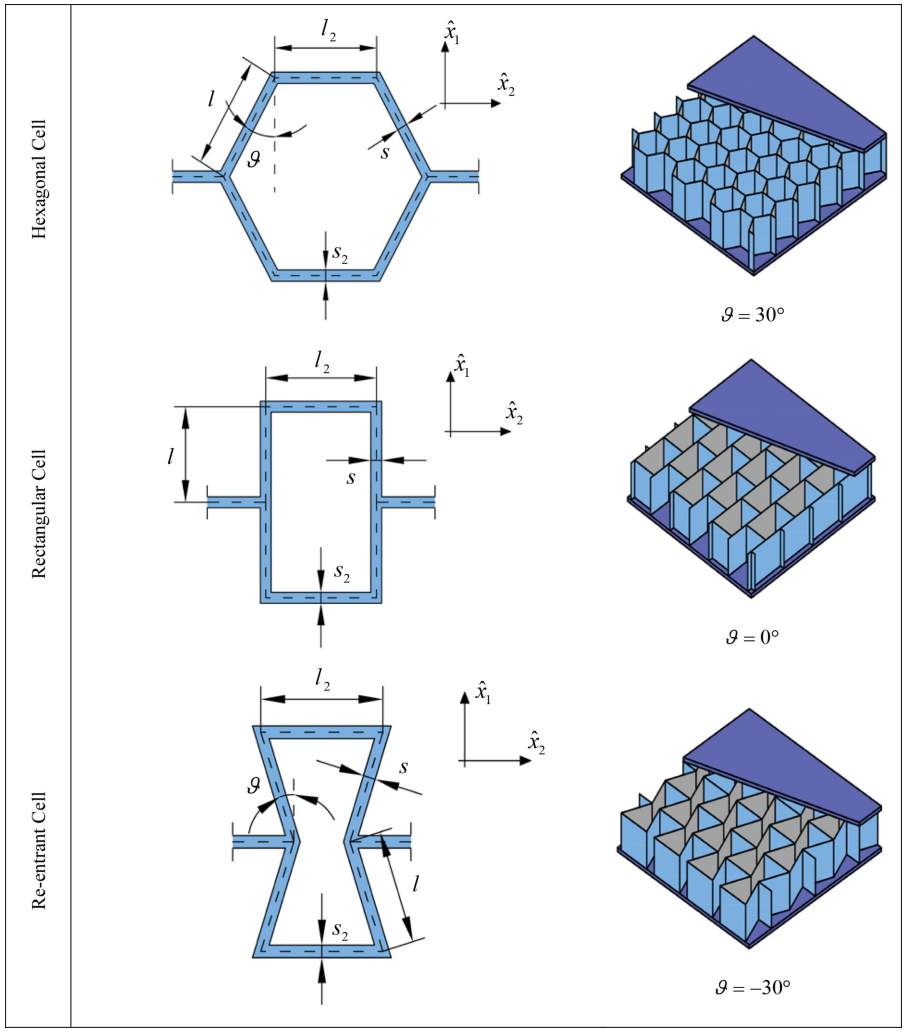

Figure 1.3. Honeycomb cell layup.

In table 1.1 we summarize the first ten natural frequencies of the rectangular plate with a central infill of hexagonal honeycomb ($\vartheta = 30°$). In this case, the equivalent elastic properties, generally orthotropic, degenerate into a transverse isotropic material, due to the perfect correspondence between the in-plane elastic moduli along α_1 and α_2. Accordingly, the symmetry of the domain and BCs is reflected on the vibration modes, that share four pairs of values, with few discrepancies related to the geometrical dimensions of L_x and L_y.The same analyses are then repeated in table 1.2 for a rectangular honeycomb unit cell ($\vartheta = 0°$), by employing different HSDTs. The 3D FEM model is developed taking into account the exact geometry of the core infill, as well as perfectly-bonded interfaces. All the internal cell walls also present the same thickness at any arbitrary point. A twofold numerical investigation

Table 1.1. Free vibration analysis of a CCCC rectangular sandwich plate with a lattice core made of hexagonal honeycomb cells, different lattice layers and layer thickness.

CCCC rectangular plate—hexagonal honeycomb								
Mode f [Hz]	3D FEM	FSDT	FSDTZ	TSDTZ	EDZ1$_{(\kappa = 5/6)}$	EDZ2$_{(\kappa = 5/6)}$	EDZ3$_{(\kappa = 1)}$	EDZ4$_{(\kappa = 1)}$
Thin layer ($b = h_2 = 5$ mm)								
DOFs	1700 490	5046	7569	12 615	7569	10 092	12 615	15 138
Thin cell wall ($s_2 = s = 0.1$ mm)								
1	497.420	562.023	499.049	499.029	540.705	489.755	499.995	499.665
2	937.430	1138.712	942.166	942.110	993.995	915.807	944.363	943.308
3	937.520	1139.725	942.875	942.819	994.694	916.480	945.074	944.017
4	1306.000	1670.009	1314.580	1314.487	1366.662	1271.120	1318.049	1316.132
5	1530.300	2024.507	1541.770	1541.649	1587.401	1485.261	1546.278	1543.554
6	1544.200	2035.337	1555.703	1555.581	1602.999	1498.889	1560.178	1557.527
7	1844.400	2524.945	1859.401	1859.243	1899.250	1786.186	1865.188	1861.512
8	1845.000	2526.375	1860.222	1860.065	1900.031	1786.955	1866.014	1862.334
9	2230.400	3203.529	2251.152	2250.939	2274.575	2153.314	2259.064	2253.690
10	2232.600	3207.605	2253.342	2253.129	2276.648	2155.362	2261.269	2255.882
Thick cell wall ($s_2 = s = 0.4$ mm)								
1	507.570	524.448	508.950	508.925	572.870	507.287	510.782	510.281
2	1005.400	1063.046	1011.036	1010.954	1124.097	1003.509	1014.852	1013.707
3	1005.400	1063.993	1011.897	1011.815	1125.027	1004.355	1015.716	1014.570
4	1446.400	1559.666	1458.681	1458.527	1606.803	1443.244	1464.401	1462.553
5	1733.900	1891.147	1751.459	1751.247	1918.189	1729.388	1758.520	1756.148
6	1745.900	1901.205	1763.338	1763.128	1932.833	1741.578	1770.423	1768.068
7	2131.300	2359.446	2156.675	2156.377	2346.730	2124.760	2165.609	2162.455
8	2132.100	2360.785	2157.807	2157.508	2347.908	2125.858	2166.746	2163.591
9	2655.400	2994.680	2694.166	2693.729	2906.987	2646.190	2705.767	2701.494
10	2658.900	2998.499	2697.293	2696.855	2910.197	2649.209	2708.911	2704.630

(*Continued*)

Table 1.1. (*Continued*)

CCCC rectangular plate—hexagonal honeycomb

Mode f [Hz]	3D FEM	FSDT	FSDTZ	TSDTZ	EDZ1$_{(\kappa = 5/6)}$	EDZ2$_{(\kappa = 5/6)}$	EDZ3$_{(\kappa = 1)}$	EDZ4$_{(\kappa = 1)}$
Thick layer ($b = h_2 = 10$ mm)								
DOFs	2606 202	5046	7569	12 615	7569	10 092	12 615	15 138
Thin cell wall ($s_2 = s = 0.1$ mm)								
1	803.600	985.369	805.519	805.493	843.671	781.480	808.063	806.722
2	1448.800	1971.116	1453.922	1453.859	1476.916	1394.118	1459.179	1455.889
3	1449.000	1972.823	1454.895	1454.832	1477.829	1395.023	1460.157	1456.863
4	1973.000	2858.961	1981.914	1981.817	1985.140	1890.367	1989.567	1984.422
5	2273.900	3444.450	2285.447	2285.328	2270.406	2172.296	2294.853	2288.098
6	2296.100	3466.138	2307.803	2307.682	2292.862	2193.156	2317.238	2310.528
7	2708.200	4257.295	2722.957	2722.808	2684.757	2580.924	2734.491	2725.981
8	2708.900	4259.593	2724.018	2723.869	2685.738	2581.904	2735.559	2727.042
9	3214.900	5346.405	3234.577	3234.388	3161.738	3054.516	3249.293	3237.800
10	3217.100	5352.810	3237.389	3237.200	3164.333	3057.114	3252.125	3240.611
Thick cell wall ($s_2 = s = 0.4$ mm)								
1	830.190	874.702	831.356	831.314	919.592	826.643	837.355	833.971
2	1608.700	1753.613	1614.633	1614.505	1750.915	1593.991	1626.554	1619.743
3	1608.800	1755.139	1615.937	1615.809	1752.262	1595.257	1627.868	1621.051
4	2278.600	2548.175	2291.807	2291.581	2453.451	2251.944	2308.985	2299.068
5	2702.900	3073.353	2721.993	2721.690	2888.812	2665.760	2742.705	2730.662
6	2725.200	3092.216	2744.324	2744.024	2915.804	2688.612	2765.219	2753.114
7	3288.700	3804.057	3315.411	3315.005	3491.702	3237.807	3340.899	3325.977
8	3289.700	3806.127	3317.016	3316.609	3493.285	3239.336	3342.518	3327.586
9	4037.900	4785.462	4078.135	4077.568	4248.043	3965.327	4110.172	4091.213
10	4041.800	4791.252	4082.468	4081.900	4252.269	3969.438	4114.544	4095.558

Geometric inputs $L_x = 0.39999$ mm, $L_y = 0.40029$ mm

Honeycomb cell configuration $l_2 = 5.1320$ mm, $l = 5.1320$ mm, $\vartheta = 30°$, $E_s = 70$ GPa, $\nu_s = 0.33$, $\rho_s = 2700$ kg/m^3

Table 1.2. Free vibration analysis of a CCCC rectangular sandwich plate with a lattice core made of rectangular honeycomb cells, different lattice layers and layer thickness.

CCCC rectangular plate—rectangular honeycomb								
Mode f [Hz]	3D FEM	FSDT	FSDTZ	TSDTZ	EDZ1$_{(\kappa = 5/6)}$	EDZ2$_{(\kappa = 5/6)}$	EDZ3$_{(\kappa = 1)}$	EDZ4$_{(\kappa = 1)}$
Thin layer ($b = h_2 = 5$ mm)								
DOFs	1938 258	5046	7569	12 615	7569	10 092	12 615	15 138
Thin cell wall ($s_2 = s = 0.1$ mm)								
1	489.070	563.844	490.427	490.408	527.369	480.055	491.460	491.072
2	907.740	1142.038	910.100	910.051	949.921	881.306	912.576	911.288
3	917.610	1143.791	923.906	923.853	967.788	895.704	926.137	924.976
4	1264.300	1675.085	1271.842	1271.760	1310.527	1225.830	1275.503	1273.322
5	1468.000	2030.916	1472.951	1472.848	1500.407	1413.434	1477.901	1474.691
6	1497.900	2042.286	1512.476	1512.364	1547.605	1453.457	1516.999	1514.112
7	1765.400	2532.091	1775.230	1775.096	1795.881	1699.354	1781.394	1777.181
8	1782.100	2534.576	1798.432	1798.291	1823.093	1722.734	1804.363	1800.338
9	2111.900	3212.577	2119.889	2119.716	2119.663	2020.124	2128.436	2122.178
10	2160.900	3219.668	2188.170	2187.976	2197.918	2088.356	2196.133	2190.412
Thick cell wall ($s_2 = s = 0.4$ mm)								
1	508.240	529.315	510.338	510.314	572.585	508.471	512.570	511.983
2	997.660	1070.243	1004.884	1004.809	1111.149	996.637	1010.104	1008.551
3	1004.400	1076.640	1015.091	1015.007	1123.566	1006.080	1018.935	1017.819
4	1432.300	1572.959	1451.033	1450.887	1589.229	1433.496	1457.642	1455.519
5	1708.800	1905.299	1731.007	1730.817	1881.658	1706.488	1740.433	1737.236
6	1733.000	1923.285	1761.302	1761.086	1919.247	1735.920	1768.177	1765.905
7	2092.100	2375.762	2127.882	2127.612	2297.935	2092.174	2138.748	2134.845
8	2106.100	2384.841	2145.765	2145.475	2320.176	2109.555	2155.042	2151.747
9	2587.400	3012.452	2636.728	2636.347	2817.787	2583.340	2651.770	2646.014
10	2631.300	3038.338	2691.050	2690.601	2885.119	2636.624	2701.948	2697.904

(*Continued*)

Table 1.2. (*Continued*)

CCCC rectangular plate—rectangular honeycomb								
Mode f [Hz]	3D FEM	FSDT	FSDTZ	TSDTZ	EDZ1$_{(\kappa = 5/6)}$	EDZ2$_{(\kappa = 5/6)}$	EDZ3$_{(\kappa = 1)}$	EDZ4$_{(\kappa = 1)}$
Thick layer ($b = h_2 = 10$ mm)								
DOFs	2791 698	5046	7569	12 615	7569	10 092	12 615	15 138
Thin cell wall ($s_2 = s = 0.1$ mm)								
1	780.090	990.465	780.884	780.860	809.609	754.781	783.532	782.090
2	1372.400	1978.452	1372.119	1372.072	1377.581	1309.840	1377.578	1373.965
3	1404.400	1985.579	1410.881	1410.814	1421.952	1348.584	1415.929	1412.610
4	1879.200	2872.050	1884.797	1884.713	1870.984	1791.332	1892.271	1886.946
5	2128.800	3459.404	2128.235	2128.153	2092.395	2014.528	2137.641	2130.485
6	2207.800	3486.323	2222.846	2222.714	2194.780	2107.097	2231.762	2225.060
7	2539.300	4272.727	2544.365	2544.251	2486.528	2403.124	2555.539	2546.757
8	2584.600	4282.427	2599.232	2599.088	2544.961	2456.548	2610.211	2601.633
9	2965.300	5362.606	2965.050	2964.926	2871.387	2789.709	2979.294	2967.410
10	3094.000	5389.763	3120.984	3120.773	3035.469	2940.949	3134.883	3123.467
Thick cell wall ($s_2 = s = 0.4$ mm)								
1	831.070	886.808	832.312	832.272	915.420	827.104	839.603	835.493
2	1582.100	1766.097	1587.074	1586.999	1706.210	1565.126	1603.054	1593.658
3	1609.600	1790.702	1622.815	1622.641	1746.890	1598.066	1634.648	1627.922
4	2242.600	2578.107	2263.274	2263.076	2402.732	2218.896	2282.641	2271.194
5	2628.300	3095.904	2647.735	2647.584	2780.954	2587.668	2674.604	2658.151
6	2706.400	3155.220	2740.575	2740.127	2886.638	2675.864	2760.124	2748.738
7	3189.500	3832.376	3226.338	3226.080	3364.440	3142.414	3256.136	3237.797
8	3237.100	3866.003	3282.220	3281.761	3427.349	3195.598	3307.949	3292.521
9	3864.000	4806.716	3909.938	3909.684	4025.016	3790.163	3949.227	3924.150
10	4004.800	4900.745	4072.182	4071.299	4206.283	3945.444	4101.454	4083.899

Geometric inputs $L_x = 0.39999$ mm, $L_y = 0.40029$ mm

Honeycomb cell configuration $l_2 = 5.1320$ mm, $l = 5.1320$ mm, $\vartheta = 0°$, $E_s = 70$ GPa, $\nu_s = 0.33$, $\rho_s = 2700$ kg/m^3

Table 1.3. Free vibration analysis of a CCCC rectangular sandwich plate with a lattice core made of re-entrant honeycomb cells, different lattice layers and layer thickness.

CCCC rectangular plate—re-entrant honeycomb								
Mode f [Hz]	3D FEM	FSDT	FSDTZ	TSDTZ	EDZ1$_{(\kappa = 5/6)}$	EDZ2$_{(\kappa = 1)}$	EDZ3$_{(\kappa = 1)}$	EDZ4$_{(\kappa = 1)}$
Thin layer ($b = h_2 = 5$ mm)								
DOFs	1224 690	5046	7569	12 615	7569	10 092	12 615	15 138
Thin cell wall ($s_2 = s = 0.1$ mm)								
1	490.960	578.921	490.972	490.954	523.359	492.172	492.155	491.673
2	901.600	1172.339	906.894	906.847	939.042	909.561	909.522	908.038
3	911.940	1174.200	907.855	907.808	939.910	910.541	910.503	909.009
4	1249.600	1719.257	1250.808	1250.733	1276.431	1254.922	1254.864	1252.265
5	1444.900	2084.327	1454.799	1454.703	1471.169	1460.100	1460.028	1456.391
6	1474.800	2096.070	1468.428	1468.331	1485.540	1473.699	1473.625	1470.064
7	1733.100	2598.238	1743.312	1743.190	1749.508	1750.008	1749.917	1745.117
8	1749.600	2600.864	1744.290	1744.168	1750.360	1751.008	1750.917	1746.101
9	2064.000	3296.048	2090.335	2090.174	2077.613	2099.392	2099.274	2092.384
10	2112.000	3303.525	2092.846	2092.686	2079.793	2101.961	2101.844	2094.910
Thick cell wall ($s_2 = s = 0.4$ mm)								
1	513.320	542.005	518.332	518.308	579.408	521.202	521.180	520.414
2	997.700	1098.256	1019.797	1019.719	1121.776	1025.419	1025.355	1023.661
3	1005.100	1099.689	1020.997	1020.919	1123.097	1026.729	1026.665	1024.938
4	1424.500	1609.960	1460.305	1460.165	1588.688	1468.487	1468.376	1465.677
5	1687.700	1954.013	1746.590	1746.395	1885.705	1756.422	1756.269	1752.840
6	1717.500	1964.699	1759.521	1759.327	1901.521	1769.460	1769.307	1765.883
7	2059.900	2434.693	2138.509	2138.243	2292.610	2150.587	2150.386	2145.919
8	2078.500	2436.723	2140.001	2139.736	2294.152	2152.206	2152.004	2147.493
9	2523.800	3092.747	2654.785	2654.394	2816.916	2669.877	2669.582	2663.627
10	2583.500	3098.528	2658.812	2658.422	2820.995	2674.234	2673.940	2667.858

(*Continued*)

Table 1.3. (*Continued*)

CCCC rectangular plate—re-entrant honeycomb								
Mode f [Hz]	3D FEM	FSDT	FSDTZ	TSDTZ	EDZ1$_{(\kappa = 5/6)}$	EDZ2$_{(\kappa = 1)}$	EDZ3$_{(\kappa = 1)}$	EDZ4$_{(\kappa = 1)}$
Thick layer ($b = h_2 = 10$ mm)								
DOFs	1764 306	5046	7569	12 615	7569	10 092	12 615	15 138
Thin cell wall ($s_2 = s = 0.1$ mm)								
1	761.020	1015.222	762.585	762.567	780.903	765.468	765.454	763.814
2	1322.100	2029.063	1324.113	1324.073	1315.261	1329.545	1329.518	1325.723
3	1343.800	2031.749	1350.842	1350.798	1345.735	1356.361	1356.332	1352.543
4	1792.000	2940.656	1799.278	1799.218	1767.993	1806.926	1806.887	1801.167
5	2030.900	3543.703	2034.329	2034.258	1983.218	2043.488	2043.440	2036.149
6	2085.300	3566.557	2100.316	2100.237	2053.782	2109.697	2109.645	2102.306
7	2408.300	4375.306	2416.547	2416.460	2341.646	2427.588	2427.532	2418.457
8	2438.400	4378.700	2453.955	2453.863	2381.229	2465.140	2465.081	2455.947
9	2809.300	5494.487	2814.552	2814.445	2706.470	2828.333	2828.262	2816.332
10	2894.500	5503.676	2920.896	2920.774	2817.532	2935.070	2934.990	2922.884
Thick cell wall ($s_2 = s = 0.4$ mm)								
1	822.070	903.605	833.190	833.162	909.920	842.329	842.313	837.082
2	1527.500	1810.490	1582.541	1582.461	1683.080	1599.107	1599.061	1589.186
3	1575.300	1811.307	1597.730	1597.644	1705.041	1614.416	1614.368	1604.484
4	2160.400	2623.223	2228.163	2228.038	2340.948	2250.824	2250.757	2236.928
5	2477.100	3170.463	2614.965	2614.780	2713.583	2640.959	2640.853	2624.587
6	2618.900	3189.702	2666.129	2665.926	2780.013	2692.817	2692.702	2676.209
7	3010.000	3913.371	3162.324	3162.110	3259.794	3193.289	3193.173	3173.485
8	3100.100	3913.836	3192.164	3191.936	3298.109	3223.563	3223.440	3203.602
9	3567.700	4933.278	3828.070	3827.738	3893.056	3864.508	3864.315	3840.410
10	3834.600	4933.800	3918.820	3918.444	4006.026	3956.664	3956.450	3931.999

Geometric inputs $L_x = 0.39999$ mm, $L_y = 0.40029$ mm, $h_1 = h_3 = 0.001$ m

Honeycomb cell configuration $l_2 = 5.1320$ mm, $l = 5.1320$ mm, $\vartheta = -30\,°$, $E_s = 70$ GPa, $\nu_s = 0.33$, $\rho_s = 2700$ kg/m^3

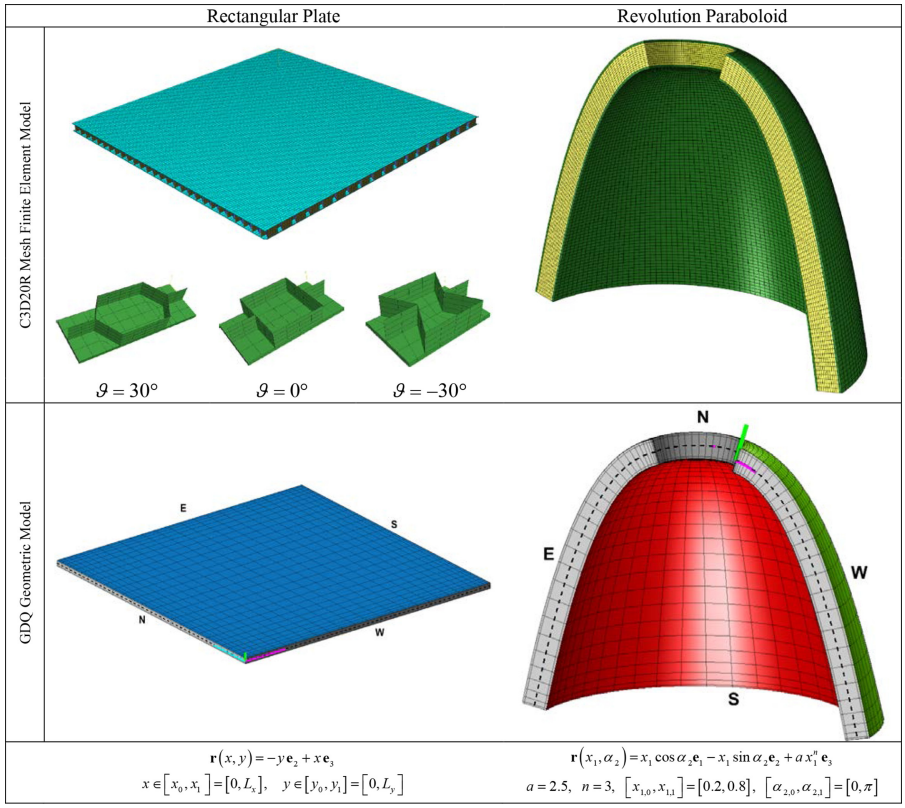

Figure 1.4. Finite element models and shell representation of the panels reinforced with a lattice infill.

is now performed for sandwich panels with thin and/or thick layers. For each case, two different thickness of the internal cell walls are selected. Based on the comparative results in table 1.2, it is worth observing an increased accuracy of GDQ-based predictions with respect to the finite element reference solution, when the zig-zag function (1.9) is embedded in the ESL displacement field (1.7). This is particularly evident when the Murakami's strategy is combined with a classical FSDT assumption. Any further increase in accuracy is observed, when implementing a third order theory. A similar behaviour can be also observed in the case of re-entrant honeycomb lattice layer ($\vartheta = -30°$). In table 1.3 we report the first ten mode frequencies for a completely clamped (CCCC) rectangular plate with a central layer made of a honeycomb re-entrant pattern. The good accordance between our GDQ-based results and finite element predictions reveal the great capability of the proposed homogenization approach and higher order theories to handle the problem. Unlike other classical homogenization methods, the present formulation is able to predict accurately the actual value of the shear modulus, G_{23}, which is usually computed by interpolating the values provided by a static and a kinematic admissible problem. The non-linear interpolation proposed in equation (1.39) is calibrated on a series of validation examples conducted on a rectangular plate [39]

and represents a valid alternative to the original Grediac formulation [29] assessed by Scarpa *et al* [30]. In this way, also for the re-entrant case, the eigenfrequencies are properly predicted for a large variety of cell cases, taking into account different cell configurations in terms of wall thickness and layer height. From a direct comparison between tables 1.1–1.3, it can be stated that the honeycomb grid does not affect the dynamic behaviour, for lower frequencies, whereas higher modes depend significantly on the cell geometric configuration. In particular, the internal cell angle ϑ is a key design parameter. For re-entrant honeycomb angles, indeed, a meaningful increase in vibration frequencies can be noticed for any cell configuration. On the other hand, since a re-entrant honeycombs turns into a negative equivalent in plane Poisson's ratio, ν_{12}, the auxetic behaviour of the central core features complicated interfacial phenomena. As a consequence, only the EDZ4 theory seems to agree with the FEM-based solution in terms of vibration modes, especially for thick layer ($h_2 = 0.001$ m) layups.

As also visible in figure 1.5, the proposed approach is capable of providing very complex in-plane and out-of-plane deformation phenomena. In addition, for a honeycomb cell, the variation of the cell geometry can affect significantly the mode shapes, especially for higher modes. Despite the symmetry of the geometry and BCs, different eigenvectors are associated with the problem in figure 1.5, by simply tuning the internal cell angle ϑ. For instance, if we consider three different unit cells with $\vartheta = 30°, 0°, -30°$, the vibration modes 5 and 6 move from a central-symmetric deformation with four waves for the hexagonal honeycomb, to a three-waves mode in the case of rectangular cell, and eventually to a four-waves mode in the case of auxetic configuration. For lower modes, the orthogonality of the deformation field is induced from different constitutive lattices and in-plane properties.

Another validation analysis is performed on a paraboloidal panel, whose mode frequencies are summarized in tables 1.4, 1.5. In figure 1.4 we report the representative geometric parameters for each selected shell structure. In this case we model the central core with a continuum model based on the equivalent elastic properties of the grid pattern computed as in equation (1.27). A fine structured mesh is used for the discretization of the domain, here modelled with C3D20R parabolic elements. The laminate consists of two external thin layers made of isotropic aluminum and a thick central core made of a lattice layer rather than a cellular material. The unit cell is made by four rib families: two of them ($\phi_i = 0°$ and $\phi_i = 90°$) are stretched along the α_1 and α_2 principal lines, whereas the other two classes of frames are symmetrically sorted along directions $\phi_i = \pm 45°$ with respect to α_1. Employing the effective compact notation (1.28), the unit cell can be identified univocally with the notation $\mathrm{F}[-45^{\delta_1}_{a_1=0.1414\ \mathrm{m}} / 0^{\delta_2}_{a_2=0.1\ \mathrm{m}} / 45^{\delta_3}_{a_3=0.1414\ \mathrm{m}} / 90^{\delta_4}_{a_4=0.1\ \mathrm{m}}]$, where a_i is the interspace between two adjacent ribs and δ_i the width of each frame. A modal analysis is adopted for a paraboloidal panel with two different BCs and different values of δ_i. A cantilevered configuration (FCFF) of the structure is first analysed, whose mode frequencies are listed in table 1.4. The same study is, thus, repeated for the same structure constrained on the two lateral edges along two different meridian lines (CFCF), as summarized in table 1.5. The 3D FEM solution has been

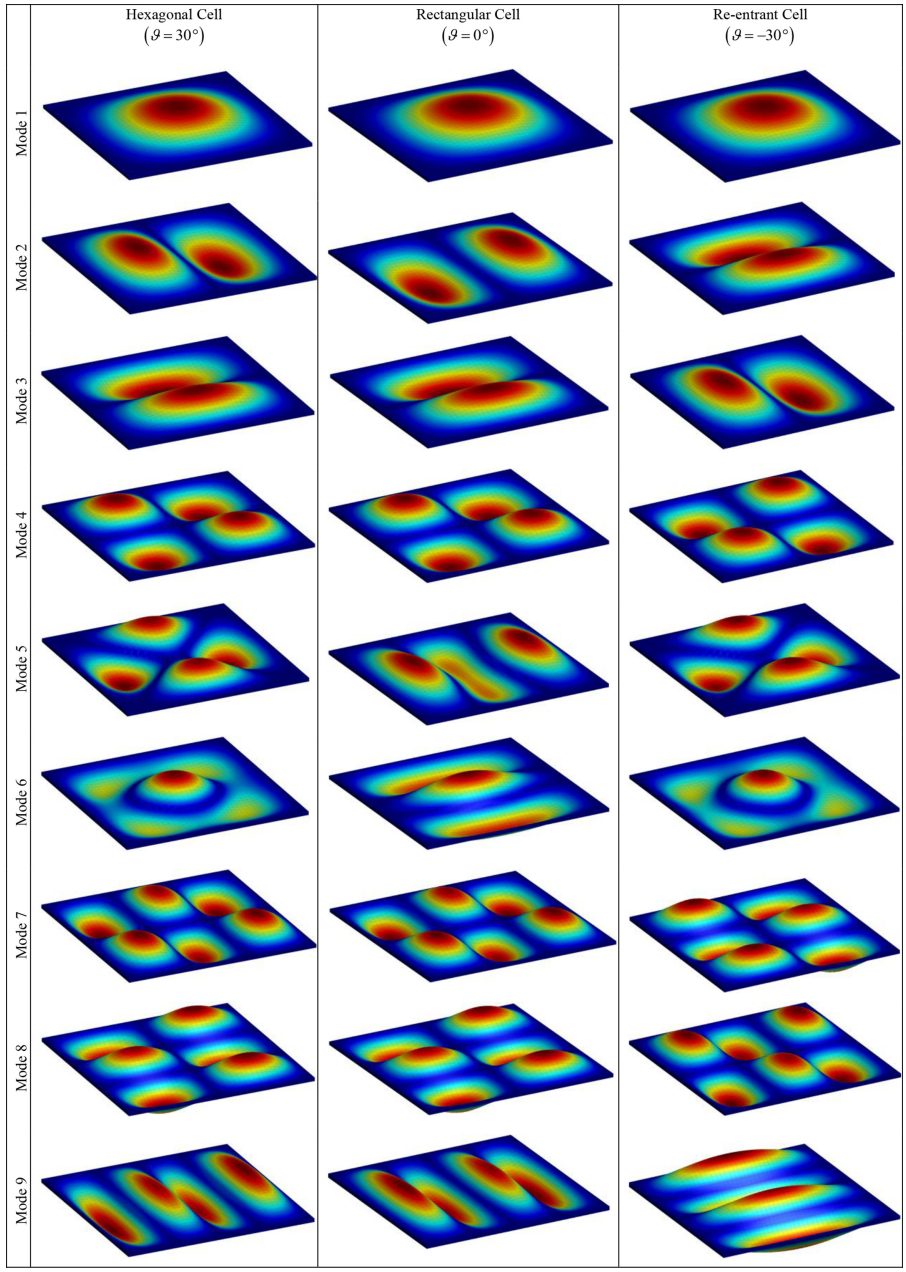

Figure 1.5. Mode shapes of a rectangular plate with a central lattice honeycomb layer.

compared with predictions from the homogenized model based on different orders of expansion. Differently from the previous cases, the influence of the Murakami's function (1.9) is trivial, since the central core is predominant within the thickness profile with respect to the external skins, leading to reduced

Table 1.4. Natural frequencies of a FCFF revolution paraboloid with a central core made of a grid layer with four families, and two external skins of aluminum. Both helical and meridian loops have been considered, together with stiffeners in two opposite directions. The shell reference surface equation and homogenized geometric representation, can be found in figure 1.4.

FCFF revolution paraboloid—pantographic central layer							
f [Hz]	3D FEM	FSDTZ	TSDTZ	EDZ1$_{(\kappa = 5/6)}$	EDZ2$_{(\kappa = 5/6)}$	EDZ3$_{(\kappa = 1)}$	EDZ4$_{(\kappa = 1)}$
DOFs	1310 499	7569	12 615	7569	10 092	12 615	15 138
Thin stiffeners ($\delta_1 = \delta_2 = \delta_3 = \delta_4 = 0.005$ m)							
1	197.410	197.545	197.523	198.567	196.350	198.363	197.651
2	267.397	267.396	267.384	268.052	267.185	267.955	267.664
3	385.044	385.684	385.495	389.842	381.401	387.663	385.697
4	539.214	539.390	539.194	535.283	531.698	540.389	539.511
5	588.531	588.636	588.501	587.027	584.747	590.020	589.122
6	670.093	670.288	670.080	672.600	666.002	671.916	670.612
7	727.782	729.362	728.983	741.227	719.380	734.569	729.612
8	788.498	789.735	789.328	783.922	773.627	793.757	789.912
9	918.067	918.195	918.126	919.194	918.061	918.982	918.554
10	981.492	982.141	982.006	976.770	971.487	982.675	981.844
Moderately thick stiffeners ($\delta_1 = \delta_2 = \delta_3 = \delta_4 = 0.01$ m)							
1	177.717	177.774	177.753	179.442	177.624	178.837	178.001
2	244.693	244.677	244.660	245.543	244.793	245.284	244.930
3	349.296	349.507	349.371	356.036	349.063	352.767	350.147
4	496.037	496.012	495.857	495.626	492.764	497.359	496.324
5	540.241	540.228	540.073	540.893	537.864	542.315	540.896
6	615.749	615.709	615.542	620.390	614.837	618.163	616.347
7	673.654	674.456	674.147	692.963	673.221	683.205	676.118
8	738.421	738.963	738.558	742.612	731.677	745.374	740.238
9	844.757	844.817	844.739	846.000	844.973	845.612	845.142
10	898.704	898.953	898.848	898.927	898.372	899.212	898.877

Thick stiffeners ($\delta_1 = \delta_2 = \delta_3 = \delta_4 = 0.02$ m)							
1	155.691	155.731	155.687	157.298	156.151	156.846	156.000
2	222.326	222.312	222.284	223.181	222.627	222.959	222.552
3	304.759	304.880	304.716	311.167	306.699	308.713	305.823
4	442.910	442.984	442.708	444.390	441.770	445.228	443.543
5	484.702	484.688	484.521	486.227	484.458	486.506	485.247
6	556.241	556.238	556.044	561.056	557.242	559.375	557.097
7	598.588	599.171	598.740	617.705	604.198	610.047	601.713
8	659.484	659.961	659.351	667.906	659.631	667.754	661.789
9	776.035	776.038	775.961	777.040	776.386	776.739	776.327
10	819.391	819.495	819.379	819.645	819.184	819.798	819.506

Geometric inputs $a = 2.5$, $n = 3$, $[\alpha_{1,0}, \alpha_{1,1}] = [0.2, 0.8]$, $[\alpha_{2,0}, \alpha_{2,1}] = [0, \pi]$, $h_1 = h_3 = 0.01m$, $h_2 = 0.1$m

Grid unit pattern layup $\mathrm{F}\left[-45^{\delta_1}_{a_1=0.1414\mathrm{m}}/0^{\delta_2}_{a_2=0.1\mathrm{m}}/45^{\delta_3}_{a_3=0.1414\mathrm{m}}/90^{\delta_4}_{a_4=0.1\mathrm{m}}\right]$, $E_s = 70$GPa, $\nu_s = 0.3$, $\rho_s = 2707\mathrm{kg/m}^3$

Table 1.5. Natural frequencies of a CFCF revolution paraboloid with a central core made of a grid layer with four families, and two external skins of aluminum. Both helical and meridian loops have been considered, together with stiffeners in two opposite directions. The shell reference surface equation and homogenized geometric representation, can be found in figure 1.4.

CFCF revolution paraboloid—pantographic central layer							
f [Hz]	3D FEM	FSDTZ	TSDTZ	EDZ1$_{(\kappa = 5/6)}$	EDZ2$_{(\kappa = 1)}$	EDZ3$_{(\kappa = 1)}$	EDZ4$_{(\kappa = 1)}$
DOFs	1310 499	7569	12 615	7569	10 092	12 615	15 138
Thin stiffeners ($\delta_1 = \delta_2 = \delta_3 = \delta_4 = 0.005$ m)							
1	295.670	296.285	295.985	299.202	291.347	298.450	296.300
2	409.346	409.822	409.505	407.900	402.856	411.461	409.722
3	628.255	629.058	628.661	627.579	621.357	631.094	628.805
4	708.349	709.402	708.859	705.684	698.032	711.923	709.090
5	859.502	859.725	859.525	856.245	841.490	861.486	859.944
6	861.205	862.800	861.794	860.760	855.388	867.819	862.506
7	893.055	894.837	894.185	896.128	881.368	898.637	894.444
8	1115.651	1116.622	1116.284	1119.101	1109.399	1118.722	1116.311
9	1137.401	1138.870	1138.308	1145.233	1126.499	1143.560	1138.928
10	1202.283	1204.644	1203.908	1196.650	1181.066	1209.728	1204.120
Moderately thick stiffeners ($\delta_1 = \delta_2 = \delta_3 = \delta_4 = 0.01$ m)							
1	272.760	272.909	272.748	279.271	272.213	276.565	273.680
2	381.659	381.742	381.550	383.314	378.910	384.328	382.239
3	580.204	580.441	580.192	583.573	577.412	583.950	581.016
4	660.616	660.986	660.676	663.923	656.660	665.070	661.634
5	791.469	791.474	791.354	795.846	790.848	794.140	792.094
6	817.706	818.170	817.482	822.272	807.693	826.796	819.710
7	835.960	836.730	836.343	843.632	831.064	842.713	837.623
8	1019.993	1020.486	1020.240	1026.127	1019.000	1023.307	1020.685
9	1059.821	1060.638	1060.241	1074.950	1056.831	1068.969	1062.067
10	1123.590	1124.650	1124.117	1132.625	1117.776	1132.854	1125.842

Thick stiffeners ($\delta_1 = \delta_2 = \delta_3 = \delta_4 = 0.02$ m)							
1	240.014	240.073	239.882	246.970	242.083	244.572	241.247
2	343.452	343.503	343.239	346.847	343.432	346.921	344.361
3	520.225	520.334	520.027	525.276	520.772	524.621	521.332
4	596.731	596.985	596.586	602.645	597.044	602.235	598.170
5	720.441	720.458	720.306	725.039	721.646	723.532	721.250
6	736.676	737.099	736.161	747.189	735.965	748.075	739.631
7	758.181	758.752	758.205	768.046	758.879	766.526	760.426
8	918.893	919.153	918.879	924.957	920.201	922.586	919.765
9	960.832	961.519	960.976	978.244	964.884	972.360	963.913
10	1017.534	1018.357	1017.567	1031.658	1019.558	1029.504	1020.747

Geometric inputs $a = 2.5,\ n = 3,\ [\alpha_{1,0}, \alpha_{1,1}] = [0.2, 0.8], [\alpha_{2,0}, \alpha_{2,1}] = [0, \pi], h_1 = h_3 = 0.01m, h_2 = 0.1\text{m}$

Grid unit pattern layup $\mathrm{F}\left[-45^{\delta_1}_{a_1=0.1414\text{m}}/0^{\delta_2}_{a_2=0.1\text{m}}/45^{\delta_3}_{a_3=0.1414\text{m}}/90^{\delta_4}_{a_4=0.1\text{m}}\right]$, $E_s = 70\text{GPa}$, $\nu_s = 0.3$, $\rho_s = 2707\text{kg/m}^3$

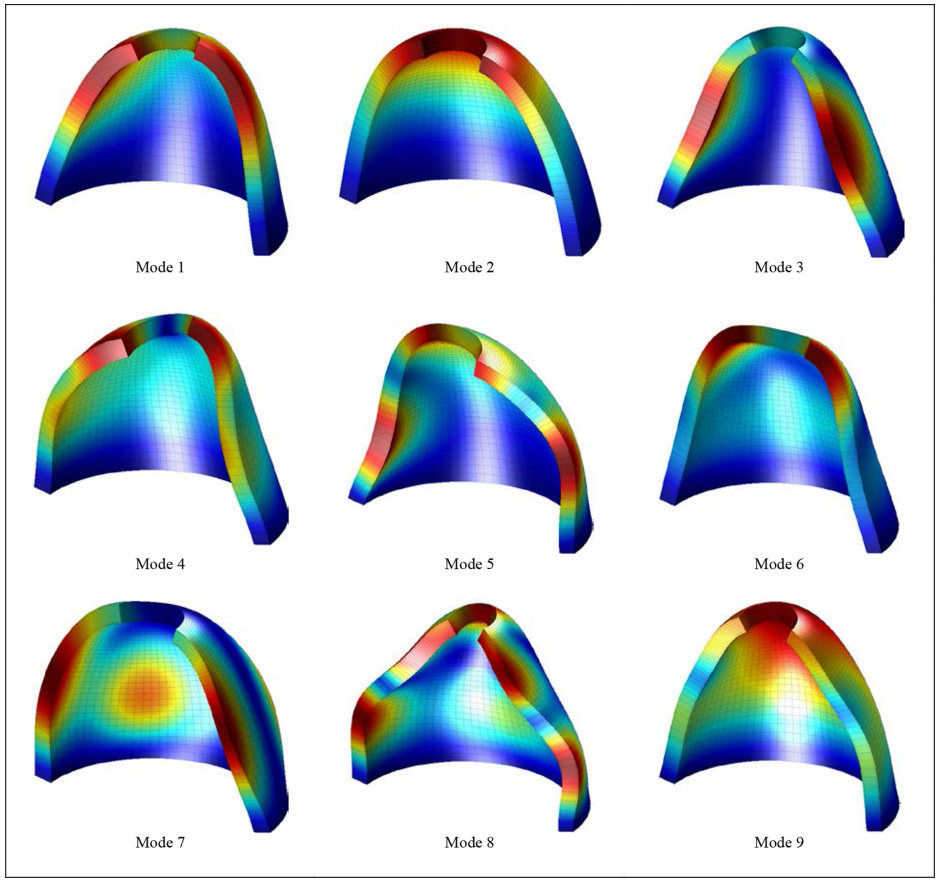

Figure 1.6. Mode shapes of a cantilever (FCFF) revolution paraboloidal panel with a lattice core made of a grid with four symmetric moderately thick rib families.

interlaminar phenomena. For this reason, even a classical third order theory by Reddy [53] behaves well together with the zig-zag strategy (1.9). The accuracy of the proposed model for grid structures seems to be unaffected by the width δ_i for each frame, as visible in both tables 1.4 and 1.5, except for CFCF shell structures with thick stiffeners $\delta_i = 0.02$ m, for which the EDZ4 formulation seems to provide the highest level of accuracy among results. Figure 1.6 depicts the first nine mode shapes of a moderately thick cantilevered paraboloidal panel. In this case, the influence of geometry becomes crucial for the overall response, because of the transversely-isotropic behaviour of the unit cell made of four ribs families. Actually, the proposed higher order model is capable of providing both symmetric and antisymmetric modal deformations, as well as all possible complex stretching effects that occur along the shell thickness, due to the interlaminar interactions.

The last set of examples considers a doubly-curved shell structure reinforced by a honeycomb central layer with $h = 5$ mm. More specifically, a helicoidal panel is modelled according to an ESL method, whose geometry definition in the principal

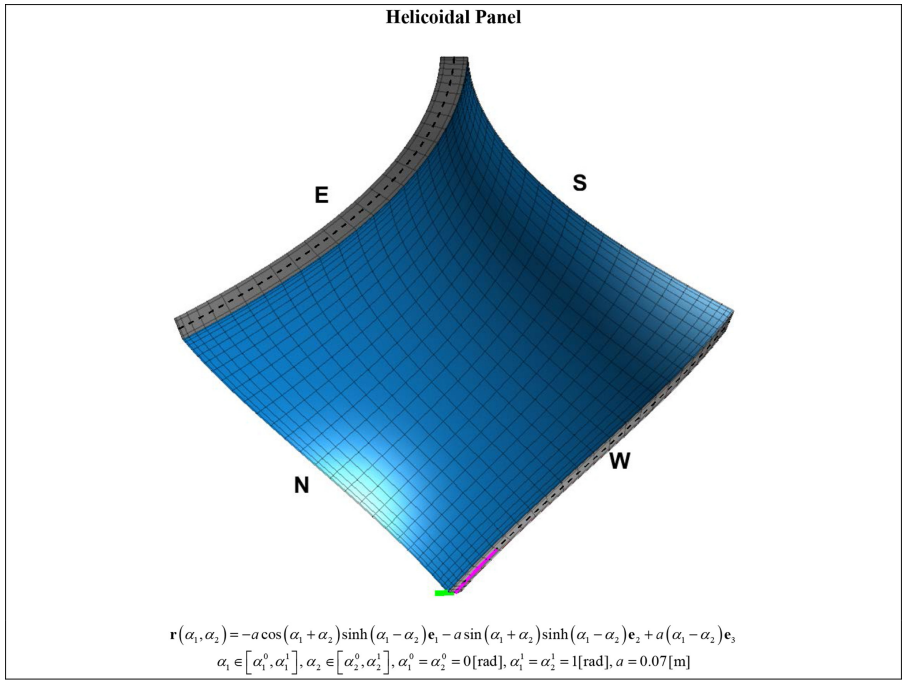

Figure 1.7. Geometric representation of a helicoidal panel in the principal reference system.

reference system can be found in figure 1.7. Also, in this case we compute the first ten mode frequencies of the structure, while keeping a CFFC boundary restraint. Three different unit cells are here implemented, with geometrical properties as defined in figure 1.3. For each selected case, the helicoidal panel assumes both thin ($s_2 = s = 0.1$ mm) and thick ($s_2 = s = 0.4$ mm) cell walls, whose results are summarized in table 1.6 under the assumption of hexagonal ($\vartheta = 30\,°$) honeycomb softcore. We recall that a transversely isotropic behaviour is provided by the cell unit at issue. For both thin cells or thick walls, the numerical results for each mode, always converge to the frequency predictions by the EDZ4 theory. Similarly, in table 1.7 we summarize the natural frequencies for the helicoidal panel (figure 1.7) with a lattice layer consisting of a series of rectangular thin-walled cells, as predicted by different HSDTs. Assuming the EDZ4-based solution as the reference one, it is worth noticing that lower order theories embedding a reduced number of DOFs provide results with a lower precision, and a higher dispersion. The same behaviour can be observed in table 1.8 for a helicoidal structure embedding a lattice layer with re-entrant cells. Based on results in this table, the accuracy of the proposed model depends on the shear correction factor assumption, $k(\zeta)$, when lower EDZ-N theories are taken on. In this case, results based on the EDZ1 theory are very accurate (if compared to EDZ4 predictions), when keeping $k(\zeta) = 5/6$. On the other hand, an EDZ2 theory does not require any shear correction factor, which corresponds to the assumption $k(\zeta) = 1$. Figure 1.8 plots the first nine mode shapes for the helicoidal shell with a central layer infilled by re-entrant cells, as computed

Table 1.6. Natural frequencies of a CFFC helicoid with a central layer made of a hexagonal honeycomb pattern. Both lattice layer and laminated structure are obtained using an isotropic aluminum material. The shell reference surface equation and homogenized geometric representation, can be found in figure 1.7.

CFFC helicoid—hexagonal honeycomb ($\vartheta = 30$ °)							
f [Hz]	FSDT	FSDTZ	TSDTZ	EDZ1$_{(\kappa = 5/6)}$	EDZ2$_{(\kappa = 1)}$	EDZ3$_{(\kappa = 1)}$	EDZ4$_{(\kappa = 1)}$
DOFs	5046	7569	12 615	7569	10 092	12 615	15 138
Thin cell wall ($s_2 = s = 0.1$ mm)							
1	1901.469	1384.682	1369.790	1397.930	1372.781	1372.574	1371.561
2	5440.802	3075.498	3024.351	2978.919	3040.084	3039.625	3033.426
3	7200.263	5736.547	5619.536	5510.106	5678.348	5677.392	5616.769
4	9808.352	6071.326	6028.289	5984.357	6048.407	6048.172	6025.510
5	12 458.479	6650.659	6597.278	6503.599	6636.379	6635.752	6598.467
6	12 500.523	7120.994	7039.499	6992.425	7079.268	7078.641	7038.838
7	15 075.318	8079.437	7913.276	7776.675	8043.259	8041.805	7918.052
8	15 129.797	8276.879	8171.826	8057.320	8245.237	8244.043	8173.664
9	17 601.664	8796.553	8664.116	8458.876	8777.101	8775.519	8665.228
10	17 672.505	9601.631	9515.206	9415.605	9588.348	9586.988	9515.458
Thick cell wall ($s_2 = s = 0.4$ mm)							
1	1831.307	1619.522	1617.284	1685.304	1621.252	1621.129	1615.236
2	5245.850	4069.307	4057.935	4036.202	4069.460	4069.004	4066.557
3	6951.404	6427.256	6421.781	6407.768	6429.068	6428.884	6426.882
4	9459.418	7943.127	7921.035	7801.382	7941.569	7940.807	7924.483
5	12 027.494	8216.985	8190.301	8109.838	8226.726	8225.500	8192.869
6	12 080.949	8826.772	8803.462	8664.301	8841.335	8839.626	8806.206
7	14 555.770	10 927.142	10 893.238	10 758.833	10 939.184	10 937.711	10 898.382
8	14 619.663	11 387.890	11 343.713	11 088.905	11 410.372	11 408.197	11 348.666
9	17 022.254	11 947.596	11 890.926	11 566.973	11 969.830	11 967.607	11 897.558
10	17 079.829	12 867.759	12 822.489	12 544.019	12 894.360	12 891.985	12 832.541
Geometric inputs $a = 0.07$, $[\alpha_{1,0}, \alpha_{1,1}] = [0, 1]$, $[\alpha_{2,0}, \alpha_{2,1}] = [0, 1]$, $h_1 = h_3 = 0.001$ m, $h_2 = 0.005$ m							
Honeycomb cell configuration $l_2 = 5.1320$ mm, $l = 5.1320$ mm, $E_s = 70$ GPa, $\nu_s = 0.33$, $\rho_s = 2700$ kg/m^3							

Table 1.7. Natural frequencies of a CFFC helicoid with a central layer made of rectangular honeycomb patterns. Both lattice layer and laminated structure are obtained using an isotropic aluminum material. The shell reference surface equation and homogenized geometric representation, can be found in figure 1.7.

CFFC helicoid—rectangular honeycomb ($\vartheta = 0\,°$)							
f [Hz]	FSDT	FSDTZ	TSDTZ	EDZ1$_{(\kappa = 5/6)}$	EDZ2$_{(\kappa = 1)}$	EDZ3$_{(\kappa = 1)}$	EDZ4$_{(\kappa = 1)}$
DOFs	5046	7569	12 615	7569	10 092	12 615	15 138
Thin cell wall ($s_2 = s = 0.1$ mm)							
1	1899.474	1398.420	1384.941	1413.976	1387.832	1387.623	1387.372
2	5435.346	3115.892	3068.028	3018.652	3083.371	3082.947	3076.455
3	7194.844	5859.476	5747.672	5622.272	5804.487	5803.542	5743.433
4	9798.266	6082.516	6042.589	5997.343	6061.101	6060.878	6039.218
5	12 446.595	6680.345	6628.924	6529.338	6668.063	6667.481	6628.443
6	12 489.314	7168.996	7093.391	7045.314	7129.120	7128.514	7092.721
7	15 058.076	8319.927	8170.666	8013.312	8272.609	8271.356	8170.866
8	15 147.805	8417.657	8305.618	8162.537	8403.019	8401.691	8311.268
9	17 586.229	8723.656	8593.832	8395.159	8705.914	8704.431	8594.762
10	17 655.802	9686.337	9608.275	9501.697	9672.919	9671.624	9606.560
Thick cell wall ($s_2 = s = 0.4$ mm)							
1	1824.397	1623.346	1621.351	1691.256	1625.614	1625.479	1621.495
2	5226.970	4102.912	4092.635	4074.371	4104.457	4104.008	4101.463
3	6932.722	6427.125	6422.306	6407.380	6428.664	6428.481	6425.164
4	9424.258	7996.494	7979.099	7901.775	7995.142	7994.445	7984.782
5	11 983.870	8430.859	8404.748	8301.309	8446.400	8444.920	8406.706
6	12 044.475	8756.603	8734.862	8579.431	8770.994	8769.354	8734.729
7	14 493.179	11 078.160	11 051.632	10 949.204	11 095.344	11 093.916	11 057.247
8	14 688.463	11 474.772	11 432.019	11 184.910	11 495.588	11 493.472	11 436.203
9	16 959.363	12 341.060	12 290.581	11 945.627	12 371.351	12 368.905	12 299.895
10	17 038.859	12 887.904	12 845.014	12 473.943	12 918.498	12 915.807	12 849.926

Geometric inputs $a = 0.07$, $[\alpha_{1,0}, \alpha_{1,1}] = [0, 1]$, $[\alpha_{2,0}, \alpha_{2,1}] = [0, 1]$, $h_1 = h_3 = 0.001\ m$, $h_2 = 0.005$ m

Honeycomb cell configuration $l_2 = 5.1320$ mm, $l = 5.1320$ mm, $E_s = 70$ GPa, $\nu_s = 0.33$, $\rho_s = 2700$ kg/m^3

Table 1.8. Natural frequencies of an helicoid with general constraints (CFFC) with a central layer made of re-entrant honeycomb patterns. Cell configurations and geometric layups are reported in the table. Both the lattice layer and the laminated structure are obtained from isotropic aluminum. Shell reference surface equation, as well as an homogenized geometric representation, can be found in figure 1.7.

CFFC helicoid—re-entrant honeycomb ($\vartheta = -30°$)

f [Hz]	FSDT	FSDTZ	TSDTZ	EDZ1$_{(\kappa = 5/6)}$	EDZ2$_{(\kappa = 1)}$	EDZ3$_{(\kappa = 1)}$	EDZ4$_{(\kappa = 1)}$
DOFs	5046	7569	12 615	7569	10 092	12 615	15 138
Thin cell wall ($s_2 = s = 0.1$ mm)							
1	1882.924	1453.037	1443.648	1479.484	1446.649	1446.475	1446.692
2	5389.094	3310.940	3274.628	3216.800	3288.546	3288.170	3281.727
3	7132.567	6166.235	6143.234	6067.371	6153.501	6153.330	6140.107
4	9714.606	6318.167	6228.764	6103.897	6279.411	6278.451	6223.805
5	12 345.413	6972.306	6921.356	6777.417	6963.239	6962.501	6917.637
6	12 385.037	7387.383	7335.057	7288.318	7358.028	7357.434	7334.676
7	14 937.200	8828.222	8727.181	8545.861	8801.618	8800.386	8727.314
8	15 032.210	9175.225	9070.433	8827.154	9172.266	9170.825	9073.699
9	17 430.734	9200.075	9076.879	8831.276	9182.041	9180.536	9076.947
10	17 510.058	10 028.989	9962.868	9828.811	10 017.484	10 016.177	9957.399
Thick cell wall ($s_2 = s = 0.4$ mm)							
1	1768.134	1611.534	1610.122	1686.200	1615.997	1615.806	1613.245
2	5069.486	4171.982	4164.742	4173.226	4178.608	4178.079	4174.547
3	6719.991	6315.639	6311.870	6307.958	6317.130	6316.699	6309.437
4	9138.789	7997.866	7987.234	7982.568	8001.452	8000.628	7995.157
5	11 643.630	8761.084	8740.231	8692.208	8788.224	8786.395	8743.833
6	11 683.228	8909.241	8893.312	8708.274	8931.379	8929.270	8891.586
7	14 098.480	11 227.478	11 208.324	11 170.876	11 253.354	11 251.477	11 210.687
8	14 282.876	11 851.278	11 819.548	11 610.178	11 882.096	11 879.703	11 828.328
9	16 438.322	12 954.898	12 920.986	12 691.910	13 000.381	12 997.732	12 939.300
10	16 519.338	13 336.736	13 303.328	12 874.136	13 376.037	13 372.435	13 304.305
Geometric inputs $a = 0.07$, $[\alpha_{1,0}, \alpha_{1,1}] = [0, 1]$, $[\alpha_{2,0}, \alpha_{2,1}] = [0, 1]$, $h_1 = h_3 = 0.001\ m$, $h_2 = 0.005$ m							
Honeycomb cell configuration $l_2 = 5.1320$ mm, $l = 5.1320$ mm, $E_s = 70$ GPa, $\nu_s = 0.33$, $\rho_s = 2700$ kg/m^3							

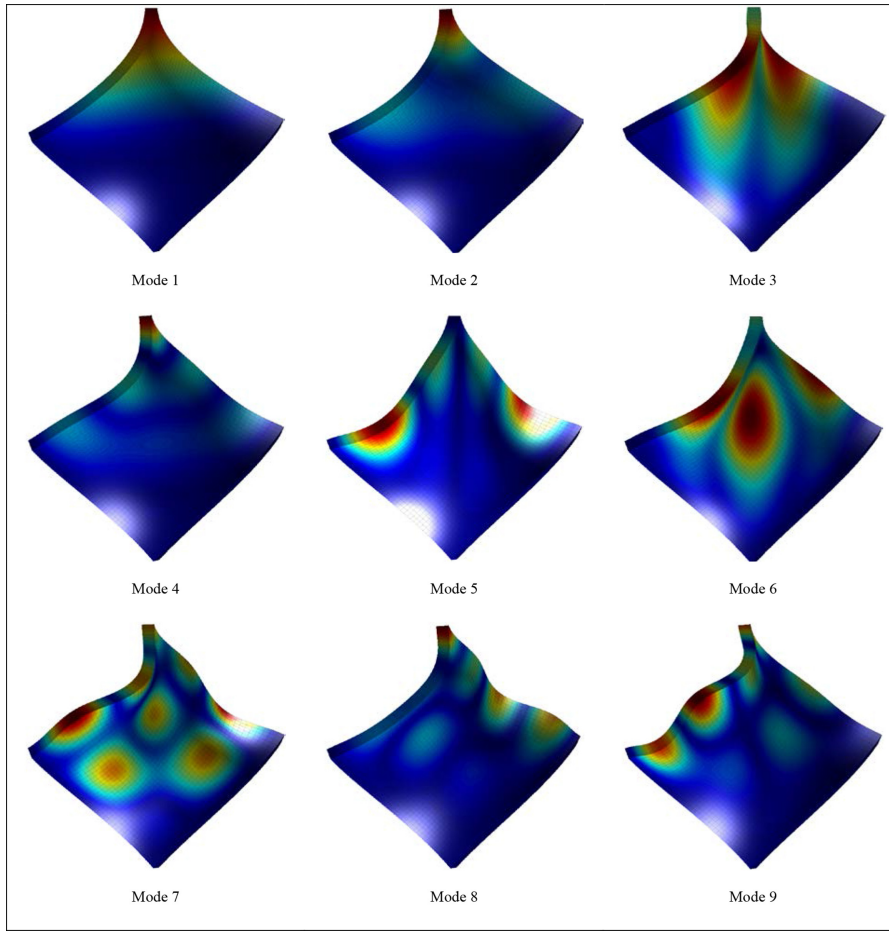

Figure 1.8. Mode shapes of a CFFC helicoidal panel with a re-entrant ($\vartheta = -30\,°$) lattice core.

with an EDZ4 theory. Based on these plots, the present approach is confirmed to be capable of getting the bending deformations in each principal direction. For higher vibration modes, the out-of-plane waves are visible in both principal directions, together with the warping effects.

1.4 Conclusions

In the present chapter an innovative strategy based on the GDQ method has been proposed for the free vibration analysis of sandwich and laminated structures with variable curvatures with a central layer made of a honeycomb pattern or stiffeners system. The fundamental equations have been derived employing the ESL approach, where a generalized through-the-thickness assumption has been considered along with different higher order theories. Within each layer, a completely anisotropic elastic behaviour has been modelled, once a general rotation of the material reference system has been provided. Based on a homogenization method, a smeared

orthotropic continuum has been provided, depending on the material properties and geometric features. A different in-plane constitutive behaviour has been provided, based on the variation of the internal cell angle. After the definition of a repetitive unit, the rib unit cell has been homogenized by assuming a thin-walled hypothesis, taking into account the axial contribution of each frame and the independence from the number of grid nodes. The fundamental equation of the problem together with the BCs are derived from the Hamiltonian Principle in its variational formulation. After the assembly procedure of the governing equations by means of the GDQ method, a free vibration analysis has been provided for different lattice and honeycomb shells. The results have been systematically compared to those provided by highly computational demanding finite elements, with a great accordance in terms of mode frequencies and shapes. The proposed higher order formulation based on a homogenized continuum modelling has been revealed to be a reliable design tool to treat complicated structures with latticed and honeycomb cores, with respect to high demanding 3D finite element simulations.

References

[1] Bauer J, Meza L R, Schaedler T A, Schwaiger R and Valdevit L 2017 Nanolattices: an emerging class of mechanical metamaterials *Adv. Mater.* **29** 1701850

[2] Dell'Isola F, Seppecher P, Alibert J J and Lekszycki T *et al* 2019 Pantographic metamaterials: an example of mathematically driven design and of its technological challenges *Continuum Mech. Thermodyn.* **31** 854–84

[3] Liddell I 2015 Frei Otto and the development of gridshells *Case Stud. Struct. Eng.* **4** 39–49

[4] Haftka R T and Grandhi R V 1986 Structural shape optimization—a survey *Comput. Meth. Appl. Mech. Eng.* **57** 91–106

[5] Ashby M F and Cebon D 1993 Materials selection in mechanical design *J. Phys. IV* **3** C7–1

[6] Vasiliev V V, Barynin V A and Rasin A F 2001 Anisogrid lattice structures—survey of development and application *Compos. Struct.* **54** 361–70

[7] Vasiliev V V, Barynin V A and Rasin A F 2009 Anisogrid composite lattice structures—development and space applications *Compos. Nanostruct.* **3** 38–50

[8] Van Quyen N, Van Thanh N, Quan T Q and Duc N D 2021 Nonlinear forced vibration of sandwich cylindrical panel with negative Poisson's ratio auxetic honeycombs core and CNTRC face sheets *Thin-Walled Struct.* **162** 107571

[9] Kalamkarov A L, Andrianov I V and Danishevsâ V V 2009 Asymptotic homogenization of composite materials and structures *Appl. Mech. Rev.* **62** 030802

[10] Gitman I, Askes H and Sluys L 2007 Representative volume: existence and size determination *Eng. Fract. Mech.* **74** 2518–34

[11] Tornabene F, Dimitri R and Brischetto S 2019 Higher-order formulation for the mechanical analysis of laminated and latticed shells with complex geometries and materials *Advances in Boundary Element and Meshless Techniques XX* ed I Benedetti, A Milazzo and F M H Aliabadi (Eastleigh (UK): EC Ltd))

[12] Tornabene F and Dimitri R 2020 Higher-order modelling of anisogrid lattice shell structures with complex geometries *18th Int. Conf. of Numerical Analysis and Applied Mathematics (ICNAAM2020) Proc. (Rhodes, Greece, 17–23 September)*

[13] Khisaeva Z F and Ostoja-Starzewski M 2006 On the size of RVE in finite elasticity of random composites *J. Elast.* **85** 153
[14] Belytschko T, Loehnert S and Song J H 2008 Multiscale aggregating discontinuities: a method for circumventing loss of material stability *Int. J. Numer. Methods Eng.* **73** 869–94
[15] Oliver J 1996 Modelling strong discontinuities in solid mechanics via strain softening constitutive equations. Part 1: Fundamentals *Int. J. Numer. Methods Eng.* **39** 3575–600
[16] Oliver J and Huespe A E 2004 Continuum approach to material failure in strong discontinuity settings *Comput. Meth. Appl. Mech. Eng.* **193** 3195–220
[17] Oliver J and Huespe A E 2004 Theoretical and computational issues in modelling material failure in strong discontinuity scenarios *Comput. Meth. Appl. Mech. Eng.* **193** 2987–3014
[18] Burton W S and Noor A K 1997 Assessment of continuum models for sandwich panel honeycomb cores *Comput. Meth. Appl. Mech. Eng.* **145** 341–60
[19] Lee J, Choi J B and Choi K 1996 Application of homogenization FEM analysis to regular and re-entrant honeycomb structures *J. Mater. Sci.* **31** 4105–10
[20] Potluri R and Rao U K 2017 Determination of elastic properties of reverted hexagonal honeycomb core: FEM approach *Mater. Today Proc.* **4** 8645–53
[21] Burlayenko V N and Sadowski T 2010 Effective elastic properties of foam-filled honeycomb cores of sandwich panels *Compos. Struct.* **92** 2890–900
[22] Réthoré J, Dang T B T and Kaltenbrunner C 2017 Anisotropic failure and size effects in periodic honeycomb materials: a gradient-elasticity approach *J. Mech. Phys. Solids* **99** 35–49
[23] Catapano A and Montemurro M 2014 A multi-scale approach for the optimum design of sandwich plates with honeycomb core. Part I: homogenization of core properties *Compos. Struct.* **118** 664–76
[24] Gibson L J and Ashby M F 1999 *Cellular Solids: Structure and Properties* (Cambridge: Cambridge University Press)
[25] Chen D H, Horii H and Ozaki S 2009 Analysis of in-plane elastic modulus for a hexagonal honeycomb core: analysis of Young's modulus and shear modulus *J. Comput. Sci. Technol.* **3** 1–12
[26] Sorohan S, Sandu M, Constantinescu D M and Sandu A G 2016 Estimation of out of plane shear moduli for honeycomb cores with modal finite element analyses *Romanian J. Tech. Sci. Appl. Mech.* **61** 71–88
[27] Xu X F and Qiao P 2002 Homogenized elastic properties of honeycomb sandwich with skin effect *Int. J. Solids Struct.* **39** 2153–88
[28] Kelsey S, Gellatly R and Clark B 1958 The shear modulus of foil honeycomb cores *Aircr. Eng. Aerosp. Technol.* **30** 294–302
[29] Grediac M 1993 A finite element study of the transverse shear in honeycomb cores *Int. J. Solids Struct.* **30** 1777–88
[30] Scarpa F and Tomlin P 2000 On the transverse shear modulus of negative Poisson ratio honeycomb structures *Fatigue Fract. Eng. Mater. Struct.* **23** 717–20
[31] Malek S and Gibson L 2015 Effective elastic properties of periodic hexagonal honeycombs *Mech. Mater.* **91** 226–40
[32] Timoshenko S and Goodier J 2011 *Theory of Elasticity* (New York: Mc-Graw Hill)
[33] Roark R J, Young W C and Plunkett R 1976 Formulas for stress and strain *J. Appl. Mech.* **43** 522
[34] Sorohan S, Sandu M, Constantinescu D M and Sandu A G 2015 On the evaluation of mechanical properties of honeycombs by using finite element analyses *INCAS Bull.* **7** 135–50

[35] Fu M-H and Yin J R 1999 Equivalent elastic parameters of the honeycomb core *Acta Mech. Sin.* **15** 113–18
[36] Torabi K, Afshari H and Aboutalebi F H 2019 Vibration and flutter analyses of cantilever trapezoidal honeycomb sandwich plates *J. Sandw. Struct. Mater.* **21** 2887–920
[37] Sorohan S, Constantinescu D M, Sandu M and Sandu A G 2018 On the homogenization of hexagonal honeycombs under axial and shear loading. Part I: analytical formulation for free skin effect *Mech. Mater.* **119** 74–91
[38] Sorohan S, Constantinescu D M, Sandu M and Sandu A G 2018 On the homogenization of hexagonal honeycombs under axial and shear loading. Part II: comparison of free skin and rigid skin effects on effective core properties *Mech. Mater.* **119** 92–108
[39] Tornabene F, Viscoti M, Dimitri R and Aiello M A 2021 Higher Order Formulations for doubly-curved shell structures with a honeycomb core *Thin-Walled Struct.* **164** 107789
[40] Tornabene F, Viscoti M, Dimitri R and Aiello M A 2021 Higher-order modelling of anisogrid composite lattice structures with complex geometries *Eng. Struct.* **244** 112686
[41] Calladine C R 1989 *Theory of Shell Structures* (Cambridge: Cambridge University Press)
[42] Kraus H 1967 *Thin Elastic Shells* (New York: Wiley)
[43] Gould P L 1999 *Analysis of Plates and Shells* (Upper Saddle River, NJ: Prentice-Hall)
[44] Li D 2020 Layer-wise theories of laminated composite structures and their applications: A review *Arch. Comput. Meth. Eng.* **28** 577–600
[45] Reddy J N 1993 An evaluation of equivalent-single-layer and layerwise theories of composite laminates *Compos. Struct.* **25** 21–35
[46] Tornabene F, Fantuzzi N, Viola E and Batra R C 2015 Stress and strain recovery for functionally graded free-form and doubly-curved sandwich shells using higher-order equivalent single layer theory *Compos. Struct.* **119** 67–89
[47] Love A E H 1944 *A Treatise on the Mathematical Theory of Elasticity* (New York: Dover Publication)
[48] Germain S 2013 *Recherches sur la théorie des surfaces élastiques* (Cambridge: Cambridge University Press)
[49] Reissner E 1945 The effect of transverse shear deformation on the bending of elastic plates *J. Appl. Mech. ASME* **12** 66–77
[50] Mindlin R D 1951 Thickness-shear and flexural vibrations of crystal plates *J. Appl. Phys.* **22** 316–23
[51] Arefi M, Mohammadi M, Tabatabaeian A, Dimitri R and Tornabene F 2018 Two-dimensional thermo-elastic analysis of FG-CNTRC cylindrical pressure vessels *Steel Compos. Struct.* **27** 525–36
[52] Reddy J N 2003 *Mechanics of Laminated Composite Plates and Shells* (Boca Raton, FL: CRC Press)
[53] Reddy J N 1986 A refined shear deformation theory for the analysis of laminated plates *NASA Contractor Report* 3955
[54] Mohammadi M, Arefi M, Dimitri R and Tornabene F 2019 Higher-order thermo-elastic analysis of FG-CNTRC cylindrical vessels surrounded by a Pasternak foundation *Nanomaterials* **9** 79
[55] Washizu K 1975 *Variational Methods in Elasticity and Plasticity* (Oxford: Pergamon)
[56] Reddy J N 1987 A generalization of two-dimensional theories of laminated composite plates *Commun. Appl. Numer. Methods* **3** 173–80

[57] Tornabene F and Bacciocchi M 2018 *Anisotropic Doubly-Curved Shells. Higher-Order Strong and Weak Formulations for Arbitrarily Shaped Shell Structures* (Bologna: Società Editrice Esculapio)
[58] Tornabene F, Bacciocchi M, Fantuzzi N and Viola E 2016 *Laminated Composite Doubly-Curved Shell Structures: Differential Geometry Higher-Order Structural Theories* (Bologna: Società Editrice Esculapio)
[59] Tornabene F 2016 General higher-order layer-wise theory for free vibrations of doubly-curved laminated composite shells and panels *Mech. Adv. Mater. Struct.* **23** 1046–67
[60] Tornabene F, Viscoti M and Dimitri R 2022 Generalized higher order layerwise theory for the dynamic study of anisotropic doubly-curved shells with a mapped geometry *Eng. Anal. Bound. Elem.* **134** 147–83
[61] Lopatin A V, Morozov E V and Shatov A V 2016 An analytical expression for fundamental frequency of the composite lattice cylindrical shell with clamped edges *Compos. Struct.* **141** 232–39
[62] Lopatin A V, Morozov E V and Shatov A V 2018 Fundamental frequency of a composite anisogrid lattice cylindrical panel with clamped edges *Compos. Struct.* **201** 200–7
[63] Morozov E V, Lopatin A V and Nesterov V A 2011 Finite-element modelling and buckling analysis of anisogrid composite lattice cylindrical shells *Compos. Struct.* **93** 308–23
[64] Shu C 2000 *Differential Quadrature and Its Application in Engineering* (London: Springer)
[65] Shu C, Ding H and Yeo K S 2003 Local radial basis function-based differential quadrature method and its application to solve two-dimensional incompressible Navier–Stokes equations *Comput. Meth. Appl. Mech. Eng.* **192** 941–54
[66] Bellman R and Casti J 1971 Differential quadrature and long-term integration *J. Math. Anal. Appl.* **34** 235–38
[67] Zong Z and Zhang Y 2009 *Advanced Differential Quadrature Methods* (Boca Raton, FL: CRC Press)
[68] Tornabene F, Fantuzzi N, Ubertini F and Viola E 2015 Strong formulation finite element method based on differential quadrature: a survey *Appl. Mech. Rev.* **67** 20801
[69] Quan J R and Chang C T 1989 New insights in solving distributed system equations by the quadrature method—I. Analysis *Comput. Chem. Eng.* **13** 779–88
[70] Tornabene F, Liverani A and Caligiana G 2011 FGM and laminated doubly curved shells and panels of revolution with a free-form meridian: a 2-D GDQ solution for free vibrations *Int. J. Mech. Sci.* **53** 446–70
[71] Tornabene F and Reddy J N 2013 FGM and laminated doubly-curved and degenerate shells resting on nonlinear elastic foundations: a GDQ solution for static analysis with *a posteriori* stress and strain recovery *J. Indian Inst. Sci.* **93** 635–88
[72] Tornabene F and Bacciocchi M 2018 Effect of curvilinear reinforcing fibers on the linear static behavior of soft-core sandwich structures *J. Compos. Sci.* **2** 14
[73] Tornabene F, Bacciocchi M, Fantuzzi N and Reddy J N 2019 Multiscale approach for three-phase CNT/polymer/fiber laminated nanocomposite structures *Polym. Compos.* **40** E102–26
[74] Zare Jouneghani F, Dimitri R, Bacciocchi M and Tornabene F 2017 Free vibration analysis of functionally graded porous doubly-curved shells based on the first-order shear deformation theory *Appl. Sci.* **7** 1252
[75] Shen J, Wang H and Zheng S 2018 Size-dependent pull-in analysis of a composite laminated micro-beam actuated by electrostatic and piezoelectric forces: generalized differential quadrature method *Int. J. Mech. Sci.* **135** 353–61
[76] Hua L I and Lam K Y 1998 Frequency characteristics of a thin rotating cylindrical shell using the generalized differential quadrature method *Int. J. Mech. Sci.* **40** 443–59

[77] Dastjerdi S, Malikan M, Dimitri R and Tornabene F 2021 Nonlocal elasticity analysis of moderately thick, porous functionally graded plates in a hygro-thermal environment *Compos. Struct.* **255** 112925
[78] Bert C W and Malik M 1996 Differential quadrature method in computational mechanics: a review *Appl. Mech. Rev.* **49** 1–28
[79] Shu C, Chen W, Xue H and Du H 2001 Numerical study of grid distribution effect on accuracy of DQ analysis of beams and plates by error estimation of derivative approximation *Int. J. Numer. Methods Eng.* **51** 159–79
[80] Fazzolari F A, Viscoti M, Dimitri R and Tornabene F 2020 1D-hierarchical Ritz and 2D-GDQ formulations for the free vibration analysis of circular/elliptical cylindrical shells and beam structures *Compos. Struct.* **258** 113338
[81] Tornabene F, Fantuzzi N and Bacciocchi M 2018 Strong and weak formulations based on differential and integral quadrature methods for the free vibration analysis of composite plates and shells: convergence and accuracy *Eng. Anal. Boundary Elem.* **92** 3–37
[82] Fantuzzi N, Tornabene F, Bacciocchi M and Ferreira A J M 2018 On the convergence of laminated composite plates of arbitrary shape through finite element models *J. Compos. Sci.* **2** 16
[83] Shu C and Wee K H A 2002 Numerical simulation of natural convection in a square cavity by simple generalized differential quadrature method *Comput. Fluids* **31** 209–26
[84] Chen C N 2000 A generalized differential quadrature element method *Comput. Meth. Appl. Mech. Eng.* **188** 553–66
[85] Dimitri R, Fantuzzi N, Tornabene F and Zavarise G 2016 Innovative numerical methods based on SFEM and IGA for computing stress concentrations in isotropic plates with discontinuities *Int. J. Mech. Sci.* **118** 166–87
[86] Dimitri R, Tornabene F and Reddy J N 2020 Numerical study of the mixed-mode behaviour of generally-shaped composite interfaces *Compos. Struct.* **237** 111935
[87] Dimitri R, Fantuzzi N, Li Y and Tornabene F 2017 Numerical computation of the crack development and SIF in composite materials with XFEM and SFEM *Compos. Struct.* **160** 468–90
[88] Hong C C 2017 GDQ analysis of a beam-plate with delamination *Compos. Struct.* **182** 237–41
[89] Viola E, Dilena M and Tornabene F 2007 Analytical and numerical results for vibration analysis of multi-stepped and multi-damaged circular arches *J. Sound Vib.* **299** 143–63
[90] Shu C and Du H 1997 A generalized approach for implementing general boundary conditions in the GDQ free vibration analysis of plates *Int. J. Solids Struct.* **34** 837–46
[91] Shu C and Wang C M 1999 Treatment of mixed and nonuniform boundary conditions in GDQ vibration analysis of rectangular plates *Eng. Struct.* **21** 125–34
[92] Brischetto S, Tornabene F, Fantuzzi N and Bacciocchi M 2017 Interpretation of boundary conditions in the analytical and numerical shell solutions for mode analysis of multi-layered structures *Int. J. Mech. Sci.* **122** 18–28
[93] Tornabene F and Viola E 2013 Static analysis of functionally graded doubly-curved shells and panels of revolution *Meccanica* **48** 901–30
[94] Tornabene F, Viscoti M, Dimitri R and Reddy J N 2021 Higher order theories for the vibration study of doubly-curved anisotropic shells with a variable thickness and isogeometric mapped geometry *Compos. Struct.* **267** 113829
[95] Tornabene F, Fantuzzi N and Bacciocchi M 2018 *DiQuMASPAB: Differential Quadrature for Mechanics of Anisotropic Shells, Plates, Arches and Beams* (Bologna: Società Editrice Esculapio)

Full list of references

Chapter 1

[1] Bauer J, Meza L R, Schaedler T A, Schwaiger R and Valdevit L 2017 Nanolattices: an emerging class of mechanical metamaterials *Adv. Mater.* **29** 1701850

[2] Dell'Isola F, Seppecher P, Alibert J J and Lekszycki T *et al* 2019 Pantographic metamaterials: an example of mathematically driven design and of its technological challenges *Continuum Mech. Thermodyn.* **31** 854–84

[3] Liddell I 2015 Frei Otto and the development of gridshells *Case Stud. Struct. Eng.* **4** 39–49

[4] Haftka R T and Grandhi R V 1986 Structural shape optimization—a survey *Comput. Meth. Appl. Mech. Eng.* **57** 91–106

[5] Ashby M F and Cebon D 1993 Materials selection in mechanical design *J. Phys. IV* **3** C7–1

[6] Vasiliev V V, Barynin V A and Rasin A F 2001 Anisogrid lattice structures—survey of development and application *Compos. Struct.* **54** 361–70

[7] Vasiliev V V, Barynin V A and Rasin A F 2009 Anisogrid composite lattice structures—development and space applications *Compos. Nanostruct.* **3** 38–50

[8] Van Quyen N, Van Thanh N, Quan T Q and Duc N D 2021 Nonlinear forced vibration of sandwich cylindrical panel with negative Poisson's ratio auxetic honeycombs core and CNTRC face sheets *Thin-Walled Struct.* **162** 107571

[9] Kalamkarov A L, Andrianov I V and Danishevsâ V V 2009 Asymptotic homogenization of composite materials and structures *Appl. Mech. Rev.* **62** 030802

[10] Gitman I, Askes H and Sluys L 2007 Representative volume: existence and size determination *Eng. Fract. Mech.* **74** 2518–34

[11] Tornabene F, Dimitri R and Brischetto S 2019 Higher-order formulation for the mechanical analysis of laminated and latticed shells with complex geometries and materials *Advances in Boundary Element and Meshless Techniques XX* ed I Benedetti, A Milazzo and F M H Aliabadi (Eastleigh (UK): EC Ltd))

[12] Tornabene F and Dimitri R 2020 Higher-order modelling of anisogrid lattice shell structures with complex geometries *18th Int. Conf. of Numerical Analysis and Applied Mathematics (ICNAAM2020) Proc. (Rhodes, Greece, 17–23 September)*

[13] Khisaeva Z F and Ostoja-Starzewski M 2006 On the size of RVE in finite elasticity of random composites *J. Elast.* **85** 153

[14] Belytschko T, Loehnert S and Song J H 2008 Multiscale aggregating discontinuities: a method for circumventing loss of material stability *Int. J. Numer. Methods Eng.* **73** 869–94

[15] Oliver J 1996 Modelling strong discontinuities in solid mechanics via strain softening constitutive equations. Part 1: Fundamentals *Int. J. Numer. Methods Eng.* **39** 3575–600

[16] Oliver J and Huespe A E 2004 Continuum approach to material failure in strong discontinuity settings *Comput. Meth. Appl. Mech. Eng.* **193** 3195–220

[17] Oliver J and Huespe A E 2004 Theoretical and computational issues in modelling material failure in strong discontinuity scenarios *Comput. Meth. Appl. Mech. Eng.* **193** 2987–3014

[18] Burton W S and Noor A K 1997 Assessment of continuum models for sandwich panel honeycomb cores *Comput. Meth. Appl. Mech. Eng.* **145** 341–60

[19] Lee J, Choi J B and Choi K 1996 Application of homogenization FEM analysis to regular and re-entrant honeycomb structures *J. Mater. Sci.* **31** 4105–10

[20] Potluri R and Rao U K 2017 Determination of elastic properties of reverted hexagonal honeycomb core: FEM approach *Mater. Today Proc.* **4** 8645–53
[21] Burlayenko V N and Sadowski T 2010 Effective elastic properties of foam-filled honeycomb cores of sandwich panels *Compos. Struct.* **92** 2890–900
[22] Réthoré J, Dang T B T and Kaltenbrunner C 2017 Anisotropic failure and size effects in periodic honeycomb materials: a gradient-elasticity approach *J. Mech. Phys. Solids* **99** 35–49
[23] Catapano A and Montemurro M 2014 A multi-scale approach for the optimum design of sandwich plates with honeycomb core. Part I: homogenization of core properties *Compos. Struct.* **118** 664–76
[24] Gibson L J and Ashby M F 1999 *Cellular Solids: Structure and Properties* (Cambridge: Cambridge University Press)
[25] Chen D H, Horii H and Ozaki S 2009 Analysis of in-plane elastic modulus for a hexagonal honeycomb core: analysis of Young's modulus and shear modulus *J. Comput. Sci. Technol.* **3** 1–12
[26] Sorohan S, Sandu M, Constantinescu D M and Sandu A G 2016 Estimation of out of plane shear moduli for honeycomb cores with modal finite element analyses *Romanian J. Tech. Sci. Appl. Mech.* **61** 71–88
[27] Xu X F and Qiao P 2002 Homogenized elastic properties of honeycomb sandwich with skin effect *Int. J. Solids Struct.* **39** 2153–88
[28] Kelsey S, Gellatly R and Clark B 1958 The shear modulus of foil honeycomb cores *Aircr. Eng. Aerosp. Technol.* **30** 294–302
[29] Grediac M 1993 A finite element study of the transverse shear in honeycomb cores *Int. J. Solids Struct.* **30** 1777–88
[30] Scarpa F and Tomlin P 2000 On the transverse shear modulus of negative Poisson ratio honeycomb structures *Fatigue Fract. Eng. Mater. Struct.* **23** 717–20
[31] Malek S and Gibson L 2015 Effective elastic properties of periodic hexagonal honeycombs *Mech. Mater.* **91** 226–40
[32] Timoshenko S and Goodier J 2011 *Theory of Elasticity* (New York: Mc-Graw Hill)
[33] Roark R J, Young W C and Plunkett R 1976 Formulas for stress and strain *J. Appl. Mech.* **43** 522
[34] Sorohan S, Sandu M, Constantinescu D M and Sandu A G 2015 On the evaluation of mechanical properties of honeycombs by using finite element analyses *INCAS Bull.* **7** 135–50
[35] Fu M-H and Yin J R 1999 Equivalent elastic parameters of the honeycomb core *Acta Mech. Sin.* **15** 113–18
[36] Torabi K, Afshari H and Aboutalebi F H 2019 Vibration and flutter analyses of cantilever trapezoidal honeycomb sandwich plates *J. Sandw. Struct. Mater.* **21** 2887–920
[37] Sorohan S, Constantinescu D M, Sandu M and Sandu A G 2018 On the homogenization of hexagonal honeycombs under axial and shear loading. Part I: analytical formulation for free skin effect *Mech. Mater.* **119** 74–91
[38] Sorohan S, Constantinescu D M, Sandu M and Sandu A G 2018 On the homogenization of hexagonal honeycombs under axial and shear loading. Part II: comparison of free skin and rigid skin effects on effective core properties *Mech. Mater.* **119** 92–108
[39] Tornabene F, Viscoti M, Dimitri R and Aiello M A 2021 Higher Order Formulations for doubly-curved shell structures with a honeycomb core *Thin-Walled Struct.* **164** 107789
[40] Tornabene F, Viscoti M, Dimitri R and Aiello M A 2021 Higher-order modelling of anisogrid composite lattice structures with complex geometries *Eng. Struct.* **244** 112686

[41] Calladine C R 1989 *Theory of Shell Structures* (Cambridge: Cambridge University Press)
[42] Kraus H 1967 *Thin Elastic Shells* (New York: Wiley)
[43] Gould P L 1999 *Analysis of Plates and Shells* (Upper Saddle River, NJ: Prentice-Hall)
[44] Li D 2020 Layer-wise theories of laminated composite structures and their applications: A review *Arch. Comput. Meth. Eng.* **28** 577–600
[45] Reddy J N 1993 An evaluation of equivalent-single-layer and layerwise theories of composite laminates *Compos. Struct.* **25** 21–35
[46] Tornabene F, Fantuzzi N, Viola E and Batra R C 2015 Stress and strain recovery for functionally graded free-form and doubly-curved sandwich shells using higher-order equivalent single layer theory *Compos. Struct.* **119** 67–89
[47] Love A E H 1944 *A Treatise on the Mathematical Theory of Elasticity* (New York: Dover Publication)
[48] Germain S 2013 *Recherches sur la théorie des surfaces élastiques* (Cambridge: Cambridge University Press)
[49] Reissner E 1945 The effect of transverse shear deformation on the bending of elastic plates *J. Appl. Mech. ASME* **12** 66–77
[50] Mindlin R D 1951 Thickness-shear and flexural vibrations of crystal plates *J. Appl. Phys.* **22** 316–23
[51] Arefi M, Mohammadi M, Tabatabaeian A, Dimitri R and Tornabene F 2018 Two-dimensional thermo-elastic analysis of FG-CNTRC cylindrical pressure vessels *Steel Compos. Struct.* **27** 525–36
[52] Reddy J N 2003 *Mechanics of Laminated Composite Plates and Shells* (Boca Raton, FL: CRC Press)
[53] Reddy J N 1986 A refined shear deformation theory for the analysis of laminated plates *NASA Contractor Report* 3955
[54] Mohammadi M, Arefi M, Dimitri R and Tornabene F 2019 Higher-order thermo-elastic analysis of FG-CNTRC cylindrical vessels surrounded by a Pasternak foundation *Nanomaterials* **9** 79
[55] Washizu K 1975 *Variational Methods in Elasticity and Plasticity* (Oxford: Pergamon)
[56] Reddy J N 1987 A generalization of two-dimensional theories of laminated composite plates *Commun. Appl. Numer. Methods* **3** 173–80
[57] Tornabene F and Bacciocchi M 2018 *Anisotropic Doubly-Curved Shells. Higher-Order Strong and Weak Formulations for Arbitrarily Shaped Shell Structures* (Bologna: Società Editrice Esculapio)
[58] Tornabene F, Bacciocchi M, Fantuzzi N and Viola E 2016 *Laminated Composite Doubly-Curved Shell Structures: Differential Geometry Higher-Order Structural Theories* (Bologna: Società Editrice Esculapio)
[59] Tornabene F 2016 General higher-order layer-wise theory for free vibrations of doubly-curved laminated composite shells and panels *Mech. Adv. Mater. Struct.* **23** 1046–67
[60] Tornabene F, Viscoti M and Dimitri R 2022 Generalized higher order layerwise theory for the dynamic study of anisotropic doubly-curved shells with a mapped geometry *Eng. Anal. Bound. Elem.* **134** 147–83
[61] Lopatin A V, Morozov E V and Shatov A V 2016 An analytical expression for fundamental frequency of the composite lattice cylindrical shell with clamped edges *Compos. Struct.* **141** 232–39

[62] Lopatin A V, Morozov E V and Shatov A V 2018 Fundamental frequency of a composite anisogrid lattice cylindrical panel with clamped edges *Compos. Struct.* **201** 200–7
[63] Morozov E V, Lopatin A V and Nesterov V A 2011 Finite-element modelling and buckling analysis of anisogrid composite lattice cylindrical shells *Compos. Struct.* **93** 308–23
[64] Shu C 2000 *Differential Quadrature and Its Application in Engineering* (London: Springer)
[65] Shu C, Ding H and Yeo K S 2003 Local radial basis function-based differential quadrature method and its application to solve two-dimensional incompressible Navier–Stokes equations *Comput. Meth. Appl. Mech. Eng.* **192** 941–54
[66] Bellman R and Casti J 1971 Differential quadrature and long-term integration *J. Math. Anal. Appl.* **34** 235–38
[67] Zong Z and Zhang Y 2009 *Advanced Differential Quadrature Methods* (Boca Raton, FL: CRC Press)
[68] Tornabene F, Fantuzzi N, Ubertini F and Viola E 2015 Strong formulation finite element method based on differential quadrature: a survey *Appl. Mech. Rev.* **67** 20801
[69] Quan J R and Chang C T 1989 New insights in solving distributed system equations by the quadrature method—I. Analysis *Comput. Chem. Eng.* **13** 779–88
[70] Tornabene F, Liverani A and Caligiana G 2011 FGM and laminated doubly curved shells and panels of revolution with a free-form meridian: a 2-D GDQ solution for free vibrations *Int. J. Mech. Sci.* **53** 446–70
[71] Tornabene F and Reddy J N 2013 FGM and laminated doubly-curved and degenerate shells resting on nonlinear elastic foundations: a GDQ solution for static analysis with *a posteriori* stress and strain recovery *J. Indian Inst. Sci.* **93** 635–88
[72] Tornabene F and Bacciocchi M 2018 Effect of curvilinear reinforcing fibers on the linear static behavior of soft-core sandwich structures *J. Compos. Sci.* **2** 14
[73] Tornabene F, Bacciocchi M, Fantuzzi N and Reddy J N 2019 Multiscale approach for three-phase CNT/polymer/fiber laminated nanocomposite structures *Polym. Compos.* **40** E102–26
[74] Zare Jouneghani F, Dimitri R, Bacciocchi M and Tornabene F 2017 Free vibration analysis of functionally graded porous doubly-curved shells based on the first-order shear deformation theory *Appl. Sci.* **7** 1252
[75] Shen J, Wang H and Zheng S 2018 Size-dependent pull-in analysis of a composite laminated micro-beam actuated by electrostatic and piezoelectric forces: generalized differential quadrature method *Int. J. Mech. Sci.* **135** 353–61
[76] Hua L I and Lam K Y 1998 Frequency characteristics of a thin rotating cylindrical shell using the generalized differential quadrature method *Int. J. Mech. Sci.* **40** 443–59
[77] Dastjerdi S, Malikan M, Dimitri R and Tornabene F 2021 Nonlocal elasticity analysis of moderately thick, porous functionally graded plates in a hygro-thermal environment *Compos. Struct.* **255** 112925
[78] Bert C W and Malik M 1996 Differential quadrature method in computational mechanics: a review *Appl. Mech. Rev.* **49** 1–28
[79] Shu C, Chen W, Xue H and Du H 2001 Numerical study of grid distribution effect on accuracy of DQ analysis of beams and plates by error estimation of derivative approximation *Int. J. Numer. Methods Eng.* **51** 159–79
[80] Fazzolari F A, Viscoti M, Dimitri R and Tornabene F 2020 1D-hierarchical Ritz and 2D-GDQ formulations for the free vibration analysis of circular/elliptical cylindrical shells and beam structures *Compos. Struct.* **258** 113338

[81] Tornabene F, Fantuzzi N and Bacciocchi M 2018 Strong and weak formulations based on differential and integral quadrature methods for the free vibration analysis of composite plates and shells: convergence and accuracy *Eng. Anal. Boundary Elem.* **92** 3–37
[82] Fantuzzi N, Tornabene F, Bacciocchi M and Ferreira A J M 2018 On the convergence of laminated composite plates of arbitrary shape through finite element models *J. Compos. Sci.* **2** 16
[83] Shu C and Wee K H A 2002 Numerical simulation of natural convection in a square cavity by simple generalized differential quadrature method *Comput. Fluids* **31** 209–26
[84] Chen C N 2000 A generalized differential quadrature element method *Comput. Meth. Appl. Mech. Eng.* **188** 553–66
[85] Dimitri R, Fantuzzi N, Tornabene F and Zavarise G 2016 Innovative numerical methods based on SFEM and IGA for computing stress concentrations in isotropic plates with discontinuities *Int. J. Mech. Sci.* **118** 166–87
[86] Dimitri R, Tornabene F and Reddy J N 2020 Numerical study of the mixed-mode behaviour of generally-shaped composite interfaces *Compos. Struct.* **237** 111935
[87] Dimitri R, Fantuzzi N, Li Y and Tornabene F 2017 Numerical computation of the crack development and SIF in composite materials with XFEM and SFEM *Compos. Struct.* **160** 468–90
[88] Hong C C 2017 GDQ analysis of a beam-plate with delamination *Compos. Struct.* **182** 237–41
[89] Viola E, Dilena M and Tornabene F 2007 Analytical and numerical results for vibration analysis of multi-stepped and multi-damaged circular arches *J. Sound Vib.* **299** 143–63
[90] Shu C and Du H 1997 A generalized approach for implementing general boundary conditions in the GDQ free vibration analysis of plates *Int. J. Solids Struct.* **34** 837–46
[91] Shu C and Wang C M 1999 Treatment of mixed and nonuniform boundary conditions in GDQ vibration analysis of rectangular plates *Eng. Struct.* **21** 125–34
[92] Brischetto S, Tornabene F, Fantuzzi N and Bacciocchi M 2017 Interpretation of boundary conditions in the analytical and numerical shell solutions for mode analysis of multi-layered structures *Int. J. Mech. Sci.* **122** 18–28
[93] Tornabene F and Viola E 2013 Static analysis of functionally graded doubly-curved shells and panels of revolution *Meccanica* **48** 901–30
[94] Tornabene F, Viscoti M, Dimitri R and Reddy J N 2021 Higher order theories for the vibration study of doubly-curved anisotropic shells with a variable thickness and isogeometric mapped geometry *Compos. Struct.* **267** 113829
[95] Tornabene F, Fantuzzi N and Bacciocchi M 2018 *DiQuMASPAB: Differential Quadrature for Mechanics of Anisotropic Shells, Plates, Arches and Beams* (Bologna: Società Editrice Esculapio)

Chapter 2

[1] Lu Z, Lu X, Lu W and Masri S F 2012 Experimental studies of the effects of buffered particle dampers attached to a multi-degree-of-freedom system under dynamic loads *J. Sound Vib.* **331** 2007–22
[2] Ahmad N, Ranganath R and Ghosal A 2019 Modeling of the coupled dynamics of damping particles filled in the cells of a honeycomb sandwich plate and experimental validation *J. Vib. Control* **25** 1706–19
[3] Ahmad N, Ranganath R and Ghosal A 2017 Modeling and experimental study of a honeycomb beam filled with damping particles *J. Sound Vib.* **391** 20–34

[4] Ahmad N, Ranganath R and Ghosal A 2016 Assessment of particle damping device for large laminated structures under acoustic excitations Presented at the Proc. of 14th ISAMPE National Conf. on Composites (INCCOM-14) *(Hyderabad)*
[5] Cundall P A and Strack O D L 1979 A discrete numerical model for granular assemblies *Géotechnique* **29** 47–65
[6] Goldsmith W 2001 *Impact(Dover Civil and Mechanical Engineering)* (Mineola, NY: Dover Publications Inc.)
[7] Tsuji Y, Tanaka T and Ishida T 1992 Lagrangian numerical simulation of plug flow of cohesionless particles in a horizontal pipe *Powder Technol.* **71** 239–50
[8] Fang X, Tang J and Luo H 2007 Granular damping analysis using an improved discrete element approach *J. Sound Vib.* **308** 112–31
[9] Saeki M 2005 Analytical study of multi-particle damping *J. Sound Vib.* **281** 1133–44
[10] Johnson K L 1985 *Contact Mechanics.* (Cambridge: Cambridge University Press)
[11] Mindlin R D and Deresiewicz H 1953 Elastic spheres in contact under varying oblique forces *ASME J. Appl. Mech* **20** 327–44
[12] Maw N, Barber J R and Fawcett J N 1976 The oblique impact of elastic spheres *Wear* **38** 101–14
[13] Olson S E 2003 An analytical particle damping model *J. Sound Vib.* **264** 1155–66

Chapter 3

[1] Nair P S and Durvasula S 1973 Vibration of skew plates *J. Sound Vib.* **26** 1–19
[2] Sathyamoorthy M 1977 Shear and rotary inertia effects on large amplitude vibration of skew plates *J. Sound Vib.* 155–63
[3] Mizusawa T, Katija T and Naruoka M 1979 Vibration of skew plates by using B-spline functions *J. Sound Vib.* **62** 301–8
[4] Mizusawa T, Kajita T and Naruoka M 1980 Analysis of skew plate problems with various constraints *J. Sound Vib.* **73** 575–84
[5] Mizusawa T and Katija T 1987 Vibration of skew plates resting on point supports *J. Sound Vib.* **115** 243–51
[6] Liew K M and Lam K Y 1990 Application of two-dimensional orthogonal plate function to flexural vibration of skew plates *J. Sound Vib.* **139** 241–52
[7] Liew K M, Xiang Y, Kitipornchai S and Wang C M 1993 Vibration of thick skew plates based on Mindlin shear deformation plate theory *J. Sound Vib.* **168** 39–69
[8] Singh B and Chakraverty S 1994 Flexural vibration of skew plates using boundary characteristic orthogonal polynomials in two variables *J. Sound Vib.* **173** 157–78
[9] Wang S 1997 Free vibration analysis of skew fibre-reinforced composite laminates based on first-order shear deformation plate theory *Comput. Struct.* **63** 525–38
[10] Žitňan P 1999 Vibration analysis of rectangular and skew plates by the Rayleigh-Ritz method *J. Sound Vib.* **221** 342–9
[11] Krishna Reddy A R and Palaninathan R 1999 Free vibration of skew laminates *Comput. Struct.* **70** 415–23
[12] Wang C M, Ang K K and Yang L 2000 Free vibration of skew sandwich plates with laminated facings *J. Sound Vib.* **235** 317–40
[13] Mizusawa T and Kondo Y 2001 Application of the spline element method to analyze vibration of skew Mindlin plates with varying thickness in one direction *J. Sound Vib.* **241** 485–501

[14] Upadhyay A K and Shukla K K 2013 Geometrically nonlinear static and dynamic analysis of functionally graded skew plates *Commun. Nonlinear Sci. Numer. Simul.* **18** 2252–79
[15] Chakraverty S and Pradhan K K 2017 Flexural vibration of functionally graded thin skew plates resting on elastic foundations *Int. J. Dyn. Control* **6** 97–121
[16] Memar Ardestani M, Zhang L W and Liew K M 2017 Isogeometric analysis of the effect of CNT orientation on the static and vibration behaviors of CNT-reinforced skew composite plates *Comput. Methods Appl. Mech. Eng.* **317** 341–79
[17] Kiani Y, Dimiti R and Tornabene F 2018 Free vibration of FG-CNT reinforced composite skew cylindrical shells using the Chebyshev–Ritz formulation *Composites* **B147** 169–77
[18] Vinyas M, Nischith G, Loja M A R, Ebrahimi F and Duc N D 2019 Numerical analysis of the vibration response of skew magneto-electro-elastic plates based on the higher-order shear deformation theory *Compos. Struct.* **214** 132–42
[19] Zhang L W 2017 On the study of the effect of in-plane forces on the frequency parameters of CNT-reinforced composite skew plates *Compos. Struct.* **160** 824–37
[20] Xue Y, Jin G, Ding H and Chen M 2018 Free vibration analysis of in-plane functionally graded plates using a refined plate theory and isogeometric approach *Compos. Struct.* **192** 193–205
[21] Reissner E 1975 On transverse bending of plates including the effects of transverse shear deformation *Int. J. Solids Struct.* **25** 495–502
[22] Reddy J N 1984 A refined nonlinear theory of plates with transverse shear deformation *Int. J. Solids Struct.* **20** 881–96
[23] Reddy J N and Phan N D 1985 Stability and vibration of isotropic, orthotropic and laminated plates according to a higher-order shear deformation theory *J. Sound Vib.* **98** 157–70
[24] Reddy J N 1984 A simple higher-order theory for laminated composite plates *J. Appl. Mech.* **51** 745–52
[25] Nayak A K, Moy S S J and Shenoi R A 2002 Free vibration analysis of composite sandwich plates based on Reddy's higher-order theory *Composites* **B33** 505–19
[26] Hosseini-Hashemi S and Arsanjani M 2005 Exact characteristic equations for some classical boundary conditions of vibrating moderately thick rectangular plates *Int. J. Solids Struct.* **42** 819–53
[27] Shimpi R P and Patel H G 2006 Free vibrations of plates using two variable refined plate theory *J. Sound Vib.* **296** 979–99
[28] Shimpi R P, Patel H G and Arya H 2007 New first-order shear deformation plate theories *J. Appl. Mech.* **74** 523–33
[29] Aydogdu M 2009 A new shear deformation theory for laminated composite plates *Compos. Struct.* **89** 94–101
[30] Xiang S, Wang K, Ai Y, Sha Y and Shi H 2009 Analysis of isotropic, sandwich and laminated plates by a meshless method and various shear deformation theories *Compos. Struct.* **91** 31–7
[31] Hosseini-Hashemi S, Fadaee M and Taher H R D 2011 Exact solutions for free flexural vibration of Lévy-type rectangular thick plates via third order shear deformation plate theory *Appl. Math. Model.* **35** 708–27
[32] Thai C H, Ferreira A J M, Bordas S P A, Rabczuk T and Nguyen-Xuan H 2014 Isogeometric analysis of laminated composite and sandwich plates using a new inverse trigonometric shear deformation theory *Eur. J. Mech.* **A43** 89–108

[33] Pradhan K K and Chakraverty S 2015 Transverse vibration of isotropic thick rectangular plates based on new inverse trigonometric shear deformation theories *Int. J. Mech. Sci.* **95** 211–31
[34] Pradhan K K and Chakraverty S 2015 Generalized power-law exponent based shear deformation theory for free vibration of functionally graded beams *Appl. Math. Comput.* **268** 1240–58
[35] Durvasula S 1968 Natural frequencies and modes of skew membranes *J. Acoust. Soc. Am.* **44** 1636–46
[36] Durvasula S and Nair P S 1974 Application of partition method to vibration problems of plates *J. Sound Vib.* **37** 429–45
[37] Durvasula S 1969 Natural frequencies and modes of clamped skew plates *Astronaut. Am. Inst. Aeronaut. J.* **7** 1164–7
[38] Liew K M and Lam K Y 1991 Vibration analysis of multispan plates having orthogonal straight edges *J. Sound Vib.* **147** 255–64
[39] Chakraverty S and Pradhan K K 2017 Flexural vibration of functionally graded thin skew plates resting on elastic foundations *Int. J. Dynam. Control* **6** 97–121

Chapter 4

[1] Birman V and Byrd L W 2007 Modeling and analysis of functionally graded materials and structures *Appl. Mech. Rev.* **60** 195–216
[2] Miyamoto Y, Kaysser W A, Rabin B H, Kawasaki A and Ford R G 2013 *Functionally Graded Materials: Design, Processing and Applications* (New York: Springer)
[3] Noda N 1999 Thermal stresses in functionally graded materials *J. Therm. Stress* **22** 477–512
[4] Shen H S 2016 *Functionally Graded Materials: Nonlinear Analysis of Plates and Shells* (Boca Raton, FL: CRC Press)
[5] Allahkarami F, Tohidi H, Dimitri R and Tornabene F 2020 Dynamic stability of bi-directional functionally graded porous cylindrical shells embedded in an elastic foundation *Appl. Sci.* **10** 1345
[6] Li H, Lam K Y and Ng T Y 2005 *Rotating Shell Dynamics* (Oxford: Elsevier)
[7] Di Taranto R A and Lessen M 1964 Coriolis acceleration effect on the vibration of a rotating thin-walled circular cylinder *J. Appl. Mech.* **31** 700–1
[8] Srinivasan A V and Lauterbach G F 1971 Traveling waves in rotating cylindrical shells *J. Eng. Ind.* **93** 1229–32
[9] Eshleman R L and Eubanks R A 1967 On the critical speeds of a continuous shaft-disk system *J. Eng. Ind.* **89** 1180–88
[10] Eshleman R L and Eubanks R A 1969 On the critical speeds of a continuous rotor *J. Eng. Ind.* **91** 1180–88
[11] Chivens D R and Nelsen H D 1975 The natural frequencies and critical speeds of a rotating, flexible shaft-disk system *J. Eng. Ind.* **97** 881–86
[12] Nelson H D 1980 A finite rotating shaft element using Timoshenko beam theory *J. Mech. Design* **102** 793–803
[13] Dimarogonas A D and Papadopoulus C A 1983 Vibration of cracked shafts in bending *J. Sound Vib.* **91** 583–93
[14] Özgüven H N 1984 On the critical speed of continuous shaft-disk systems *J. Vib. Acoust.* **106** 59–61

[15] Kim C-D and Bert C W 1993 Critical speed analysis of laminated composite, hollow drive shafts *Compos. Eng.* **3** 633–43
[16] Ng T Y and Lam K Y 1999 Vibration and critical speed of a rotating cylindrical shell subjected to axial loading *Appl. Acoust.* **56** 273–82
[17] Daneshjou K, Talebitooti M, Talebitooti R and Googarchin H S 2013 Dynamic analysis and critical speed of rotating laminated conical shells with orthogonal stiffeners using generalized differential quadrature method *Lat. Am. J. Solids Struct.* **10** 349–90
[18] Daneshjou K, Talebitooti M and Talebitooti R 2013 Free vibration and critical speed of moderately thick rotating laminated composite conical shell using generalized differential quadrature method *Appl. Math. Mech. Engl. Ed.* **34** 437–56
[19] Barooti M M, Safarpour H and Ghadiri M 2017 Critical speed and free vibration analysis of spinning 3D single-walled carbon nanotubes resting on elastic foundations *Eur. Phys. J. Plus* **132** 6
[20] Tornabene F and Bacciocchi M 2018 Dynamic stability of doubly-curved multi-layered shells subjected to arbitrarily oriented angular velocities: numerical evaluation of the critical speed *Compos. Struct.* **201** 1031–55
[21] Tornabene F 2019 On the critical speed evaluation of arbitrarily oriented rotating doubly-curved shells made of functionally graded materials *Thin-Walled Struct.* **140** 85–98
[22] Cheng Z-Q and Batra R C 2000 Deflection relationships between the homogeneous plate theory and different functionally graded plate theories *Arch. Mech.* **52** 143–58
[23] Yang J and Shen H-S 2003 Nonlinear bending analysis of shear deformable functionally graded plates subjected to thermo-mechanical loads under various boundary conditions *Compos. Part B Eng.* **34** 103–15
[24] Batra R C 2006 Torsion of a functionally graded cylinder *AIAA J.* **44** 1363–65
[25] Efraim E and Eisenberger M 2007 Exact vibration analysis of variable thickness thick annular isotropic and FGM plates *J. Sound Vib.* **299** 720–38
[26] Tornabene F 2009 Free vibration analysis of functionally graded conical, cylindrical and annular shell structures with a four-parameter power-law distribution *Comput. Methods Appl. Mech. Engrg.* **198** 2911–35
[27] Mori T and Tanaka K 1973 Average stress in matrix and average elastic energy of materials with misfitting inclusions *Acta Metal.* **21** 571–74
[28] Mura T 1982 *Micromechanics of Defects in Solids* (The Hague: Martinus Nijhoff)
[29] Hashin Z 1983 Analysis of composite materials—a survey *J. Appl. Mech.* **50** 481–505
[30] Benveniste Y 1987 A new approach to the application of Mori–Tanaka's theory in composite materials *Mech. Mat.* **6** 147–57
[31] Iijima S 1994 Synthesis of carbon nanotubes *Nature* **354** 56–8
[32] Bouaziz O, Kim H S and Estrin Y 2013 Architecturing of metal-based composites with concurrent nanostructuring: a new paradigm of materials design *Adv. Eng. Mater.* **15** 336–40
[33] Beygelzimer Y, Estrin Y and Kulagin R 2015 Synthesis of hybrid materials by severe plastic deformation: a new paradigm of SPD processing *Adv. Eng. Mater.* **17** 1853–61
[34] Estrin Y, Beygelzimer Y and Kulagin R 2019 Design of architectured materials based on mechanically driven structural and compositional patterning *Adv. Eng. Mater.* **21** 1900487
[35] Ashrafi B, Hubert P and Vengallatore S 2006 Carbon nanotube-reinforced composites as structural materials for micro actuators in micro electromechanical systems *Nanotechnology* **17** 4895–903

[36] Rafiee M, Yang J and Kitipornchai S 2013 Thermal bifurcation buckling of piezoelectric carbon nanotube reinforced composite beams *Comput. Math. Appl.* **66** 1147–60
[37] Araneo R, Bini F, Rinaldi A, Notargiacomo A, Pea M and Celozzi S 2015 Thermal-Electric model for piezoelectric ZnO nanowires *Nanotechnology* **26** 265402
[38] Ng T Y, Lam K Y and Liew K M 2000 Effects of FGM materials on the parametric resonance of plate structures *Comput. Meth. Appl. Mech. Eng.* **190** 953–62
[39] Praveen G N and Reddy J N 1998 Nonlinear transient thermo elastic analysis of functionally graded ceramic–metal plates *Int. J. Solids Struct.* **33** 4457–76
[40] He X Q, Ng T Y, Sivashanker S and Liew K M 2001 Active control of FGM plates with integrated piezoelectric sensors and actuators *Int. J. Solids Struct.* **38** 1641–55
[41] Tornabene F, Viola E and Inman D J 2009 2-D differential quadrature solution for vibration analysis of functionally graded conical, cylindrical shell and annular plate structures *J. Sound Vib.* **328** 259–90
[42] Kiani Y, Dimitri R and Tornabene F 2018 Free vibration study of composite conical panels reinforced with FG-CNTs *Eng. Struct.* **172** 472–82
[43] Sofiyev A H, Tornabene F, Dimitri R and Kuruoglu N 2020 Buckling behavior of FG-CNT reinforced composite conical shells subjected to a combined loading *Nanomaterials* **10** 419
[44] Jena S K, Chakraverty S, Malikan M and Tornabene F 2020 Effects of surface energy and surface residual stresses on vibro-thermal analysis of chiral, zigzag, and armchair types of SWCNTs using refined beam theory *Mech. Based Des. Struct. Mach.*
[45] Ghasemi A R, Mohandes M, Dimitri R and Tornabene F 2019 Agglomeration effects on the vibrations of CNTs/fiber/polymer/metal hybrid laminates cylindrical shell *Compos. Part B: Eng.* **167** 700–16
[46] Mohammadi M, Arefi M, Dimitri R and Tornabene F 2019 Higher-order thermo-elastic analysis of FG-CNTRC cylindrical vessels surrounded by a pasternak foundation *Nanomaterials* **9** 79
[47] Jena S K, Chakraverty S, Malikan M and Tornabene F 2020 Effects of surface energy and surface residual stresses on vibro-thermal analysis of chiral, zigzag, and armchair types of SWCNTs using refined beam theory *Mech. Based Des. Struct. Mach.*
[48] Karami B, Janghorban M, Shahsavari D, Dimitri R and Tornabene F 2019 Nonlocal buckling analysis of composite curved beams reinforced with functionally graded carbon nanotubes *Molecules (Basel)* **24** 2750
[49] Noroozi A R, Malekzadeh P, Dimitri R and Tornabene F 2020 Meshfree radial point interpolation method for the vibration and buckling analysis of FG-GPLRC perforated plates under an in-plane loading *Eng. Struct.* **221** 111000
[50] Shu C 2000 *Differential Quadrature and Its Application in Engineering* (Berlin: Springer)
[51] Bellman R and Casti J 1971 Differential quadrature and long-term integration *J. Math. Anal. Appl.* **34** 235–38
[52] Bert C and Malik M 1996 Differential quadrature method in computational mechanics *Appl. Mech. Rev.* **49** 1–27
[53] Shu C and Du H 1997 Free vibration analysis of composites cylindrical shells by DQM *Compos. Part B Eng.* **28B** 267–74
[54] Liu F-L and Liew K M 1999 Differential quadrature element method: a new approach for free vibration of polar Mindlin plates having discontinuities *Comput. Methods Appl. Mech. Eng.* **179** 407–23

[55] Tornabene F and Viola E 2007 Vibration analysis of spherical structural elements using the GDQ method *Comput. Math. Appl.* **53** 1538–60
[56] Marzani A, Tornabene F and Viola E 2008 Nonconservative stability problems via generalized differential quadrature method *J. Sound Vib.* **315** 176–96
[57] Tornabene F and Viola E 2008 2-D solution for free vibrations of parabolic shells using generalized differential quadrature method *Eur. J. Mech. A-Solid* **27** 1001–25
[58] Tornabene F 2011 2-D GDQ solution for free vibrations of anisotropic doubly-curved shells and panels of revolution *Compos. Struct.* **93** 1854–76
[59] Tornabene F 2011 Free vibrations of anisotropic doubly-curved shells and panels of revolution with a free-form meridian resting on Winkler–Pasternak elastic foundations *Compos. Struct.* **94** 186–206
[60] Tornabene F and Reddy J N 2013 FGM and laminated doubly-curved and degenerate shells resting on nonlinear elastic foundations: a GDQ solution for static analysis with *a posteriori* stress and strain recovery *J. Indian Inst. Sci.* **93** 635–88
[61] Mosallaie Barzoki A A, Ghorbanpour Arani A, Kolahchi R, Mozdianfard M R and Loghman A 2013 Nonlinear buckling response of embedded piezoelectric cylindrical shell reinforced with BNNT under electro–thermo-mechanical loadings using HDQM *Compos. Part B Eng.* **44** 722–27
[62] Khani S, Tabandeh N and Ghomshei M M 2014 Natural frequency analysis of non-uniform smart beams with piezoelectric layers, using differential quadrature method *Compos. Part B Eng.* **58** 303–11
[63] Tornabene F, Fantuzzi N, Ubertini F and Viola E 2015 Strong formulation finite element method based on differential quadrature: a survey *Appl. Mech. Rev.* **67** 020801
[64] Tornabene F, Dimitri R and Viola E 2016 Transient dynamic response of generally-shaped arches based on a GDQ-time-stepping method *Int. J. Mech. Sci.* **114** 277–314
[65] Tornabene F and Brischetto S 2018 3D capability of refined GDQ models for the bending analysis of composite and sandwich plates, spherical and doubly-curved shells *Thin-Walled Struct.* **129** 94–124
[66] Brischetto S and Tornabene F 2018 Advanced GDQ models and 3D stress recovery in multilayered plates, spherical and double-curved panels subjected to transverse shear loads *Compos. Part B: Eng.* **146** 244–69
[67] Dimitri R, Tornabene F and Zavarise G 2018 Analytical and numerical modeling of the mixed-mode delamination process for composite moment-loaded double cantilever beams *Compos. Struct.* **187** 535–53
[68] Tornabene F and Dimitri R 2018 A numerical study of the seismic response of arched and vaulted structures made of isotropic or composite materials *Eng. Struct.* **159** 332–66
[69] Dimitri R, Tornabene F and Reddy J N 2020 Numerical study of the mixed-mode behavior of generally-shaped composite interfaces *Compos. Struct.* **237** 111935
[70] Ng T Y, Lam K Y and Liew K M 2000 Effect of FGM materials on the parametric resonance of plate structures *Comput. Methods Appl. Mech. Eng.* **190** 953–62
[71] Yang J, Kitipornchai S and Liew K M 2003 Large amplitude vibration of thermo-electro-mechanically stressed FGM laminated plates *Comput. Methods Appl. Mech. Eng.* **192** 3861–85
[72] Wu C P and Tsai Y H 2004 Asymptotic DQ solutions of functionally graded annular spherical shells *Eur. J. Mech A-Solids* **23** 283–99

[73] Liew M, He X Q and Kitipornchai S 2004 Finite element method for the feedback control of FGM shells in the frequency domain via piezoelectric sensors and actuators *Comput. Methods Appl. Mech. Eng.* **193** 257–73
[74] Della Croce L and Venini P 2004 Finite elements for functionally graded Reissner–Mindlin plates *Comput. Methods Appl. Mech. Eng.* **193** 705–25
[75] Elishakoff I, Gentilini C and Viola E 2005 Forced vibrations of functionally graded plates in the three-dimensional setting *AIAA J.* **43** 2000–7
[76] Elishakoff I, Gentilini C and Viola E 2005 Three-dimensional analysis of an all-around clamped plate made of functionally graded materials *Acta Mech.* **180** 21–36
[77] Patel B P, Gupta S S, Loknath M S and Kadu C P 2005 Free vibration analysis of functionally graded elliptical cylindrical shells using higher-order theory *Compos. Struct.* **69** 259–70
[78] Abrate S 2006 Free vibration, buckling, and static deflection of functionally graded plates *Compos. Sci. Technol.* **66** 2383–94
[79] Zenkour A M 2006 Generalized shear deformation theory for bending analysis of functionally graded plates *Appl. Math. Model.* **30** 67–84
[80] Pelletier J L and Vel S S 2006 An exact solution for the steady-state thermoelastic response of functionally graded orthotropic cylindrical shells *Int. J. Solids Struct.* **43** 1131–58
[81] Arciniega R A and Reddy J N 2007 Large deformation analysis of functionally graded shells *Int. J. Solids Struct.* **44** 2036–52
[82] Arciniega R A and Reddy J N 2007 Tensor-based finite element formulation for geometrically nonlinear analysis of shell structures *Comput. Methods Appl. Mech. Eng.* **196** 1048–73
[83] Roque C M C, Ferreira A J M and Jorge R M N 2007 A radial basis function for the free vibration analysis of functionally graded plates using refined theory *J. Sound Vib.* **300** 1048–70
[84] Nie G J and Zhong Z 2007 Semi-analytical solution for three dimensional vibration of functionally graded circular plates *Comput. Methods Appl. Mech. Engrg.* **196** 4901–10
[85] Yang J and Shen H S 2007 Free vibration and parametric resonance of shear deformable functionally graded cylindrical panels *J. Sound Vib.* **261** 871–93
[86] Tornabene F 2016 General higher order layer-wise theory for free vibrations of doubly-curved laminated composite shells and panels *Mech. Adv. Mater. Struct.* **23** 1046–67
[87] Tornabene F, Fantuzzi N, Bacciocchi M and Viola E 2018 Mechanical behavior of damaged laminated composites plates and shells: higher-order shear deformation theories *Compos. Struct.* **189** 304–29
[88] Tornabene F, Fantuzzi N and Bacciocchi M 2019 Refined shear deformation theories for laminated composite arches and beams with variable thickness: natural frequency analysis *Eng. Anal. Bound. Elem.* **100** 24–47
[89] Kraus H 1967 *Thin Elastic Shells* (New York: Wiley)
[90] Tornabene F and Bacciocchi M 2018 *Anisotropic Doubly-Curved Shells. Higher-Order Strong and Weak Formulations for Arbitrarily Shaped Shell Structures* (Bologna: Esculapio)
[91] Carrera E 2003 Historical review of zig-zag theories for multi-layered plates and shells *Appl. Mech. Rev.* **56** 287–308
[92] Carrera E 2004 On the use of the Murakami's zig-zag function in the modeling of layered plates and shells *Comput. Struct.* **82** 541–54
[93] Tornabene F, Fantuzzi N and Bacciocchi M 2019 Foam core composite sandwich plates and shells with variable stiffness: effect of curvilinear fiber path on the modal response *J. Sandw. Struct. Mater.* **21** 320–65

[94] Tornabene F, Viola E and Fantuzzi N 2013 General higher-order equivalent single layer theory for free vibrations of doubly-curved laminated composite shells and panels *Compos. Struct.* **104** 94–117
[95] Shi D-L, Huang Y Y, Hwang K-C and Gao H 2004 The effect of nanotube waviness and agglomeration on the elastic property of carbon nanotube-reinforced composites *J. Eng. Mater. – T. ASME* **126** 250–57
[96] Tornabene F and Viola E 2013 Static analysis of functionally graded doubly-curved shells and panels of revolution *Meccanica* **48** 901–30
[97] Tornabene F, Fantuzzi N and Bacciocchi M 2014 Free vibrations of free-form doubly-curved shells made of functionally graded materials using higher-order equivalent single layer theories *Compos. Part B Eng.* **67** 490–509
[98] Tornabene F, Fantuzzi N, Viola E and Batra R C 2015 Stress and strain recovery for functionally graded free-form and doubly-curved sandwich shells using higher-order equivalent single layer theory *Compos. Struct.* **119** 67–89
[99] Odegard G M, Gates T S, Wise K E, Park C and Siochi E J 2003 Constitutive modeling of nanotube-reinforced polymer composites *Compos. Sci. Technol.* **63** 1671–87
[100] Hill R 1965 A self-consistent mechanics of composite materials *J. Mech. Phys. Solids* **13** 213–22
[101] Walpole L J 1969 On the overall elastic moduli of composite materials *J. Mech. Phys. Solids* **17** 235–51
[102] Dong X N, Zhang X, Huang Y Y and Guo X E 2005 A generalized self-consistent estimate for the effective elastic moduli of fiber-reinforced composite materials with multiple transversely isotropic inclusions *Int. J. Mech. Sci.* **47** 922–40
[103] Popov V N, Van Doren V E and Balkanski M 2000 Elastic properties of crystals of single-walled carbon nanotubes *Solid State Commun.* **114** 395–99
[104] Tornabene F and Dimitri R 2020 Generalized differential and integral quadrature: theory and applications *Mathematical Methods in Interdisciplinary Sciences* ed S Chakraverty (New York: Wiley) ch 14
[105] Kim N-I and Lee J 2014 Divergence and flutter behavior of Beck's type of laminated box beams *Int. J. Mech. Sci.* **84** 91–101
[106] Leipholz H 1978 *Stability of Elastic Structures* (New York: Springer)
[107] Leipholz H 1987 Stability theory *An Introduction to the Stability of Dynamic Systems and Rigid Bodies* 2nd edn (New York: Springer)
[108] Bigoni D and Noselli G 2011 Experimental evidence of flutter and divergence instabilities induced by dry friction *J. Mech. Phys. Solids* **59** 2208–26
[109] Tornabene F, Fantuzzi N, Bcciocchi M and Viola E 2016 Effect of agglomeration on the natural frequencies of functionally graded carbon nanotube-reinforced laminated composite doubly-curved shells *Compos. Part B: Eng.* **89** 187–218
[110] Tornabene F, Fantuzzi N, Bacciocchi M and Dimitri R 2015 Dynamic analysis of thick and thin elliptic shell structures made of laminated composite materials *Compos. Struct.* **133** 278–99
[111] Dong Y H, Li Y H, Chen D and Yang J 2018 Vibration characteristics of functionally graded graphene reinforced porous nanocomposite cylindrical shells with spinning motion *Compos. Part B Eng.* **145** 1–13

[112] Liew K M, Ng T Y, Zhao X and Reddy J N 2002 Harmonic reproducing kernel particle method for free vibration analysis of rotating cylindrical shells *Comput. Methods Appl. Mech. Eng.* **191** 4141–57
[113] Jafari A A and Bagheri M 2006 Free vibration of rotating ring stiffened cylindrical shells with non-uniform stiffener distribution *J. Sound Vib.* **296** 353–67

Chapter 5

[1] Malvern L E 1969 *Introduction to the Mechanics of a Continuous Medium* (Upper Saddle River, NJ: Prentice-Hall)
[2] Reddy J N 1993 *An Introduction to the Finite Element Method* (New York: McGraw-Hill), p 27
[3] Cowin S C and Doty S B 2007 *Tissue Mechanics* (Springer: Berlin)
[4] Majdoub M, Sharma P and Cagin T 2008 Enhanced size-dependent piezoelectricity and elasticity in nanostructures due to the flexoelectric effect *Phys. Rev.* **B77** 125424
[5] Cosserat E and Cosserat F 1909 *Théorie des corps déformables*
[6] Eringen A C 2002 *Nonlocal Continuum Field Theories* (Springer: Berlin)
[7] Reddy J 2007 Nonlocal theories for bending, buckling and vibration of beams *Int. J. Eng. Sci.* **45** 288–307
[8] Witmer E 1991-1992 *Elementary Bernoulli-Euler Beam Theory*MIT Unified Engineering Course Notes (Cambridge, MA: MIT Press), pp 114–64
[9] Elishakoff I 2020 *Handbook on Timoshenko-Ehrenfest Beam and Uflyand-Mindlin Plate Theories* (World Scientific: Singapore)
[10] Love A E H 1888 XVI. The small free vibrations and deformation of a thin elastic shell *Phil. Trans. R. Soc.* **A179** 491–546
[11] Mindlin R 1951 Influence of rotatory inertia and shear on flexural motions of isotropic, elastic plates *J. Appl. Mech.* **18** 31–8
[12] Sarkar S and Reddy J 2016 Exploring the source of non-locality in the Euler–Bernoulli and Timoshenko beam models *Int. J. Eng. Sci.* **104** 110–5

Chapter 6

[1] Dowell E H 1970 Panel flutter: a review of the aeroelastic stability of plates and shells *AIAA J.* **8** 385–99
[2] Tawfik M, Ro J J and Mei C 2002 Thermal post-buckling and aeroelastic behaviour of shape memory alloy reinforced plates *Smart Mater. Struct.* **11** 297–307
[3] Li F M 2012 Active aeroelastic flutter suppression of a supersonic plate with piezoelectric material *Int. J. Eng. Sci.* **51** 190–203
[4] Song Z G and Li F M 2012 Active aeroelastic flutter analysis and vibration control of supersonic composite laminated plate *Compos. Struct.* **94** 702–13
[5] Asadi H and Wang Q 2017 An investigation on the aeroelastic flutter characteristics of FG-CNTRC beams in the supersonic flow *Compos. Part B-Eng.* **116** 486–99
[6] Stankovich S, Dikin D, Dommett G, Kohlhaas K, Zimney E J, Stach E, Piner R, Nguyen S and Ruoff R 2006 Graphene-based composite materials *Nature* **442** 282–86
[7] Potts J R, Dreyer D R, Bielawski C W and Ruoff R S 2011 Graphene-based polymer nanocomposites *Polymer* **52** 5–25
[8] Zhao S Y, Zhao Z, Yang Z C, Ke L L, Kitipornchai S and Yang J 2020 Functionally graded graphene reinforced composite structures: a review *Eng. Struct.* **210** 110339

[9] Laws N, Dvorak G J and Hejazi M 1983 Stiffness changes in unidirectional composites caused by crack systems *Mech. Mater.* **2** 123–37
[10] Dvorak G, Laws N and Hejazi M 1985 Analysis of progressive matrix cracking in composite laminates I. Thermoelastic properties of a ply with cracks *J. Compos. Mater.* **19** 216–34
[11] Fan Y and Wang H 2016 Nonlinear dynamics of matrix-cracked hybrid laminated plates containing carbon nanotube-reinforced composite layers resting on elastic foundations *Nonlinear Dyn.* **84** 1181–99
[12] Fan Y and Wang H 2016 Thermal postbuckling and vibration of postbuckled matrix cracked hybrid laminated plates containing carbon nanotube reinforced composite layers on elastic foundation *Compos. Struct.* **157** 386–97
[13] Lei Z X, Zhang L W and Liew K M 2018 Modeling large amplitude vibration of matrix cracked hybrid laminated plates containing CNTR-FG layers *Appl. Math. Modell.* **55** 33–48
[14] Pan Z Z, Zhang L W and Liew K M 2019 Modeling geometrically nonlinear large deformation behaviors of matrix cracked hybrid composite deep shells containing CNTRC layers *Comput. Meth. Appl. Mech. Eng.* **355** 753–78
[15] Guo H L, Yang T Z, Żur K K and Reddy J N 2021 On the flutter of matrix cracked laminated composite plates reinforced with graphene nanoplatelets *Thin-Walled Struct.* **158** 107161
[16] Mei C, Abdel-Motagaly K and Chen R 1999 Review of nonlinear panel flutter at supersonic and hypersonic speeds *Appl. Mech. Rev.* **52** 321–32
[17] Sohn K J and Kim J H 2008 Structural stability of functionally graded panels subjected to aero-thermal loads *Compos. Struct.* **82** 317–25
[18] Shiau L C, Kuo S Y and Liu Y P 2012 Aerothermoelastic analysis of composite laminated plates *Compos. Struct.* **94** 1982–90
[19] Ibrahim H H, Tawfik M and Al-Ajmi M 2007 Thermal buckling and nonlinear flutter behavior of functionally graded material panels *J. Aircr.* **44** 1610–18
[20] Ibrahim H H, Tawfik M and Negm H M 2011 Thermal buckling and nonlinear flutter behavior of shape memory alloy hybrid composite plates *J. Vib. Control* **17** 321–33
[21] Fazelzadeh S A, Pouresmaeeli S and Ghavanloo E 2015 Aeroelastic characteristics of functionally graded carbon nanotube-reinforced composite plates under a supersonic flow *Comput. Meth. Appl. Mech. Eng.* **285** 714–29
[22] Chai Y Y, Song Z G and Li F M 2018 Investigations on the aerothermoelastic properties of composite laminated cylindrical shells with elastic boundaries in supersonic airflow based on the Rayleigh-Ritz method *Aerosp. Sci.Technol.* **82–83** 534–44
[23] Marzocca P, Fazelzadeh S A and Hosseini M 2011 A review of nonlinear aero-thermo-elasticity of functionally graded panels *J. Therm. Stresses* **34** 536–68
[24] Liew K M, Lei Z X, Yu J L and Zhang L W 2014 Postbuckling of carbon nanotube-reinforced functionally graded cylindrical panels under axial compression using a meshless approach *Comput. Meth. Appl. Mech. Eng.* **268** 1–17
[25] Zhang L W and Liew K M 2014 An improved moving least-squares Ritz method for two-dimensional elasticity problems *Appl. Math. Comput.* **246** 268–82
[26] Guo H L, Cao S Q, Yang T Z and Chen Y S 2018 Vibration of laminated composite quadrilateral plates reinforced with graphene nanoplatelets using the element-free IMLS-Ritz method *Int. J. Mech. Sci.* **142** 610–21
[27] Guo H L, Cao S Q, Yang T Z and Chen Y S 2018 Geometrically nonlinear analysis of laminated composite quadrilateral plates reinforced with graphene nanoplatelets using the element-free IMLS-Ritz method *Compos. Part B-Eng.* **154** 216–24

[28] Huang K, Guo H L, Qin Z H, Cao S Q and Chen Y S 2020 Flutter analysis of laminated composite quadrilateral plates reinforced with graphene nanoplatelets using the element-free IMLS-Ritz method *Aerosp. Sci.Technol.* **103** 105915
[29] De Villoria R G and Miravete A 2007 Mechanical model to evaluate the effect of the dispersion in nanocomposites *Acta Mater.* **55** 3025–31
[30] Reddy J N 2004 *Mechanics of Laminated Composite Plates and Shells: Theory and Analysis* 2nd edn. (Boca Raton, FL: CRC Press)
[31] Lin K, Lu P and Tarn J 1989 Flutter analysis of composite panels using high-precision finite elements *Comput. Struct.* **33** 561–74
[32] Thai C H, Ferreira A J M, Tran T D and Phung-Van P 2019 Free vibration, buckling and bending analyses of multilayer functionally graded graphene nanoplatelets reinforced composite plates using the NURBS formulation *Compos. Struct.* **220** 749–59
[33] Song M T, Kitipornchai S and Yang J 2017 Free and forced vibrations of functionally graded polymer composite plates reinforced with graphene nanoplatelets *Compos. Struct.* **159** 579–88
[34] Reddy J N 2015 *An Introduction to Nonlinear Finite Element Analysis* 2nd edn (Oxford: Oxford University Press)
[35] Shiau L C, Kuo S Y and Liu Y P 2012 Aerothermoelastic analysis of composite laminated plates *Compos. Struct.* **94** 1982–90
[36] Wu H L, Kitipornchai S and Yang J 2017 Thermal buckling and postbuckling of functionally graded graphene nanocomposite plates *Mater. Des.* **132** 430–41

Chapter 7

[1] Fahrner W 2005 *Nanotechnology and Nanoelectronics* (Berlin: Springer)
[2] Kabychenkov A F and Lisovskii F V 2019 Flexomagnetic and flexoantiferromagnetic effects in centrosymmetric antiferromagnetic materials *Tech. Phys.* **64** 980–3
[3] Eliseev E A, Morozovska A N, Glinchuk M D and Blinc R 2009 Spontaneous flexoelectric/flexomagnetic effect in nanoferroics *Phys. Rev.* B **79** 165433
[4] Lukashev P and Sabirianov R F 2010 Flexomagnetic effect in frustrated triangular magnetic structures *Phys. Rev.* B **82** 094417
[5] Yudin P V and Tagantsev A K 2013 Fundamentals of flexoelectricity in solids *Nanotechnology* **24** 432001
[6] Sidhardh S and Ray M C 2018 Flexomagnetic response of nanostructures *J. Appl. Phys.* **124** 244101
[7] Zhang N, Zheng S and Chen D 2019 Size-dependent static bending of flexomagnetic nanobeams *J. Appl. Phys.* **126** 223901
[8] Malikan M and Eremeyev V A 2020 Free vibration of flexomagnetic nanostructured tubes based on stress-driven nonlocal elasticity, Springer Nature, analysis of shells, plates, and beams *Adv. Struct. Mater.* **134**
[9] Malikan M and Eremeyev V A 2020 On the geometrically nonlinear vibration of a piezo-flexomagnetic nanotube *Math. Methods Appl. Sci.* https://doi.org/10.1002/mma.6758
[10] Malikan M, Uglov N S and Eremeyev V A 2020 On instabilities and post-buckling of piezomagnetic and flexomagnetic nanostructures *Int. J. Eng. Sci.* **157** 103395
[11] Malikan M and Eremeyev V A 2020 On nonlinear bending study of a piezo-flexomagnetic nanobeam based on an analytical-numerical solution *Nanomaterials* **10** 10091762

[12] Song X and Li S-R 2007 Thermal buckling and post-buckling of pinned–fixed Euler–Bernoulli beams on an elastic foundation *Mech. Res. Commun.* **34** 164–71
[13] Reddy J N 2010 Nonlocal nonlinear formulations for bending of classical and shear deformation theories of beams and plates *Int. J. Eng. Sci.* **48** 1507–18
[14] Moory-Shirbani M, Sedighi H M, Ouakad H M and Najar F 2018 Experimental and mathematical analysis of a piezoelectrically actuated multilayered imperfect microbeam subjected to applied electric potential *Compos. Struct.* **184** 950–60
[15] Ouakad H M and Sedighi H M 2019 Static response and free vibration of MEMS arches assuming out-of-plane actuation pattern *Int. J. Non Linear Mech.* **110** 44–57
[16] Chen W-R, Chen C-S and Chang H 2020 Thermal buckling analysis of functionally graded Euler–Bernoulli beams with temperature-dependent properties *J. Appl. Comput. Mech.* **6** 457–70
[17] Malikan M and Eremeyev V A 2020 On the dynamics of a visco-piezo-flexoelectric nanobeam *Symmetry* **12** 643
[18] Lim C W, Zhang G and Reddy J N 2015 A Higher-order nonlocal elasticity and strain gradient theory and its applications in wave propagation *J. Mech. Phys. Solids* **78** 298–313
[19] Malikan M and Eremeyev V A 2020 A new hyperbolic-polynomial higher-order elasticity theory for mechanics of thick FGM beams with imperfection in the material composition *Compos. Struct.* **249** 112486
[20] Malikan M, Eremeyev V A and Sedighi H M 2020 Buckling analysis of a non-concentric double-walled carbon nanotube *Acta Mech.* **231** 5007–20
[21] Li L, Han B, Zhang Q-C, Zhao Z-Y and Lu T J 2019 Dynamic response of clamped sandwich beams: analytical modeling *Theor. Appl. Mech. Lett.* **9** 391–6
[22] Malikan M, Nguyen V B and Tornabene F 2018 Damped forced vibration analysis of single-walled carbon nanotubes resting on viscoelastic foundation in thermal environment using nonlocal strain gradient theory *Eng. Sci. Technol. Int. J.* **21** 778–86
[23] Lu L, Guo X and Zhao J 2017 Size-dependent vibration analysis of nanobeams based on the nonlocal strain gradient theory *Int. J. Eng. Sci.* **116** 12–24
[24] Rajput A B, Hazra S and Nath Ghosh N 2013 Synthesis and characterisation of pure single-phase $CoFe_2O_4$ nanopowder via a simple aqueous solution-based EDTA-precursor route *J. Exp. Nanosci.* **8** 629–39
[25] Malikan M, Krasheninnikov M and Eremeyev V A 2020 Torsional stability capacity of a nano-composite shell based on a nonlocal strain gradient shell model under a three-dimensional magnetic field *Int. J. Eng. Sci.* **148** 103210
[26] Malikan M and Eremeyev V A 2020 Post-critical buckling of truncated conical carbon nanotubes considering surface effects embedding in a nonlinear Winkler substrate using the Rayleigh-Ritz method *Mater. Res. Express* **7** 025005
[27] Malikan M, Dimitri R and Tornabene F 2019 Transient response of oscillated carbon nanotubes with an internal and external damping *Compos. Part B: Eng.* **158** 198–205

Chapter 8

[1] Younis M I 2011 *MEMS Linear and Nonlinear Statics and Dynamics* (Cham: Springer), p 20
[2] Rahaeifard M, Kahrobaiyan M H, Asghari M and Ahmadian M T 2011 Static pull-in analysis of microcantilevers based on the modified couple stress theory *Sens. Actuators A: Phys.* **171** 370–4

[3] Yin L, Qian Q and Wang L 2011 Size effect on the static behavior of electrostatically actuated microbeams *Acta Mech. Sin.* **27** 445
[4] Kong S L 2013 Size effect on pull-in behaviors of electrostatically actuated cantilever microbeams *Appl. Mech. Mater.* **300** 889–92
[5] Abdel-Rahman E M, Younis M I and Nayfeh A H 2002 Characterization of the mechanical behavior of an electrically actuated microbeam *J. Micromech. Microeng.* **12** 759
[6] Gurtin M E and Murdoch A I 1975 A continuum theory of elastic material surfaces *Arch. Ration. Mech. Anal.* **57** 291–323
[7] Koochi A, Kazemi A, Khandani F and Abadyan M 2012 Influence of surface effects on size-dependent instability of nano-actuators in the presence of quantum vacuum fluctuations *Phys. Scr.* **85** 035804
[8] Soroush R, Koochi A, Kazemi A S, Noghrehabadi A, Haddadpour H and Abadyan M 2010 Investigating the effect of Casimir and van der Waals attractions on the electrostatic pull-in instability of nano-actuators *Phys. Scr.* **82** 045801
[9] Beni Y T, Koochi A and Abadyan M 2011 Theoretical study of the effect of Casimir force, elastic boundary conditions and size dependency on the pull-in instability of beam-type NEMS *Phys. E: Low-Dimens. Syst. Nanostruct.* **43** 979–88
[10] Hosseini-Hashemi S, Nazemnezhad R and Bedroud M 2014 Surface effects on nonlinear free vibration of functionally graded nanobeams using nonlocal elasticity *Appl. Math. Model.* **38** 3538–53
[11] Sedighi H M, Daneshmand F and Abadyan M 2015 Dynamic instability analysis of electrostatic functionally graded doubly-clamped nano-actuators *Compos. Struct.* **124** 55–64
[12] Lei X W, Natsuki T, Shi J X and Ni Q Q 2012 Surface effects on the vibrational frequency of double-walled carbon nanotubes using the nonlocal Timoshenko beam model *Compos. Part B: Eng.* **43**(1) 64–9
[13] Hughes T J, Cottrell J A and Bazilevs Y 2005 Isogeometric analysis: CAD, finite elements, NURBS, exact geometry and mesh refinement *Compu. Methods Appl. Mech. Eng.* **194** 4135–95
[14] Reali A 2006 An isogeometric analysis approach for the study of structural vibrations *J. Earthq. Eng.* **10** 1–30
[15] Cottrell J A, Reali A, Bazilevs Y and Hughes T J 2005 Isogeometric analysis of structural vibrations *Comp. Methods Appl. Mech. Eng.* **195** 5257–96
[16] Weeger O, Wever U and Simeon B 2013 Isogeometric analysis of nonlinear Euler–Bernoulli beam vibrations *Nonlinear Dyn.* **72** 813–35
[17] Zare A, Eghtesad M and Daneshmand F 2017 Numerical investigation and dynamic behavior of pipes conveying fluid based on isogeometric analysis *Ocean Eng.* **140** 388–400
[18] Jockovic M 2016 Free vibration analysis of beam element using Isogeometric analysis *4th Int. Conf. on Contemporary Achievements in Civil Engineering* 22 269–78
[19] Vinh Loc T, Hoang Chien T and Xuan Hung N 2013 Geometrically nonlinear and dynamic analysis of Euler–Bernoulli beams using isogeometric approach *J. Sci.* **3** 2–9
[20] Shojaee S, Izadpanah E, Valizadeh N and Kiendl J 2012 Free vibration analysis of thin plates by using a NURBS-based isogeometric approach *Finite Elem. Anal. Des.* **61** 23–34
[21] Stoykov S, Hofreither C and Margenov S 2014 Isogeometric analysis for nonlinear dynamics of Timoshenko beams *Int. Conf. on Numerical Methods and Applications* (Cham: Springer), 138–46

[22] Yang F A C M, Chong A C M, Lam D C C and Tong P 2002 Couple stress based strain gradient theory for elasticity *Int. J. Solids Struct.* **39** 2731–43
[23] Reddy J N 2017 *Energy Principles and Variational Methods in Applied Mechanics* (New York: Wiley)
[24] Park S K and Gao X L 2006 Bernoulli–Euler beam model based on a modified couple stress theory *J. Micromech. Microeng.* **16** 2355
[25] Gurtin M E and Murdoch A I 1978 Surface stress in solids *Int. J. Solids Struct.* **14** 431–40
[26] Huang J M, Liew K M, Wong C H, Rajendran S, Tan M J and Liu A Q 2001 Mechanical design and optimization of capacitive micromachined switch *Sens. Actuators A: Phys.* **93** 273–85
[27] Israelachvili J N 1992 *Intermolecular and Surface Forces* (New York: Academic)
[28] Hosaka H, Itao K and Kuroda S 1995 Damping characteristics of beam-shaped micro-oscillators *Sens. Actuators A: Phys.* **49** 87–95
[29] Fox R W, McDonald A T and Pritchard P J 1998 *Introduction to Fluid Mechanics* (New York: Wiley)
[30] Wazwaz A M 1999 A reliable modification of Adomian decomposition method *Appl. Math. Comput.* **102** 77–86
[31] Rach R 1984 A convenient computational form for the Adomian polynomials *J. Math. Anal. Appl.* **102** 415–9
[32] Wazwaz A M 2001 The numerical solution of sixth-order boundary value problems by the modified decomposition method *Appl. Math. Comput.* **118** 311–25
[33] Cottrell J A, Hughes T J and Bazilevs Y 2009 *Isogeometric Analysis: toward Integration of CAD and FEA* (New York: Wiley)
[34] Piegl L and Tiller W 2012 *The NURBS Book* (Cham: Springer)
[35] Rogers D F 2000 *An Introduction to NURBS: With Historical Perspective* (Amsterdam: Elsevier)
[36] Rao S S 1995 *Mechanical Vibrations Laboratory Manual* (New York: Addison-Wesley)
[37] Shabani R, Hatami H, Golzar F G, Tariverdilo S and Rezazadeh G 2013 Coupled vibration of a cantilever micro-beam submerged in a bounded incompressible fluid domain *Acta Mech.* **224** 841–50

Chapter 9

[1] Brischetto S 2014 A continuum elastic three-dimensional model for natural frequencies of single-walled carbon nanotubes *Composites* **B61** 222–8
[2] Brischetto S 2015 A continuum shell model including van der Waals interaction for free vibrations of double-walled carbon nanotubes *Comput. Model. Eng. Sci.* **104** 305–27
[3] Brischetto S, Tornabene F, Fantuzzi N and Bacciocchi M 2015 Refined 2D and exact 3D shell models for the free vibration analysis of single- and double-walled carbon nanotubes *Technologies* **3** 259–84
[4] Brischetto S 2014 Three-dimensional exact free vibration analysis of spherical, cylindrical and flat one-layered panels *Shock Vib.* **2014** 1–29
[5] Brischetto S 2013 Exact elasticity solution for natural frequencies of functionally graded simply-supported structures *Comput. Model. Eng. Sci.* **95** 391–430
[6] Brischetto S 2014 An exact 3D solution for free vibrations of multilayered cross-ply composite and sandwich plates and shells *Int. J. Appl. Mech.* **6** 1–42

[7] Brischetto S and Torre R 2014 Exact 3D solutions and finite element 2D models for free vibration analysis of plates and cylinders *Curved Layer. Struct.* **1** 59–92
[8] Leissa A W 1969 *Vibration of Plates SP-160* NACA, Washington
[9] Leissa A W 1973 *Vibration of Shells SP-160* NACA, Washington
[10] Hildebrand F B, Reissner E and Thomas G B 1949 *Notes on the Foundations of the Theory of Small Displacements of Orthotropic Shells Technical Note No. 1833* NACA, Washington
[11] Tornabene F 2012 *Meccanica delle Strutture a Guscio in Materiale Composito* (Bologna: Societá Editrice Esculapio)
[12] Soedel W 2004 *Vibration of Shells and Plates* (New York: Marcel Dekker)
[13] Reddy J N 2004 *Mechanics of Laminated Composite Plates and Shells. Theory and Analysis* 2nd edn (New York: CRC Press)
[14] Soldatos K P and Ye J 1995 Axisymmetric static and dynamic analysis of laminated hollow cylinders composed of monoclinic elastic layers *J. Sound Vibr.* **184** 245–59
[15] Messina A 2009 Three dimensional free vibration analysis of cross-ply laminated plates through 2D and exact models *3rd Int. Conf. on Integrity, Reliability and Failure (Porto, 20–24 July)*
[16] Open document *Systems of Differential equations* free available on http://www.math.utah.edu/gustafso/ (accessed 23rd May 2013)
[17] Boyce W E and DiPrima R C 2001 *Elementary Differential equations and Boundary Value Problems* (New York: Wiley)
[18] Zwillinger D 1997 *Handbook of Differential equations* (New York: Academic)
[19] Molery C and Van Loan C 2003 Nineteen dubious ways to compute the exponential of a matrix, twenty-five years later *SIAM Rev.* **45** 1–46
[20] Simsek M 2010 Vibration analysis of a single-walled carbon nanotube under action of a moving harmonic load based on nonlocal elasticity theory *Physica* **E43** 182–91
[21] Aydogdu M 2009 A general non local beam theory: its application to nanobeam bending, buckling and vibration *Physica* **E41** 1651–5
[22] Cinefra M, Carrera E and Brischetto S 2011 Refined shell models for the vibration analysis of multiwalled carbon nanotubes *Mech. Adv. Mater. Struct.* **18** 476–83
[23] Chen X and Cao G 2006 A structural mechanics study of single-walled carbon nanotubes generalized from atomistic simulation *Nanotechnology* **17** 1004–15
[24] de Borbón F and Ambrosini D 2012 On the influence of van der Waals coefficient on the transverse vibration of double walled carbon nanotubes *Comput. Mater. Sci.* **65** 504–8
[25] Carrera E, Brischetto S and Nali P 2011 *Plates and Shells for Smart Structures: Classical and Advanced Theories for Modeling and Analysis* (New Delhi: Wiley)
[26] Tornabene F, Viola E and Fantuzzi N 2013 General higher-order equivalent single layer theory for free vibrations of doubly-curved laminated composite shells and panels *Compos. Struct.* **104** 94–117
[27] Tornabene F 2016 General higher order layer-wise theory for free vibrations of doubly-curved laminated composite shells and panels *Mech. Adv. Mater. Struct.* **23** 1046–67

Chapter 10

[1] Griffith A A 1921 The phenomena of rupture and flow in solids *Phil. Trans. R. Soc.* **A221** 582–93
[2] Irwin G R 1957 Analysis of stresses and strains near the end of a crack traversing a plate *J. Appl. Mech.* **24** 351–69

[3] Rice J R 1968 A path independent integral and the approximate analysis of strain concentrations of notches and cracks *J. Appl. Mech.* **35** 379–86
[4] Evans A G, Dalgleish B J, He M and Hutchinson J W 1989 On crack path selection and the interface fracture energy in bimaterial systems *Acta Metall.* **37** 3249–54
[5] Evans A G, Rühle M, Dalgleish B and Charalambides B G 1990 The fracture energy of bimaterial interfaces *Metall. Trans.* **A21** 2419–29
[6] Dugdale D S 1960 Yielding of steel sheets containing slits *J. Mech. Phys. Solids* **8** 100–4
[7] Barenblatt G I 1959 The formation of equilibrium cracks during brittle fracture. General ideas and hypotheses *J. Appl. Math. Mech.* **23** 434–44
[8] Needleman A 1990 An analysis of decohesion along an imperfect interface *Int. J. Fract.* **42** 21–40
[9] Allix O and Ladevèze P 1992 Interlaminar interface modelling for the prediction of delamination *Compos. Struct.* **22** 235–42
[10] Allix O and Corigliano A 1996 Modeling and simulation of crack propagation in mixed-modes interlaminar fracture specimens *Int. J. Fract.* **77** 111–40
[11] Belytschko T and Gracie R 2007 On XFEM applications to dislocations and interfaces *Int. J. Plast.* **23** 1721–38
[12] Sukumar N, Möes N, Moran B and Belytschko T 2000 Extended finite element method for three-dimensional crack modelling *Int. J. Numer. Methods Eng.* **48** 1549–70
[13] Cazes F and Möes N 2015 Comparison of a phase-field model and of a thick level set model for brittle and quasi-brittle fracture *Int. J. Numer. Methods Eng.* **103** 114–43
[14] Latifi M, van der Meer F P and Sluys L J 2017 An interface thick level set model for simulating delamination in composites *Int. J. Numer. Methods Eng.* **111** 301–400
[15] Bourdin B, Francfort G A and Marigo J J 2008 *The Variational Approach to Fracture* (Berlin: Springer)
[16] Miehe C, Welschinger F and Hofacker M 2010 Thermodynamically consistent phase-field models of fracture: variational principles and multi-field FE implementations *Int. J. Numer. Methods Eng.* **83** 1273–11
[17] Mumford D B and Shah J 1989 Optimal approximations by piecewise smooth functions and associated variational problems *Commun. Pure Appl. Math.* **42** 577–685
[18] Francfort G A and Marigo J J 1998 Revisiting brittle fracture as an energy minimization problem *J. Mech. Phys. Solids* **46** 1319–42
[19] Bourdin B, Francfort G and Marigo J J 2000 Numerical experiments in revisited brittle fracture *J. Mech. Phys. Solids* **48** 797–826
[20] Kasirajan P, Bhattacharya S, Rajagopal A and Reddy J N 2020 Phase field modeling of fracture in quasi-brittle materials using natural neighbor Galerkin method *Comput. Methods Appl. Mech. Eng.* **366** 113019
[21] Rajagopal A, Fischer P, Kuhl E and Steinmann P 2010 Natural element analysis of the Cahn–Hilliard phase-field model *Comput. Mech.* **46** 471–93
[22] Ambati M, Gerasimov T and De Lorenzis L 2015 Phase-field modeling of ductile fracture *Comput. Mech.* **55** 1017–40
[23] Borden M J, Hughes T J R, Landis C M, Anvari A and Lee I J 2016 A phase-field formulation for fracture in ductile materials: finite deformation balance law derivation, plastic degradation, and stress triaxiality effects *Comput. Methods Appl. Mech. Eng.* **312** 130–66

[24] Borden M J, Verhoosel C V, Scott M A, Hughes T J R and Landis C M 2012 A phase-field description of dynamic brittle fracture *Comput. Methods Appl. Mech. Eng.* **217-20** 77–95
[25] Schlüter A, Willenbücher A, Kuhn C and Müller R 2014 Phase field approximation of dynamic brittle fracture *Comput. Mech.* **54** 1141–61
[26] Zhou S, Rabczuk T and Zhuang X 2018 Phase field modeling of quasi-static and dynamic crack propagation: COMSOL implementation and case studies *Adv. Eng. Softw.* **122** 31–49
[27] Raghu P, Rajagopal A and Reddy J N 2020 Nonlocal transient dynamic analysis of laminated composite plates *Mech. Adv. Mater. Struct.* **27** 1076–84
[28] Verhoosel C V and Borst R de 2013 A phase-field model for cohesive fracture *Int. J. Numer. Methods Eng.* **96** 43–62
[29] Nguyen T T, Yvonnet J, Zhu Q Z, Bornert M and Chateau C 2016 A phase-field method for computational modeling of interfacial damage interacting with crack propagation in realistic microstructures obtained by microtomography *Comput. Methods Appl. Mech. Eng.* **312** 567–95
[30] Paggi M and Reinoso J 2017 Revisiting the problem of a crack impinging on an interface: a modeling framework for the interaction between the phase field approach for brittle fracture and the interface cohesive zone model *Comput. Methods Appl. Mech. Eng.* **321** 145–72
[31] Ambrosio L and Tortorelli V M 1990 Approximation of functional depending on jumps by elliptic functional via t-convergence *Commun. Pure Appl. Math.* **43** 999–1036
[32] Tvergaard V and Hutchinson J W 1993 The influence of plasticity on mixed mode interface toughness *J. Mech. Phys. Solids* **41** 1119–35
[33] Mohammed I and Liechti K M 2000 Cohesive zone modeling of crack nucleation at bimaterial corners *J. Mech. Phys. Solids* **48** 735–64
[34] Cui W C, Wisnom M R and Jones M 1992 A comparison of failure criteria to predict delamination of unidirectional glass/epoxy specimens waisted through the thickness *Composites* **23** 158–66
[35] Xu X P and Needleman A 1993 Void nucleation by inclusion debonding in a crystal matrix *Model. Simul. Mater. Sci. Eng.* **1** 111–32
[36] Van den Bosch M J, Schreurs P J G and Geers M G D 2006 An improved description of the exponential Xu and Needleman cohesive zone law for mixed-mode decohesion *Eng. Fract. Mech.* **73** 1220–34
[37] Reinoso J and Paggi M 2014 A consistent interface element formulation for geometrical and material nonlinearities *Comput. Mech.* **54** 1569–81
[38] Krishnan A and Xu L R 2013 Experimental studies on the interaction among cracks, notches and interfaces of bonded polymers *Int. J. Solids Struct.* **50** 1583–96
[39] Li J, Hai L and Wu J Y 2020 A phase-field damage model with micro inertia effect for the dynamic fracture of quasi-brittle solids *Eng. Fract. Mech.* **225** 106821

Chapter 11

[1] Chakraverty S and Biswas P 2020 *Recent Trends in Wave Mechanics and Vibrations Lecture Notes in Mechanical Engineering* (Cham: Springer)
[2] Qassab S Y and Ali Sultan H 2013 Modal analysis of pneumatic two finger robotic hand by finite element analysis and experimental testing *Int. J. Eng. Technol. IJET-IJENS* **13** 1–9
[3] Jeevan A N R 2015 Modeling and analysis of robot arm using ANSYS *Int. J. Sci. Eng. Technol. Res.* **4** 6692–97

[4] Warude P, Patel M, Pandit P, Patil V, Pawar H, Nate C, Gajlekar S, Atpadkar V and Roy D 2019 On the design and vibration analysis of a three-link flexible robot interfaced with a mini-gripper *Recent Trends in Wave Mechanics and VibrationsLecture Notes in Mechanical Engineering* (Singapore: Springer), pp 29–45

[5] Pawar H, Nate C, Patel M, Pandit P, Patil V, Warude P, Wankhede N, Chothe P, Atpadkar V and Roy D 2019 Design, dynamic simulation and test-run of the indigenous controller of a multi-gripper revolute robot by minimizing system trembling *Recent Trends in Wave Mechanics and VibrationsLecture Notes in Mechanical Engineering* (Singapore: Springer), pp 47–60

[6] Roy D 2019 Towards the control of inherent vibration of flexible robotic systems and associated dynamics: new proposition and model *Int. J. Robot. Res. Appl. Autom.* **1** 6–17

[7] Chitte P G and Bansode S S 2016 Structural and vibrational analysis of six axis ARISTO robot using ANSYS *Int. J. Innov. Res. Technol.* **3** 291–96

[8] Shareef I R and Zayer I A 2018 Natural frequency estimation of a free vibrated robotic arm using artificial intelligence *Int. J. Appl. Eng. Res.* **13** 5393–99

[9] Chouhan R and Kanwal F 2014 Design and development of a prototype robotic gripper *Proc. of the 2014 Int. Conf. on Robotics and Emerging Allied Technologies in Engineering (iCREATE) (Islamabad, April 22–24)* pp 317–20

[10] Datta R and Pradhan S 2015 Analysis and design optimization of a robotic gripper using multiobjective genetic algorithm *IEEE Trans. Syst. Man Cybernet.: Syst.* **46** 1–11

[11] Liu C-H 2019 Topology and size–shape optimization of an adaptive compliant gripper with high mechanical advantage for grasping irregular objects *Robotica* **37** 1383–400

[12] Abomoharam A H M 2017 Modeling and design optimization of a robot gripper mechanism *Rob. Comput. Integr. Manuf.* **46** 94–103

[13] Lanni C 2019 An optimum design algorithm for mechanisms in two-finger grippers *Proc. of the 13th WSEAS Int. Conf. on SYSTEMS* pp 63–70

[14] Bircher W G 2017 A two-fingered robot gripper with large object reorientation range Proc. of the IEEE Int. Conf. on Robotics and Automation (ICRA) *(Singapore, May 29–June 3)* pp 3453–460

[15] Sahu S and Choudhury B B 2017 Static analysis of a 6-axis industrial robot using finite element analysis *Int. J. Mech. Eng. Technol. (IJMET)* **8** 49–55

[16] Bicchi A and Kumar V 2000 Robotic grasping and contact: a review *Proc. of the IEEE Int. Conf. on Robotics and Automation* pp 348–53

[17] Badadhe S 2018 FEM based dynamic analysis of robot end gripper mechanism *Int. J. Eng. Sci. Invent. (IJESI)* **7** 50–67

[18] Roy D 2019 Control of inherent vibration of flexible robotic systems and associated dynamics *Recent Trends in Wave Mechanics and VibrationsLecture Notes in Mechanical Engineering* (Singapore: Springer)

[19] Roy D 2020 Design, modeling and indigenous firmware of a patient assistance flexible robotic system-type I: beta version *Adv. Robotics Mech. Eng.* **2** 148–59

[20] Benosman M and Vey G 2004 Control of flexible manipulators: a survey *Robotica* **22** 533–45

[21] Singer N C and Seering W C 1990 Preshaping command inputs to reduce system vibration *J. Dyn. Syst. Meas. Control-Trans. ASME* **112** 76–82

[22] Fraser A R and Daniel R W 1991 *Perturbation Techniques for Flexible Manipulators* (Norwell, MA: Kluwer)

[23] Luo Z H 1993 Direct strain feedback control of a flexible robot arm: new theoretical & experimental results *IEEE Trans. Autom. Control* **38** 1610–22
[24] Chen W 2001 Dynamic modelling of multi-link flexible robotic manipulators *Comput. Struct.* **79** 183–95
[25] Subudhi B and Morris A S 2002 Dynamic modeling, simulation and control of a manipulator with flexible links and joints *Rob. Autom. Syst.* **41** 257–70
[26] Feliu V, Somolinos J A and Garcia A 2003 Inverse dynamics based control system for a three degrees-of-freedom flexible arms *IEEE Trans. Robotics Automat.* **19** 1007–14
[27] Feliu V and Ramos F 2005 Strain gauge based control of single-link flexible very light weight robots robust to payload changes *Mechatronics* **15** 547–71
[28] Singer N C and Seering W C 1990 Preshaping command inputs to reduce system vibration *J. Dyn. Syst. Meas. Control-Trans. ASME* **112** 76–82
[29] Chen Y P and Hsu H T 2001 Regulation and vibration control of an FEM-based single-link flexible arm using sliding-mode theory *J. Vibrat. Control* **7** 741–52
[30] Tjahyadi H and Sammut K 2006 Multi-mode vibration control of a flexible cantilever beam using adaptive resonant control *Smart Mater. Struct.* **15** 270–78
[31] Trapero-Arenas J R, Mboup M, Pereira-Gonalez E and Feliu V 208 Online frequency and damping estimation in a single-link flexible manipulator based on algebraic identification *Proc. of the 16th. Mediterranean Conf. on Control & Automation (IEEE)* pp 338–43
[32] Pereirea E, Aphale S S, Feliu V and Moheimani S O R 2011 Integral resonant control for vibration damping and precise tip-positioning of a single-link flexible manipulator *IEEE ASME Trans. Mech.* **16** 232–40
[33] Gupta N K 1980 Frequency-shaped cost functionals: extension of linear-quadratic-gaussian design methods *J. Guid. Control* **3** 529–35
[34] Juang J-N, Turner J D and Chun H M 1985 Closed-form solutions for feedback control with terminal constraints *J. Guid. Control* **8** 39–43
[35] Baumgarte J 1972 Stabilization of constraints and integrals of motion in dynamic systems *Comput. Method Appl. Mech. Eng.* **1** 1–16
[36] Argyris J 1982 An excursion into large rotations *Comp. Method Appl. Mech. Eng.* **32** 85–155
[37] Atluri S and Cazzani A 1995 Rotations in computational solid mechanics *Arch. Comput. Meth. Eng.* **2** 49–138
[38] Fraeijs de Veubeke B 1976 The dynamics of flexible bodies *Int. J. Eng. Sci.* **14** 895–913
[39] Danielson D and Hodges D 1988 A beam theory for large global rotation, moderate local rotation and small strain *ASME J. Appl. Mech.* **55** 179–84
[40] Li D and Likins P 1987 Dynamics of a multi-body system with relative translation on curved flexible tracks *J. Guid.* **10** 299–306
[41] Bauchau O, Damilano G and Theron N 1995 Numerical integration of non-linear elastic multi-body systems *Int. J. Numer. Methods Eng.* **38** 2727–51
[42] Oden J and Martins J 1985 Models and computational methods for dynamic friction phenomena *Comput. Method Appl. Mech. Eng.* **52** 527–634
[43] Rauniyar A, Roy D, Pandit P and Atpadkar V 2018 Design model for the drive and actuator of the test set-up of a novel flexible robotic system *Proc. of the 2018 IEEE Int. Conf. on Computational Intelligence and Computing Research (IEEE-ICCIC-2018) (Madurai, Tamil Nadu, India, December 13–15)* [Awarded Best Paper Prize]
[44] Islam A, Sharma S, Sharma K, Sharma R, Sharma A and Roy D 2020 Real-time data monitoring through sensors in robotized shielded metal arc welding *Mater. Today: Proc.* **26** 2368–73

Chapter 12

Bandyopadhyay D and Bhattacharyya S K 2007 *Statistical Health Monitoring of Structures Using Noisy Dynamic Responses* (IIT Kharagpur, India: ICTACEM), pp 27–9

Bandyopadhyay D and Bhattacharyya S K 2008 *An Inverse Dynamic Approach of Statistical Health Monitoring of Structure from Limited Noisy Data* (Adelaide: ICTAM), pp 25–9

Cao M and Qiao P 2009 Novel Laplacian scheme and multiresolution modal curvatures for structural damage identification *Mech. Syst. Sig. Process.* **23** 1223–42

Carden E and Fanning P 2004 Vibration based condition monitoring: a review *Struct. Health Monitor.* **3** 355–77

Chatterjee P K, Datta T K and Surana C S 1994 Vibration of continuous bridges under moving vehicles *J. Sound Vib.* **340** 619–32

Ciambella J, Vestroni F and Vidoli S 2011 Damage observability, localization and assessment based on eigen frequencies and eigen vectors curvatures *Smart Struct. Syst.* **9** 191–204

Ciambella J and Vestroni F 2015 The use of modal curvatures for damage localization in beam-type structures *J. Sound Vib.* **340** 126–37

Chaurasia A, Panigrahi S K and Patel S S 2018 Damage identification of reinforced concrete beam using modal curvature approach *J Sci. Ind. Res.* **77** 337–41

Darpe A K, Gupta K and Chawla A 2004 Coupled bending, longitudinal and torsional vibrations of a cracked rotor *J. Sound Vib.* **269** 33–60

Doebling S W, Farrar C R and Prime M B 1998 A summary review of vibration-based damage identification methods *Shock Vib. Digest* **30** 91–105

Dulieu-Barton J M, Brennan M J, Holford K M and Worden K 2003 Damage assessment of structures *Proceedings of DAMAS (5th Int. Conf. on Damage Assessment of Structures)* (Freienbach: Trans Tech Publications), pp 149–54

Foti D and Campian C 2007 Structural health monitoring through dynamic identification techniques: numerical simulation of a damage scenario *Buletinul, Institutului Politechnic Din Iasi, tomul LIII (LVII)* 3–4

Fan W and Qiao P 2011 Vibration-based damage identification methods: a review and comparative study *Struct. Health Monitor.* **10** 83–111

Farrar C and Jauregui D 1996 *Fault Detection Algorithms Applied to Experimental and Numerical Modal Data from The I-40 Bridge Technical Report LA-13074-MS* Los Alamos National Laboratory

Fox C H 1992 The location of defects in structures: a comparison of the use of natural frequency and mode shape data *Proc. of the 10th Int. Modal Analysis Conf.* pp 522–8

Gandomi A H, Sahab M G, Rahaei A and Safari G M 2008 Development in mode shape-based structural fault identification technique *World Appl. Sci. J.* **5** 29–38

Humar J, Bagchi A and Xu H 2006 Performance of vibration-based techniques for the identification of structural damage *Struct. Health Monitor.* **5** 215–41

Bureau of Indian Standards 2000 *IS 456 Plain and Reinforced Concrete Code* Bureau of Indian Standards, New Delhi

Ko J M, Sun Z G and Ni Y Q 2002 Multi-stage identification scheme for detecting damage in cable-stayed KapShuiMun Bridge *Eng. Struct.* **24** 857–68

Lee P K K, Ho E and Chung H W 1987 Static and dynamic tests of concrete bridges *ASCE J. Struct. Eng.* **113** 61–73

Pandey A K, Biswas M and Samman M M 1991 Damage detection from changes in curvature mode shapes *J. Sound Vib.* **145** 321–32

Panigrahi S K, Chakraverty S and Bhattacharyya S K 2015 Damage detection of multi-storeyed shear structure using sparse and noisy modal data *Smart Struct. Syst.* **15** 1215–32

Panigrahi S K, Chakraverty S and Mishra B K 2009 Vibration based damage detection in a uniform strength beam using genetic algorithm *Meccanica* **44** 697–710

Panigrahi S K, Chakraverty S and Mishra B K 2013 Damage identification of multistory shear structure from sparse modal information *J. Comp. Civ. Eng.* **27** 1–9

Ratcliffe C P 2000 A frequency and curvature based experimental method for locating damage in structures *J. Vib. Acoustics* **122** 324–29

Ren W-X and De Roeck G 2002 Structural damage identification using modal data. I: Simulation verification *J. Struct. Eng.* **128** 87–95

Rizos P F, Aspragathos N and Dimarogonas A D 1990 Identification of crack location and magnitude in a cantilever beam from the vibration modes *J. Sound Vib.* **138** 381–88

Saleh F, Supriyadi B, Suhendro B and Tran D 2004 Damage detection in non-prismatic reinforced concrete beams using curvature mode shapes *SIF2004 Structural Integrity and Fracture* (Melbourne: Australian Fracture Group Inc.), pp 331–37

Santos J V, Dos A, Mota S C M and Pina H L G 2000 Development of a numerical model for the damage identification on composite plate structure *Compos. Struct.* **48** 59–65

Srinivasa V, Sasmala S, Ramanjaneyulua K and Jeyasehar C A 2013 Influence of test conditions on modal characteristics of reinforced concrete structures under different damage scenarios *Arch. Civil Mech. Eng.* **13** 491–505

Stubbs N and Osegueda R 1990 Global damage detection in solids: experimental verification *Int. J. Anal. Exp. Modal Anal* **5** 81–97

Unger J F, Anne T and De R G 2005 Damage detection of a prestressed concrete beam using modal strains *J. Struct. Eng.* **131** 1456–63

Wahab M M A and Roeck G D 1999 Damage detection in bridges using modal curvatures: Application to a real damage scenario *J. Sound Vibration* **226** 217–35

Yu B, Shimao H, Wenjing N, Jing G and Xueqing S 2012 Plane grid structure damage location identification by model curvature *Proc. Eng.* **31** 534—40

Zhang J, Hue P, Hue Y C, Long D Y and Yu Z H 2011 Damage detection of plane member structures based on modal curvature difference method *Adv. Mater. Res.* **163** 2848–51

Chapter 13

[1] Zenkert D 1995 *An Introduction to Sandwich Construction* (Cradley Heath: EMAS Publishing)

[2] Castanié B, Bouvet C and Ginot M 2020 Review of composite sandwich structure in aeronautic applications *Compos. Part C: Open Access* **1** 100004

[3] Wijker J J 2008 *Spacecraft Structures* (Cham: Springer)

[4] Morozov E V, Lopatin A V and Taygin V B 2015 Design, fabrication and testing of composite sandwich integral structure of spacecraft antenna *Compos. Struct.* **134** 645–53

[5] Thomsen O T 2009 Sandwich materials for wind turbine blades—present and future *J. Sandw. Struct. Mater.* **11** 7–26

[6] Nast E 1997 On honeycomb-type core moduli *38th Structures, Structural Dynamics, and Materials Conference, Structures, Structural Dynamics, and Materials and Co-located Conferences* (Reston, VA: American Institute of Aeronautics and Astronautics)

[7] Schwingshackl C W, Aglietti G S and Cunningham P R 2006 Determination of honeycomb material properties: existing theories and an alternative dynamic approach *J. Aerosp. Eng.* **19** 177–83
[8] Gibson L J, Ashby M F, Schajer G S and Robertson C I 1982 The mechanics of two-dimensional cellular materials *Proc. Royal Soc. London A. Math. Phys. Sci.* **382** 25–42
[9] Gibson L J and Ashby M F 1988 *Cellular Solids: Structure and Properties* (Oxford: Pergamon)
[10] Gibson L J and Ashby M F 1997 *Cellular Solids: Structure and Properties* (Cambridge: Cambridge University Press), pp 175–231
[11] Grediac M 1993 A finite element study of the transverse shear in honeycomb cores *Int. J. Solids Struct.* **30** 1777–88
[12] Shi G and Tong P 1995 The derivation of equivalent constitutive equations of honeycomb structures by a two scale method *Comput. Mech.* **15** 395–407
[13] Masters I G and Evans K E 1996 Models for the elastic deformation of honeycombs *Compos. Struct.* **35** 403–22
[14] Becker W 1998 The in-plane stiffnesses of a honeycomb core including the thickness effect *Arch. Appl. Mech.* **68** 334–41
[15] Xu X F and Qiao P 2002 Homogenized elastic properties of honeycomb sandwich with skin effect *Int. J. Solids Struct.* **39** 2153–88
[16] Zhang J and Ashby M F 1992 The out-of-plane properties of honeycombs *Int. J. Mech. Sci.* **34** 475–89
[17] Qiao P and Xu X F 2005 Refined analysis of torsion and in-plane shear of honeycomb sandwich structures *J. Sandwich Struct. Mater.* **7** 289–305
[18] Mujika F, Pujana J and Olave M 2011 On the determination of out-of-plane elastic properties of honeycomb sandwich panels *Polym. Test.* **30** 222–28
[19] Malek S and Gibson L 2015 Effective elastic properties of periodic hexagonal honeycombs *Mech. Mater.* **91** 226–40
[20] Mukhopadhyay T and Adhikari S 2016 Free-vibration analysis of sandwich panels with randomly irregular honeycomb core *J. Eng. Mech.* **142** 06016008
[21] Yuan J, Zhang L and Huo Z 2020 An equivalent modeling method for honeycomb sandwich structure based on orthogonal anisotropic solid element *Int. J. Aeronaut. Space Sci.* **21** 957–69
[22] Irfan S and Siddiqui F 2019 A review of recent advancements in finite element formulation for sandwich plates *Chin. J. Aeronaut.* **32** 785–98
[23] Abrate S and Di M Sciuva 2017 Equivalent single layer theories for composite and sandwich structures: a review *Compos. Struct.* **179** 482–94
[24] Ahmad Nazeer, Ranganath R. and Ghosal Ashitava 2017 Modeling and experimental study of a honeycomb beam filled with damping particles *J. Sound Vibr.* **391** 20–34

Chapter 14

[1] Giambanco G, Rizzo S and Spallino R 2001 Numerical analysis of masonry structures via interface models *Comput. Meth. Appl. Mech. Eng.* **190** 6493–511
[2] Lubliner J, Oliver S and Onate E 1989 A plastic-damage model for concrete *Int. J. Solids Struct.* **25** 299–329
[3] Lubliner J, Oliver S and Onate E 1990 Finite element nonlinear analysis of concrete structures using a plastic-damage model *Eng. Fract. Mech.* **35** 219–31

[4] Lourenço P B 1998 Experimental and numerical issues in the modelling of the mechanical behavior of masonry *Structural Analysis of Historical Constructions* ed P Roca *et al* (Barcelona: CIMNE), pp 57–91

[5] Lourenço P B 2000 A case study about using sophisticated masonry models in practice: the Lethes theatre (C. 1650) *Fifth Int. Conf. on Computational Structures Technology* ed B H V Topping and G de Roeck (Edinburgh: Civil-Comp Press), pp 433–42

[6] Naraine K and Sinha S 1989 Behavior of brick masonry under cyclic compressive loading *J. Constr. Eng. Manag. (ASCE)* **115** 1432–43

[7] Naraine K and Sinha S 1991 Cyclic behaviour of masonry in biaxial compression *J. Struct. Eng. (ASCE)* **117** 1336–55

[8] Naraine K and Sinha S 1992 Stress-strain curve for brick masonry in biaxial compression *J. Struct. Eng. (ASCE)* **118** 1451–61

[9] Abaqus/CAE documentation 2010 Section 18.5.1–18.5.3

[10] Lee J and Fenves G L 1998 A plastic-damage model for cyclic loading of concrete structures *J. Eng. Mech. ASCE* **124** 892–900

[11] Peña F, Lourenco P B, Mendes N and Oliveira D V 2010 Numerical models for the seismic assessment of an old masonry tower *Eng. Struct.* **32** 1466–78